Aluminium and manganese in the West Atlantic Ocean

A MODEL STUDY

Marco van Hulten

April 12, 2014

This is an incomplete draft of my PhD thesis. Numbering of references to included sections and other objects are likely to change with future versions, while unincluded objects are presented as '**??**'.

Nomenclature

Symbols

$\rightarrow$	"Also see..."; only used in this Nomenclature
$:=$	Definition
$\equiv$	Equality between two functions for any choice of values for the variables
$\%_m$	Percent by mass
[Tr]	Concentration of a →tracer →Tr ($\mathrm{mol\,dm^{-3}}$)
(Tr)	Activity of a tracer Tr ($\mathrm{mol\,dm^{-3}}$)
$\varnothing$	Diameter of a →particle
$A_{\_}$	Mathematical notation for →Al concentrations; subscript denotes phase
$\mathcal{A}$	Horizontal →eddy diffusion coefficient ($\mathrm{m^2\,s^{-1}}$)
α_{Tr}	Dissolution fraction of Tr from deposited dust
β_{Tr}	Dissolution fraction of Tr from sediment source
$C_{\_}$	Mathematical notation for →C concentrations; subscript denotes phase
c_{in}	Weight factor for the Al/Si incorporation ratio
$\Delta\mathcal{V}$	Gridbox volume
Δz_i	Thickness of →model layer i
γ	Activity coefficient, factor accounting for mixture effects; (Tr) = γ [Tr]
$F_{\_}$	Mathematical notation for →Fe concentrations; subscript denotes phase
f	Coriolis parameter ($\mathrm{rad\,s^{-1}}$)
f_{Tr}	Mass fraction of an element Tr
$f_{\mathrm{T1:T2}}$	Molar ratio T1/T2 in source term
Φ_{dust}	Dust deposition flux from the atmosphere on to the ocean surface ($\mathrm{g\,m^{-2}\,s^{-1}}$)
g	Gravity of the Earth, approximately $9.8\,\mathrm{m\,s^{-2}}$
I	Flow of a tracer per unit of time ($\mathrm{M\,s^{-1}}$)
K	→Eddy viscosity, or turbulent viscosity coefficient (Pa s)
log	Natural logarithm
μ	Viscosity (Pa s)
$M_{\_}$	Mathematical notation for →Mn concentrations; subscript denotes phase
m	Modelled value of a tracer
m_{Tr}	Atomic mass of Tr ($\mathrm{g\,mol^{-1}}$)
mol	Mole, about $6.022 \cdot 10^{23}$ elementary entities of a substance
µM	Micromolar, 10^{-6} $\mathrm{mol\,dm^{-3}}$
nM	Nanomolar, 10^{-9} $\mathrm{mol\,dm^{-3}}$
$\nu_{\mathcal{E}}$	Vertical →eddy diffusion coefficient ($\mathrm{m^2\,s^{-1}}$)
o	Measured value of a tracer
P	Pressure (Pa = $\mathrm{kg\,m^{-1}\,s^{-2}}$)
r_{max}	Maximum Al/Si incorporated into living diatom →frustules
$R_{\mathrm{T1:T2}}$	Reaction stoichiometry between reactants T1 and T2
$D_{\updownarrow}$	Root Mean Square Deviation, vertical distribution homogenised
S	Salinity (‰)
$S_{\_}$	Mathematical notation for →Si concentrations; subscript denotes phase
Sv	Sverdrup, 10^6 $\mathrm{m^3\,s^{-1}}$
T	Temperature (° C)

$\mathcal{T}$	Mathematical notation for an arbitrary tracer
$\dot{\mathcal{T}}_0$	Input of a tracer as an increase of the concentration of a base tracer $\mathcal{T}_0$ ($\mathrm{g\,s^{-1}}$)
Tmol	Teramole, 10^{12} mol
Tr,T1,T2	Any ocean tracer, e.g. Al, Mn, Si, C; only used in this Nomenclature
U, V, W	Zonal, meridional and vertical component of the velocity
$\mathbf{v}$	→Velocity ($\mathrm{m\,s^{-1}}$)
V_P	Phytoplankton growth rate ($\mathrm{M\,s^{-1}}$)
w_s	→Settling →speed of →particles; $-w_s\hat{z}$ is the settling velocity
$\bar{x}$	Average value of a quantity x
$\hat{z}$	Upward unit vector, (0,0,1)

Abbreviations and terminology

3-D	Three-dimensional
AABW	AntArctic Bottom Water
AAIW	AntArctic Intermediate Water
adsorption	The adhesion of a substance onto a surface of a particle
Al	Aluminium, 3rd most abundant element in the Earth's crust
$\mathrm{Al_{ads}}$	→Adsorbed Al
$\mathrm{Al_{biog}}$	Incorporated biogenic Al
$\mathrm{Al_{diat}}$	Incorporated diatom Al
$\mathrm{Al_{diss}}$	Dissolved Al: $\mathrm{Al^{3+}}$, $\mathrm{AlOH^{2+}}$ and →colloids with $\varnothing < 0.2\,\mu\mathrm{M}$
$\mathrm{Al_{part}}$	→Particulate Al: either $\mathrm{Al_{ads}}$ or $\mathrm{Al_{biog}}$, lithogenic Al not included
aluminosilicate	Lithogenic minerals mostly composed of aluminium, silicon, and oxygen
AMOC	Atlantic Meridional Overturning Circulation
BATS	Bermuda Atlantic Time-series Study (1988–)
BEC	Biogeochemical Elemental Cycling (model, previously: biogeochemistry/ecosystem/circulation)
biogenic	Created by organisms
Boussinesq approx	The assumption that density differences are sufficiently small to be neglected, except for g-dependent terms
$\mathrm{CaCO_3}$	Calcium carbonate: calcite and aragonite
clay	→Aluminosilicates with $\varnothing < 2\,\mu\mathrm{m}$
CLIVAR	Climate Variability and Predictability (2010–), project of the World Climate Programme
$\mathrm{CO_2}$	Carbon dioxide
conceptual model	Composition of concepts to clarify the working of certain phenomena
colloid	→Particle with $1\,\mathrm{nm} < \varnothing < 1\,\mu\mathrm{m}$
desorption	The release of a substance from a surface of a particle
diagenesis	The change of sediments after →sedimentation
diatom	Functional type of phytoplankton with silica frustule
DIC	Dissolved Inorganic Carbon
DOC	Dissolved Organic Carbon
DSOW	Denmark Strait Overflow Water
dust	Atmospheric →particles, mainly coming from desserts
ECMWF	European Center for Medium range Weather Forecasting
eddy diffusion	Parameterisation for subgrid advection
eddy viscosity	Parameterisation for subgrid transport and dissipation of energy
empiricism	The view that regards *sensory experience* as the main source and test of knowledge
ERA-40	→ECMWF Re-Analysis of 40 yr, a 45-year re-analysis of the atmosphere and surface conditions from September 1957 to August 2002
ERS	European Remote Sensing; refers to ERS-1 and ERS-2 satellites
euphotic zone	The surface layer of the ocean that is well-lit, i.e. more than 1% of sunlight penetration
Fe	Iron, 4th most abundant element in the Earth's crust
$\mathrm{Fe_{diss}}$	Dissolved Fe: $\mathrm{Fe^{3+}}$, ligands and colloids with $\varnothing < 0.2\,\mu\mathrm{m}$
fluid	Liquids and gasses; in case of geophysical fluids the ocean and atmosphere, respectively

frustule	Cell wall made of →biogenic →silica
GCM	General Circulation Model, a model of general circulation based on the primitive equations
GEOSECS	GEochemical Ocean SECtions Study (1972–1978)
GEOTRACES	Programme aiming to improve our understanding of ocean biogeochemical cycles (2006–)
HAMOCC	HAmburg Model for the Ocean Carbon Cycle
HOT	Hawaii Ocean Time-series (1988–)
hydrothermal vent	A fissure in the Earth's crust, typically found at spreading regions
INCA	INteraction with Chemistry and Aerosols (model)
instrumentalism	The view that a scientific theory is a useful instrument in understanding the world (agnostic about realism)
IPY	3rd International Polar Year (2007–2009)
JGOFS	Joint Global Ocean Flux Study (1989–2005)
lithogenic	Originating from the lithosphere; not →biogenic
LMDzT	Laboratoire de Météorologie Dynamique (model)
LSCE	Laboratoire des Sciences du Climat et l'Environnement
LSG	Large Scale Geostrophic →OGCM (Hamburg model)
mixed layer	Ocean layer where masses are mixed by turbulent; between the air-sea interface and the →thermocline
Mn	Manganese, 12th most abundant element in the Earth's crust
Mn_{ads}	→Adsorbed Mn
Mn(II)	Dissolved Mn: Mn^{2+} and colloids with $\varnothing < 0.2\,\mu m$
MnO_x	Oxidised Mn: MnO_x or colloids thereof
model	Structure for which at least some sentences of a theory, hypotheses or observations are satisfied; →conceptual, →numerical model
NADW	North Atlantic Deep Water
NEMO	Nucleus for European Modelling of the Ocean
numerical model	Mathematical model for which no analytical solution exists and hence is solved on a computer
O	Elemental oxygen, 1st most abundant element in the Earth's crust
OBGCM	Ocean Biogeochemical General Circulation Model
OGCM	Ocean General Circulation Model
OPA	Océan PArallélisé, ocean dynamics component of NEMO
ORCA	Any of five meshes based on the conformal mapping of Madec and Imbard [55]
ORCA2	Model configuration based on the 2°resolution →ORCA mesh, used in →NEMO
OSF	Overturning Stream Function, measure for the MOC in Sv
particle	A localised object, typically larger and heavier than →colloids
PISCES	Biogeochemical model developed by LSCE and community, component of NEMO-TOP
POC	Particulate Organic Carbon
POM	Particulate Organic Matter
rationalism	The view that regards *reason* as the chief source and test of knowledge
RMSD	Root Mean Square Deviation
SAAMW	SubAntArctic Mode Water
SAFe	Sampling and Analysis of Fe (an international standard for sampling and cross-validation)
sand	→Aluminosilicates with $\varnothing > 63\,\mu m$
sedimentation	The last step of particle →settling where →particles in seawater become part of the sediment
settling	The process of sinking of heavy particles through the seawater; → w_s
Si	Silicon, 2nd most abundant element in the Earth's crust
silica	Hydrated silicon dioxide: $SiO_2 \cdot nH_2O$
Si_{biog}	Biogenic Si
Si_{diss}	Dissolved Si or silicic acid: $Si(OH)_4$
Si_{diat}	Si incorporated into the →frustules of diatoms
silt	→Aluminosilicates with $2\,\mu m < \varnothing < 63\,\mu m$
structural realism	The view that regards only structures or relationships as real (as opposed to concrete objects

plankter	Single member of →plankton, a *floater*
plankton	Organisms in the water column that cannot swim but move with the currents
speed	The magnitude of the →velocity, $\|\|\mathbf{v}\|\|$
Sv	Sverdrup, $10^6\ \mathrm{m^3\,s^{-1}}$
thermocline	Layer with large vertical temperature gradient; between upper →mixed layer and deep ocean
TOP	Tracer in the Ocean Paradigm, biogeochemical component of NEMO
tracer	Any property of seawater, e.g. temperature, salinity, iron concentration
velocity	The rate of change of the position, denoted by the vector $\mathbf{v}$ ($\mathrm{m\,s^{-1}}$)
WOCE	World Ocean Circulation Experiment (1990–2002)

Chapter 1

Introduction

1.1 Rationale

The two trace elements aluminium (Al) (Section 1.3.2) and manganese (Mn) (Section 1.3.3) are the focus of this thesis. In the oceans, dissolved Al is present in very small concentrations. It interacts with silicon, a major nutrient for certain types of phytoplankton (Section 1.3.1), and has an influence on the remineralisation of part of these phytoplankton. Furthermore, Al can be used as a proxy for dust deposition in the ocean, which is important since dust contains essential nutrients like iron (Fe) and manganese (Mn). Manganese is an essential nutrient for phytoplankton in the ocean (and other organisms as well) and also a good tracer for hydrothermal vent plumes that are strongly enriched in dissolved Mn. Phytoplankton, with its interaction with Al and Mn, play an important role in the Earth system. Section 1.2 gives the background necessary to understand the importance and interconnectedness of these matters.

1.2 Oceans and climate

Since the formation of the Earth about 4.5 billion years ago, the climate is changing. Climate is defined as the statistical description in terms of the mean and variability of quantities like temperature and precipitation over a period of time ranging from months to thousands or millions of years. This stands in contrast with weather, which is the condition of the atmosphere at a specific place and time [159 § 1.2.2]. At least until the beginning of the industrial revolution, causes of climate change have been primarily natural, i.e. humans did not influence the climate in any significant way. Natural climate change can occur because of internal variability as well as changes in the external forcing. An example of internal climate variability is the El Niño–Southern Oscillation (ENSO) which is purely driven by feedback mechanisms between the atmosphere and the ocean. External factors may influence the climate as well, among which are variations in the Earth's orbit affecting the distribution of sunlight on the Earth, and volcanic activity which affects incoming solar radiation due to emission of volcanic dust.

These are all natural effects, but since about 1750 humans have been influencing the climate considerably [159 § 7.5.1]. Burning of fossil fuels and land use changes resulted in increased concentrations of greenhouse gasses, e.g. carbon dioxide, methane and nitrogen oxides. Greenhouse gasses absorb infrared radiation emitted by the Earth's surface. Subsequently, part of the radiation is emitted back to the surface. Hence, part of the heat is trapped. Without these gasses the worldwide average surface temperature would be significantly lower (about -18°C) than with these gasses (14°C, 1961–1990 average). Due to the anthropogenic emission of greenhouse gasses, the concentration of greenhouse gasses in the atmosphere increased significantly. As a

consequence, since ∼1900 the Earth's average temperature of the atmosphere and the upper ∼700 m of the ocean has increased notably [10 § 1, 131, 159 § 1.2.2]. Overall, the oceans have absorbed 93 % of all the extra heat due to increased greenhouse gas concentrations [159 § 3.1].

Since 1750 more than half of the anthropogenic carbon dioxide is stored in the oceans and terrestrial biospheres, while the remaining part stays in the atmosphere (causing global warming). The importance of the ocean in the climate system is apparent from the fact that 40–50 % of the anthropogenic carbon storage occurs in the oceans, while the rest is stored by the terrestrial ecosystem [159 § 6.3.1, 83]. Carbon dioxide (CO_2) in the atmosphere tends to equilibrate with the carbon dioxide in the surface layer of the ocean [159 § 3.8.1.1]. The system is never precisely in equilibrium, primarily because of the removal of Dissolved Inorganic Carbon (DIC) by two different mechanisms, namely the 'solubility pump' (Section 1.2.1) and the 'biological pump' (Section 1.2.2).

Both in the ocean and on land CO_2 is assimilated by photo-autotrophic organisms (plants), through a process named photosynthesis. Photosynthesis is the fixation, of inorganic carbon during growth of photo-autotrophs, creating complex organic compounds, namely proteins, carbohydrates and fats. Important photo-autotrophs in the ocean include diatoms and cyanobacteria. Other carbon fixers are chemo-autotrophs, who do not need sunlight and derive their energy source chemically, but they are of less importance for the overall carbon fixation.

Only a small part of DIC is fixed by phytoplankton (explained below), while most of it stays in its dissolved phase [159 § 6.1.1]. Nonetheless, the total amount of fixation in the ocean approximately equals the net fixation by the terrestrial ecosystem [60]. This stands in contrast with the much smaller organic carbon pool of aquatic compared to terrestrial plants. The amounts of carbon fixation are nevertheless similar because of the much faster biological overturning in the ocean [60, 103].

For photosynthesis, solar energy, inorganic carbon, water and nutrients are needed [42 § 3.2]. Incoming solar irradiance at the sea surface penetrates into the upper waters. It is attenuated with increasing depth until only 1 % of light remains, below which photosynthesis is negligible. The layer above that depth is often considered the *euphotic zone* [e.g. 28]. In very clear oceanic waters the euphotic zone thickness can be as much as 150 m [42 § 2.1]. The euphotic zone depth is much shallower in the presence of (self-shading) plankton, and coloured dissolved organic matter, while in coastal seas resuspension of sediment (silt, clay) gives much turbidity blocking sunlight already within a few metres or less.

The euphotic zone largely coincides with the *mixed layer*, which is regarded as the layer where all tracers (salinity, temperature, density; and dissolved tracers, e.g. O_2, major nutrients, DIC) are uniform with depth. The mixed layer depth is often defined as the depth where, going downwards, a first significant density increase is observed. Hence, the depth and intrinsic stability of the mixed layer is a function of the vertical density distribution. Alternatively, it can be defined by using a Turbulent Kinetic Energy (TKE) [118 § 7.2, 138 § 14.3] criterium, which is more difficult to measure in the real ocean but is based on the physical causes for the mixed layer. These two definitions are consistent with each other to a good approximation. The mixed layer is caused by wind, waves and buoyancy flux (turbulent heat flux, convective overturning and precipitation minus evaporation). From these quantities the TKE can be calculated. The mixed layer can vary between 10 m in calm summer conditions to 600 m or more during deep winter convection. The strong seasonality of the interplay of the euphotic zone (a few to 150 m depth) and the mixed layer (typically 10 to ∼600 m depth) strongly controls the net primary production. Specifically, if the base of the mixed layer is deeper than a critical depth, productivity will drop to almost zero. This critical depth is defined as the depth at which the primary production minus the remineralisation, integrated to the surface, equals zero; it is typically a few hundred metres deep [102 § 4.3]. Among all factors controlling oceanic

photosynthesis (light, major nutrients, trace nutrients, grazing loss) the available light is by far the most important [42 § 3.3].

The *major nutrients*, i.e. nutrients that are needed in large amounts, are nitrate, phosphate, and, for silicifying autotrophs like diatoms, silicic acid [33 § 9.1, 164]. In the central gyres of the temperate ocean, these nutrients have been utilised so much that they are depleted in surface waters, hence limiting for photosynthesis and plankton growth. Besides the major nutrients, all organisms require at least six bio-essential trace elements manganese (Mn), iron (Fe), cobalt (Co), nickel (Ni), copper (Cu) and zinc (Zn), also called *trace nutrients* [73, 165]. Also there is more and more evidence that cadmium (Cd) is also utilised, either as a substitution of Zn or for intrinsic Cd-requiring biochemical functionality [57, 67]. All these 6–7 trace elements exist in very low concentrations in seawater. Bio-limitation due to shortage of either one of these trace elements is well demonstrated (notably for Fe) or expected [e.g. 57, 80, 107, 162]. Knowledge about the distribution and availability of these nutrients is essential in predicting the amount of carbon fixation. A shortage of any essential nutrient leads to decreased carbon fixation, i.e. less photosynthetic fixation of carbon dioxide in the Earth system [102 pp. 105–7].

Temperature, salinity (dissolved sea salts) and pressure (T, S and P) are the traditional tracers in physical oceanography and utilised not only to derive the density of a water mass (a function of T, S and P), but also as the classical tracers of hydrography like ocean currents throughout the oceans. More and more other biogeochemical tracers (e.g. dissolved oxygen and major nutrient elements) and anthropogenic tracers (e.g. tritium of atomic bomb tests and chlorofluorocarbons CFCs) are also used as tracers of hydrography. The concentration of dissolved chemical and biogeochemical substances (*tracers*) in seawater is determined by air-sea interaction, local biological production and remineralisation, and by physical transport by currents, water mass mixing and settling of biogenic debris particles. External sources like rivers and groundwater discharge also play a role nearby continents, while deep-sea hydrothermal vents and marine sediments act as sources for some tracers and sinks for other tracers.

The distribution of these biogeochemical tracers (carbon, nitrate, iron etc.), and the air-sea fluxes of carbon dioxide, are governed by a combination of physics, chemistry and biology. Since the GEochemical Ocean SECtions Study (GEOSECS) in the 1970s, the number of observations of DIC and major nutrients has increased (e.g. World Ocean Circulation Experiment (WOCE), Joint Global Ocean Flux Study (JGOFS), CLImate VARiability and predictability (CLIVAR)). Nowadays the GEOTRACES programme is producing many high accuracy observations of trace elements (`www.geotraces.org`). Despite the increase, these observations are merely a snapshot both in space of the vast oceans and in time. For DIC and major nutrients there now evolves a time series database spanning some four decades [e.g. 90, 122, 139], yet for trace elements the first GEOTRACES sections still are a one-time snapshot. To interpret the observations and to obtain an integrated understanding, numerical ocean models can be used, that provide information on the time evolution of the ocean. Conversely, the measurements provide a constraint on ocean models and can therefore be used to assess the model's reliability and/or improve the representation of the physical and biogeochemical processes in the model. A thorough understanding of ocean processes is necessary for estimating, for instance, the anthropogenic uptake of CO_2 by the ocean [83], which feeds back to the entire Earth system.

1.2.1 Solubility pump

Dissolved biogeochemical tracers can be transported from the mixed layer into the ocean interior by a suite of, sometimes interacting, physical transport and mixing mechanisms. The mixed layer can become very thick during severe winter storms, leading to a uniform distribution of all tracers in the upper several hundreds of metres. During spring and summer (with seasonal

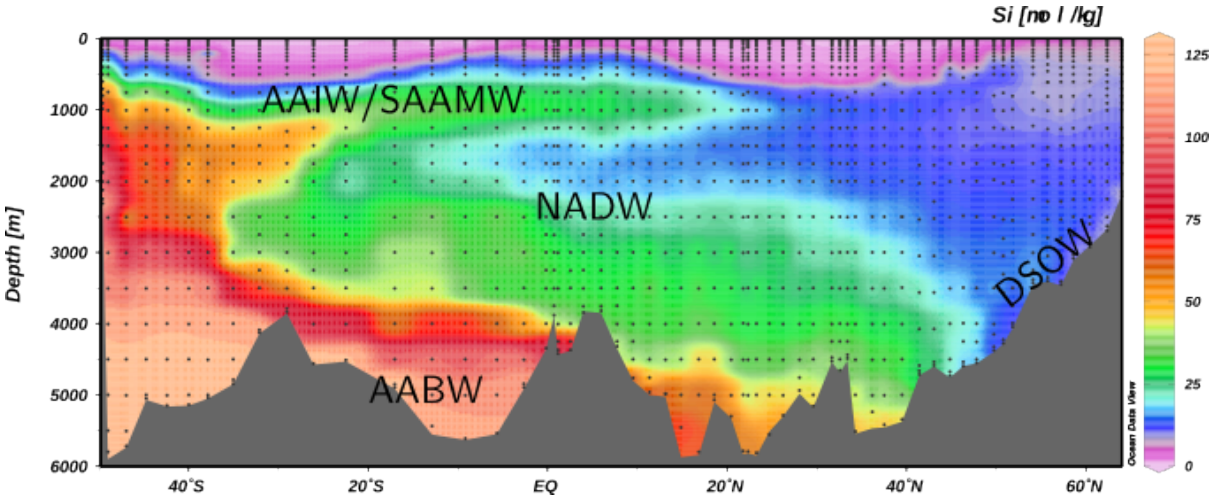

Figure 1.1: The Si_{diss} distribution (concentration in µM), with main water masses indicated.

warming of upper layers and low wind velocity) the deeper part of this becomes separated from the upper part. In general these subsurface waters that are formed by deep winter convection and subduction are named mode waters. In different ocean regions this deeper part is a major conduit for uptake of tracers from the surface, for example the SubAntarctic Mode Water (SAMW) in the South Atlantic Ocean, and the Subpolar Mode Water and the 18 Degree Water in the North Atlantic Ocean [124].

When looking at the oceans over longer annual, decadal or century time scales, i.e. quasi-steady-state distributions, the seasonal deep winter convection is partly responsible for the 3-D distribution of surfaces of uniform density (isopycnal surfaces). These surfaces are not perfectly horizontal but show curvature and some isopycnal surfaces outcrop at the ocean surface. Transport by turbulent mixing along such surfaces of uniform density is several orders of magnitude faster than transport by turbulence across isopycnal surfaces. Therefore the outcrops of isopycnals in the surface ocean serve as conduits for relatively rapid transport of tracers into the typically intermediate (∼100–∼1000 m) depth range of the ocean interior. For example for DIC and major nutrients (N, P, Si) this is known as the 'solubility pump'; it brings carbon (C) and nutrients, respectively, into the intermediate and deep ocean.

In the polar oceans, notably in the Greenland-Iceland-Norwegian Sea (GIN Sea) between Iceland and Spitsbergen, and in the Weddell Sea (Antarctica), winter cooling and seasonal sea ice formation lead to increasing density of surface waters. As a consequence, these waters sink to a depth of 1 to 4 km. This may be seen as the very extreme cases of deep winter convection and also contributes to the 'solubility pump'. In the Labrador Sea and at the Antarctic Polar Front this deep winter convection does not go deeper than about 1000–1200 m resulting in the Labrador Sea Water (LSW) and the AntArctic Intermediate Water (AAIW), respectively. In the GIN Sea the water sinks deeper, and next flows over the sills in Denmark Strait and Iceland-Faroe-Scotland Ridge into the North Atlantic as the major source water of the North Atlantic Deep Water (NADW). In the Weddell Sea the deep winter convection sinks to the bottom, forming the Weddell Sea Bottom Water (WSBW) that flows out as AntArctic Bottom Water (AABW) flowing into the three major ocean basins. Figure 1.1 presents the major water masses in the West Atlantic GEOTRACES transect (plotted over the Si_{diss} concentration, see Section 1.3.1).

The general circulation in the Atlantic Ocean of northward surface water transport, the forming of NADW and the subsequent southward current at 2–3 km depth, is called the Atlantic

Meridional Overturning Circulation (AMOC). It is not only important in transporting DIC and nutrients to the deep ocean, but variability in the AMOC also influences climate. For instance, a slower AMOC may result in a smaller flux of water towards Europe. This means that less heat is transported to Europe, which could induce a colder climate. However, in this thesis the interest in the AMOC strength and shape is based on the transport of trace metals from the surface Atlantic to the deep Atlantic Ocean.

1.2.2 Biological pump

The biological production in the euphotic zone leads to the accumulation of biomass, almost all phytoplankton and zooplankton. Large part of this plankton remineralises rapidly again within the euphotic zone or just below, but some small portion escapes such immediate remineralisation and may settle down into the intermediate and deep ocean waters as biogenic debris (dead phytoplankton, zooplankton and bacteria, faecal pellets of zooplankton). Aggregation of the debris leads to a larger size of the settling particles, that enhances the overall settling velocity [87, 168] in accordance with Stokes' law:

$$w_s = \frac{2r^2(\rho_{\text{part}} - \rho_{\text{fluid}})g}{9\mu} \,, \tag{1.1}$$

with r the radius of the particle, ρ_{part} the density of the particle, ρ_{fluid} the density of the medium, g the gravitational acceleration and μ the viscosity of the medium. Stokes' law is only valid when the particles are homogeneous spheres with smooth surfaces, the particles do not interfere with each other and the flow is laminar. Several of these assumptions are doubtful. For instance, biogenic debris can take forms different from spheres, resulting in settling velocities not following Eqn 1.1 [132]. Hence, if used at all, Stokes' law must be taken as an approximate model for particles in the real ocean.

This export of biogenic particles from the euphotic zone downwards into the deep ocean is known as the 'biological pump' and is the major pathway for transfer of carbon and major nutrients as well as many trace elements from the surface waters into the deep sea [102 pp. 102–14].

1.2.3 Carbon cycle in the ocean

Figure 1.2 presents the cycling of carbon, nutrients and trace elements in the oceans. Major nutrients (N, P, Si) and trace nutrients (Fe, Co, Mn, Ni, Cu, Zn, Cd), and other trace elements (for this thesis notably Al), enter the ocean through rivers, by dissolution of dust deposition input, diffusion from pore waters within sediments, and dissolution from resuspended sediment particles. Hydrothermal vents are a source of some elements (for this thesis notably Mn; also Fe), while other elements (e.g. Al) in hydrothermal systems are removed near the vents by quick settling. Lithogenic particles are supplied by rivers and by dust deposition, and are mostly deposited in sediments. For sake of simplicity this lithogenic pathway is not shown. During phytoplankton growth, solar radiation is the energy source for fixing carbon from CO_2 into organic carbon. In this process O_2 is released. Zooplankton consume phytoplankton (grazing) and use O_2 for respiration, releasing CO_2 as well as Dissolved Organic Carbon (DOC) and debris (dead material) here named 'organic detritus'. Most of the DOC and detritus enters the microbial loop (dotted arrows), while much smaller amounts settle into deeper waters. The microbial loop comprises heterotrophic bacteria, several types of auto-phototrophs (e.g. cyanobacteria), phagotrophic protozoa, mixotrophic eukaryotes and viruses [114], but is of relatively minor interest for this thesis. Within the typically 4 km deep water column more than half of the settling biogenic detritus is remineralised by bacteria and deep-sea animals,

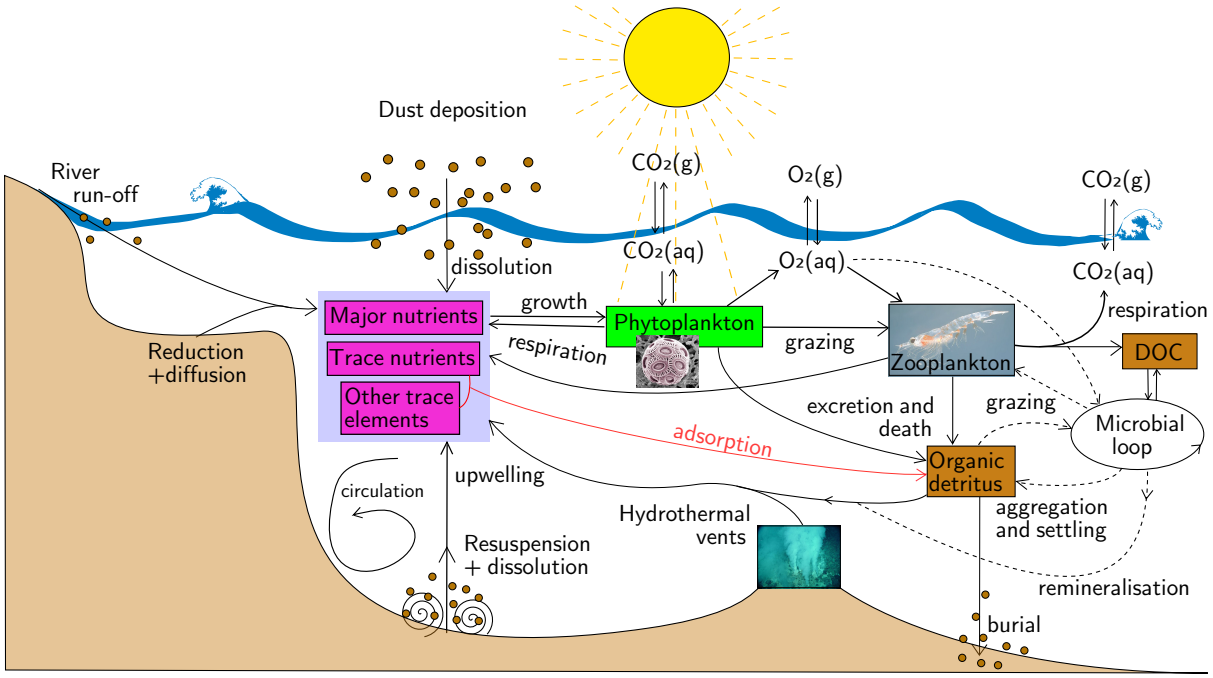

Figure 1.2: Cycling of carbon, major and trace nutrients and other trace elements in the oceans. Major nutrients and trace nutrients, and other trace elements, enter the ocean through the sources as depicted in the figure. See the text for a detailed description of the sources and internal processes. This is a simplified conceptual model of the nutrient and carbon cycle, limited to the seawater, leaving out other parts of the Earth system like the sediment. Many processes, among which nitrogen fixation and denitrification, and lithogenic particles, are not represented in this figure.

the other half reaches the seafloor where another large part is remineralised by the benthic community. Eventually, only a very small portion escapes remineralisation and becomes part of the sediment. Within the sediment this is mostly remineralised by bacteria, and only a very small fraction is buried permanently in the deeper sediment.

The red arrow signifies adsorptive scavenging of most of the bio-essential trace nutrients and also of the other trace elements onto the settling biogenic debris. For trace metal elements with multiple oxidation states in the oceans, notably Mn(II), Mn(IV) and Fe(II), Fe(III), the adsorptive scavenging is often enhanced by oxidation from its dissolved states (Mn(II) and Fe(II)) to solid phase (Mn(III) and Fe(III)). This is a simplified conceptual model of the nutrient and carbon cycle, leaving out other processes and other parts of the ocean-related Earth system, like the sediment.

Carbon fixation takes place typically through photosynthesis. This process takes place in two parts. The first is the *light reaction* during which light energy is converted to chemical energy in the form of Adenosine-5'-TriPhosphate (ATP) and Nicotinamide Adenine Dinucleotide Phosphate ($NADP^+$), hence this only takes place when there is sufficient sunlight available. In this process H_2O is split by light (photolysis) creating O_2 as a by-product [32 pp. 209–19]. The second part of photosynthesis is the *Calvin cycle* during which CO_2 is converted to glucose (sugar), using ATP and $NADP^+$ as the energy source [32 pp. 219–21]. The net reaction of the entire photosynthesis process is given by:

$$106\,CO_2 + 122\,H_2O + 16\,NO_3^- + H_2PO_4^- + 17\,H^+ \rightarrow (CH_2O)_{106}(NH_3)_{16}H_3PO_4 + 138\,O_2 \quad (1.2)$$

where the stoichiometric uptake ratio of the nutrients N and P were found by Redfield [6].

Zooplankton consume phytoplankton (grazing) and respire, releasing CO_2. The net res-

piration reaction is the opposite of Reaction 1.2. Upon excretion and death of phyto- and zooplankton, the resulting detritus (dead material) starts to settle towards the seafloor. Most of the organic detritus enters the microbial loop [16, 102 p. 122, 138, 114]. The microbial loop is presented as an ellipse in the right of Figure 1.2. It is an abstraction of the interaction between unicellular entities, i.e. bacteria and viruses, that are smaller than the typical phyto- or zooplankter. In the end, the remaining small part of the particulate material settles as aggregates and is buried in the sediment.

The red arrow in the middle of Figure 1.2 signifies adsorption of several nutrients and trace metals, among which aluminium and iron, onto detrital material. After adsorption they settle downwards with the particulate material. The combination of adsorption and settling is called *scavenging*. Most scavenged metals also desorb from particles. In that case, the process is referred to as *reversible scavenging*. By (reversible) adsorptive scavenging nutrients can be exported out of the ocean into the sediment. Besides being scavenged, nutrients are also incorporated in phytoplankton during growth, entering the food web. When marine organisms excrement or die, the nutrients are exported, similar to the nutrients adsorbed onto these detrital products. Lithogenic particles (mineral particles that are not of biological origin, i.e. clay, silt and sand) probably also play a significant role in scavenging because of their ballast effect [87]. Hence, they are important for exporting nutrients and trace metals into the sediment, but these particles are not fully presented in this conceptual model (Figure 1.2).

1.3 Nutrients and trace metals

1.3.1 Silicon

Silicon (Si) is a major nutrient that is of great importance in this thesis, because of its interaction with Al. Therefore this section gives the necessary background of Si cycling in the ocean.

Silicon is the second most abundant element in the Earth's crust (after oxygen). The element exists in the ocean as silicic acid (Si_{diss}), biogenic silica (Si_{biog}) and lithogenic Si. Silicic acid is used by diatoms, silicoflagellates, radiolaria and sponges. The silicic acid is converted to biogenic silica, $SiO_2{\cdot}nH_2O$, to form the skeletons of the organisms. For example, sponges have an internal skeleton made of either Si_{biog} or calcium carbonate, while diatoms have external silicic structures called *frustules*.[1] Diatoms form a functional class of phytoplankton which accounts for about 35–40 % of the primary production in the oceans [49, 135]. Diatoms are heavy (two times the density of seawater) because of the frustules. This makes them effective in exporting silica, organic carbon and other diatom-associated elements, into the deep ocean. This results in less recycling compared to non-diatom phytoplankton, and hence a relative export production of about 50 % of total export production. This is also referred to as the *ballast effect*. For these reasons diatoms are central to the discussion of silicon and climate change.

As a further illustration of the processes shown in Figure 1.2, consider the example of Si_{diss} as a nutrient for diatoms. A simplified representation of Si cycling is shown in the right part of Figure 1.3. Clearly, diatoms are limited in growth by the available Si_{diss} and the amount of sunlight. If either of these factors is limiting, less diatom growth occurs (bottom-up limitation). If the number of grazers of diatoms are increased, diatom growth is limited as well (top-down limitation, only represented in Figure **??**) [102 p. 138f]. Section 3.3.1 presents a mathematical model for the rate of photosynthesis.

Upon settling of Si_{biog} (bottom-right part of Figure 1.3), part of it is buried in the sediment. Based on the large amount of Si_{biog} in the upper sediment and the low $[Si_{diss}]$ in the bottom

[1] In this figure and the following, the term *biogenic silica* (Si_{biog}) is reserved for dead, sinking frustules, while *diatom silicon* (Si_{diat}), or frustules, is used for biogenic silica of living diatoms.

water, Si_{biog} should not be preserved but dissolve and subsequently diffuse out of the sediment into the water column. However, several factors prevent the dissolution and help to preserve Si_{biog} in the sediment. Dissolution depends on the specific surface area (smaller means better preserved), the organic coating and the temperature. In the sediments of the deep ocean the low temperature prevents dissolution. Hence, Si_{biog} can accumulate without diffusing out of the sediment. Furthermore, when aluminium is incorporated in, or adsorbed on to, diatoms, the solubility of Si_{biog} is decreased. This incorporation can be either *primary uptake* (biological incorporation during growth; Gehlen et al. [e.g. 72]) or, probably more significantly, *secondary uptake* (early diagenesis; Koning et al. [109]) (Section 1.3.2).

1.3.2 Aluminium

One major reason of the importance of Al is the use of Al as a tracer of aeolian dust supply into the surface ocean. Dust deposition is an important source of trace nutrients such as Fe and Mn. Aluminium is abundant in dust (about 8 $\%_m$), does not complexify and is not biologically active to such an extent as Fe, which makes it more practical than iron as a proxy for dust [e.g. 65].

Dissolution of Al from dust and other processes determining the distribution of dissolved Al are presented in Figure 1.3. It is currently assumed that the major source of Al to the open ocean is dust deposition [e.g. 78, 88, 108, 170]. A fraction of the Al in dust (1–15 %) dissolves within the upper mixed layer [23, 25, 87, 97, 99, 133, 149], while below the mixed layer the dissolution of Al from dust is deemed negligible (Chapter **??**). Most Al in dust (i.e. 85–99 %) remains in the particulate phase and sinks to the bottom of the ocean, where it is assumed to be buried in the sediment. This has been suggested by many studies on Al in the ocean [e.g. 23, 97, 99], but no explicit study has been published on the fate of lithogenic dust particles in the water column below the mixed layer.

The second significant source of Al is sediment resuspension and subsequent dissolution, presented at the bottom (centre) of Figure 1.3. Sedimented particles may contain Al within, or on, the particle. When these particles are resuspended, dissolution may occur by desorption and/or dissolution of the carrier particle, releasing Al [39, 154, 170]. Indeed, a high concentration of Al_{diss} has been measured near the sediment in the West Atlantic Ocean at 45–50°N (Figure **??**). In Chapter **??** results of simulations are presented that back this hypothesis.

Other sources do not appear to play a significant role in adding Al to the ocean. Even though rivers carry a large amount of Al, most of it is removed in estuaries and continental shelf sediments and never enters the open ocean [22, 23, 129, 151]. Finally, hydrothermal vents are not a source of Al to the deep waters of the oceans either [21, 35, 51, 141].

The primary removal mechanism of Al_{diss} from the surface ocean is the adsorptive scavenging and settling with Si_{biog} as the major carrier (light-yellow ellipse in Figure 1.3), hence this removal is large in areas with high diatom production [15, 23, 27, 30, 98]. Besides being scavenged by surface adsorption, the Al_{diss} becomes incorporated as an apparent trace substitute for Si during growth of living diatoms. Following diatom death, the incorporated Al is exported with the Si_{biog} debris [11, 27, 40, 58, 72, 123].

Incorporated Al is likely to inhibit the dissolution of Si_{biog} [4, 38, 40, 68]. This means that at a high Al_{diat}/Si_{diat} ratio in living diatoms and thus the same ratio Al_{biog}/Si_{biog} in biogenic debris, less Si_{biog} will be remineralised. Furthermore, more silica will be buried and hence lost from the system. Consequently, less Si_{diss} will be returned to the surface through upwelling, resulting in decreased diatom production. This highlights a possibly important effect that Al has on Si, and hence, potentially, the Earth system.

Converse to Al having an impact on the dissolution of Si_{biog}, Si can have an effect on the

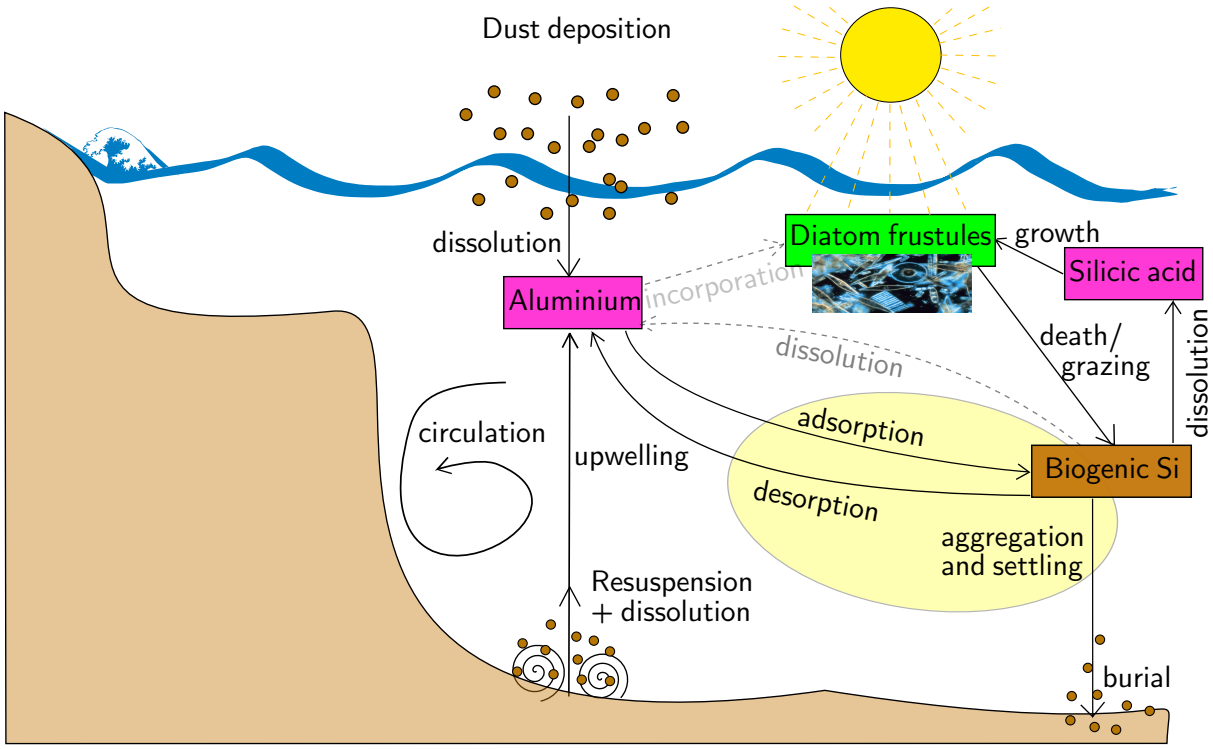

Figure 1.3: Aluminium cycling in the ocean. Just like the nutrients in Figure 1.2, dissolved Al enters the ocean through dust deposition and sediment resuspension, while rivers, hydrothermal vents and reducing sediments are negligible. Al is mostly removed by *reversible scavenging* (presented in the yellow ellipse). The dashed arrow from aluminium to diatom frustules signifies incorporation of Al into diatom frustules. The significance of this removal process is not well known yet, but it appears that it is small (Chapter **??**). Silicic acid (Si_{diss}) is presented as well, since it is an essential part of understanding Al cycling. However, not all sources of Si_{diss} are presented in this figure; for this see Figure 1.2

release of Al from resuspended sediments. This release may be caused by desorption of adsorbed Al (Al_{ads}) from Si_{biog} and dissolution of biologically incorporated Al (Al_{biog}). Also lithogenic particles may be dissolved, but the most obvious candidate for dissolution is Al_{ads} since that is on the outside of Si_{biog}, instead of built in. This hypothesis is worked out and its simulated effects are presented in Chapter **??**.

1.3.3 Manganese

While in the open ocean manganese (Mn) exists in small concentrations, it is the twelfth most plentiful element in the Earth's crust [50]. In the ocean Mn occurs in many forms, among which in dissolved form and incorporated in organisms and particles. From a chemical oceanographic perspective two phases are the most important. One is dissolved Mn, Mn(II), available for uptake by autotrophs. The other is oxidised Mn, MnO_x, not bioavailable and subject to scavenging and aggregation [e.g. 45]. After phytoplankton death, incorporated Mn sinks together with the dead material downwards, but most of the material remineralises before reaching the sea floor. All significant processes of the manganese tracers are presented in Figure 1.4.

Manganese is an essential nutrient for all life. One important function of Mn for phytoplankton is its role in photosynthesis, namely photolysis in photosystem II [18, 36, 32 pp. 209–19]. Photosystem II is the first protein complex in the light reaction (see p. 12) where photons are captured and converted to chemical energy, namely stored in $NADP^+$ (Section 1.2.3).

Reactive oxygen species like superoxide (O_2^-) tend to quickly react with photosystem II,

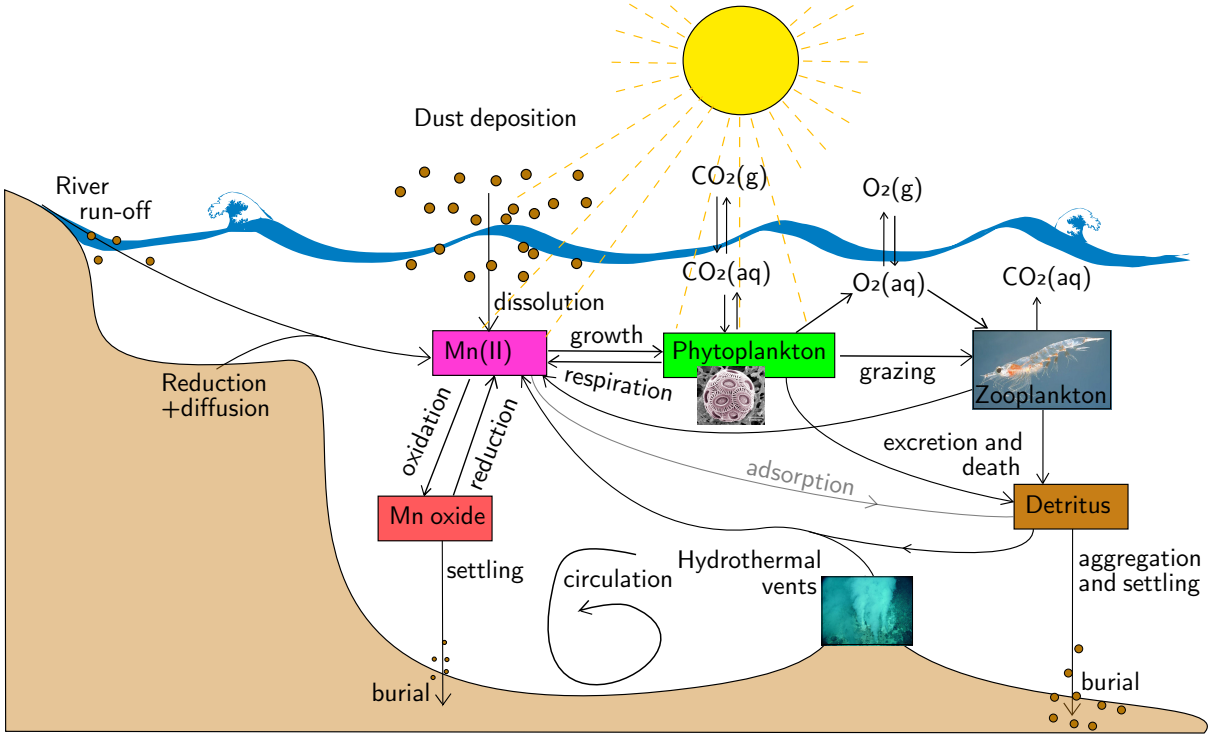

Figure 1.4: Manganese cycling in the ocean. Like all nutrients in Figure 1.2, dissolved Mn enters the ocean through dust deposition, river run-off, sediment reduction and hydrothermal vents. The reactions between Mn(II) (magenta box) and MnO_x (red box below) occur everywhere in the ocean, but reduction is significantly faster in the euphotic zone than in the aphotic zone. In this conceptual model of Mn, sediment redissolution is neglected, as is the microbial loop.

decreasing its efficiency. Superoxide dismutase (SOD) enzymes catalyse the conversion of superoxide into oxygen and hydrogen peroxide, hence protecting photosystem II. Diatoms need Mn-SOD (or, less dominantly, Fe-SOD), which is the second important function of Mn [82, 104]. Simply put, Mn- and Fe-SOD destroy reactive oxygen species. Under conditions of deficient Fe, which is used in photosynthesis as well, less Fe-SOD is created, hence less reactive oxygen species are removed. This results in a decreased efficiency of photosystem II. Manganese can compensate the destructive influence of reactive oxygen species by means of Mn-SOD. Mn can also substitute Fe in some other biologically important reactions [82]. For these reasons, Mn availability is especially important under low (bioavailable) Fe conditions [135 p. 16, and references therein]. This is also referred to as co-limitation of Fe and Mn. In other words, when too little Fe is present, Mn can compensate the effects of this deficit for a large part [162]. Co-limitation may occur in the Southern Ocean where both dissolved Fe and Mn concentrations can be low [162].

An important mechanism of storing Mn in particles other than biological incorporation is *oxidation* of dissolved Mn(II) on colloids to insoluble Mn(IV) (and possibly other oxidation states, red box in Figure 1.4) and the subsequent aggregation by particulate matter (implicitly presented as *settling* below the red box). Oxidation occurs everywhere in the ocean where oxygen is available. This process can be strongly accelerated by Mn(II)-oxidising microorganisms, primarily bacteria and fungi [29, 45, 91].

The reverse process is *reduction*, reducing Mn oxides to bioavailable dissolved Mn(II), i.e. Mn^{2+}. This process is significantly faster under the influence of sunlight, then referred to as *photoreduction*. This is the most important reason why the Mn(II) concentration is relatively

high in the photic zone. The relative speed of photoreduction compared to oxidation is important for Mn(II) availability. A higher oxidation rate means more scavenging, hence more Mn export. The full redox equilibrium reaction, in its most simple form, is given by:

$$MnO_2 + 2\ H^+ \quad \rightleftharpoons \quad Mn^{2+} + \frac{1}{2}\ O_2 + H_2O\ ,$$

where reduction is to the right and oxidation to the left.

Just like Al, Mn enters the open ocean through dust deposition and possibly resuspended sediments. Dust deposition is the second reason for high [Mn(II)] in the surface ocean. Especially in the centre/north Atlantic Ocean surface [Mn(II)] is high because of high dust input from the Sahara, in combination with MnO_x reduction [24, 47, 44, 97, 108]. Similarly, [Mn(II)] is high in the northern Indian Ocean [163]. Rivers are another source of Mn to the ocean [8, 95]. Anoxic or suboxic shelves diffuse Mn(II) because sediment microorganisms reduce MnO_x if there is no more oxygen (or nitrate) left [12, 20, 110]. Finally, plenty of evidence is found of manganese fluxing out of hydrothermal vents [9, 19, 21, 70, 140, 141].

While Al is reversibly scavenged by Si_{biog}, dissolved Mn first oxidises to MnO_x, after which it aggregates and is scavenged by particles. Probably lithogenic particles play the most significant role, since sediment traps show a strong correlation between lithogenic particles and Mn [89]. The complete process may be more complicated than described above, e.g. because possibly Mn forms ligands that stay in solution better than Mn(II) [144, 161]. These processes are not presented in the simplified conceptual model in Figure 1.4.

Finally, Mn oxides are an important scavenger of other trace metals like Fe, cobalt and zinc (A. Tagliabue, personal communication, March 2013). Hence, Mn availability does not only directly impact biology but may also play a role in removing nutrients from the surface ocean.

1.4 Research questions

The focus of this thesis is the main processes that distribute aluminium and manganese throughout the ocean, and their interaction with the carbon and silicon cycles of the ocean. For both tracers state-of-the-art models are developed and simulations discussed. The Ocean Biogeochemical General Circulation Model (OBGCM) used for studying the ocean distribution of Al and Mn is NEMO-Pisces [96]. This model and the simulated distribution of several tracers (Si, Fe and the dynamical variables) are described in Chapter 3.

As this thesis is part of the Geotraces programme, and collaborated with the West Atlantic subprogramme, its aim is to interpret chiefly these measurements. Measurements at unprecedently high resolution were taken in the West Atlantic Ocean, near the western boundary currents, because of the highly important role of the western boundary currents. To interpret the observations and to obtain an integrated understanding, numerical ocean models are used in this thesis, that provide information on the time evolution of the ocean. Conversely, the measurements provide a constraint on ocean models and can therefore be used to assess the model's reliability and/or improve the representation of the physical and biogeochemical processes in the model.

1.4.1 Aluminium

The primary focus is Al, as this element can be used as a tracer for dust, a main carrier through which many trace nutrients like Fe and Mn enter the ocean. Aluminium is important on its own since it affects the Si cycle, but this effect is not studied thoroughly in this thesis. There are several questions concerning mainly the processes of Al_{diss} and its distribution.

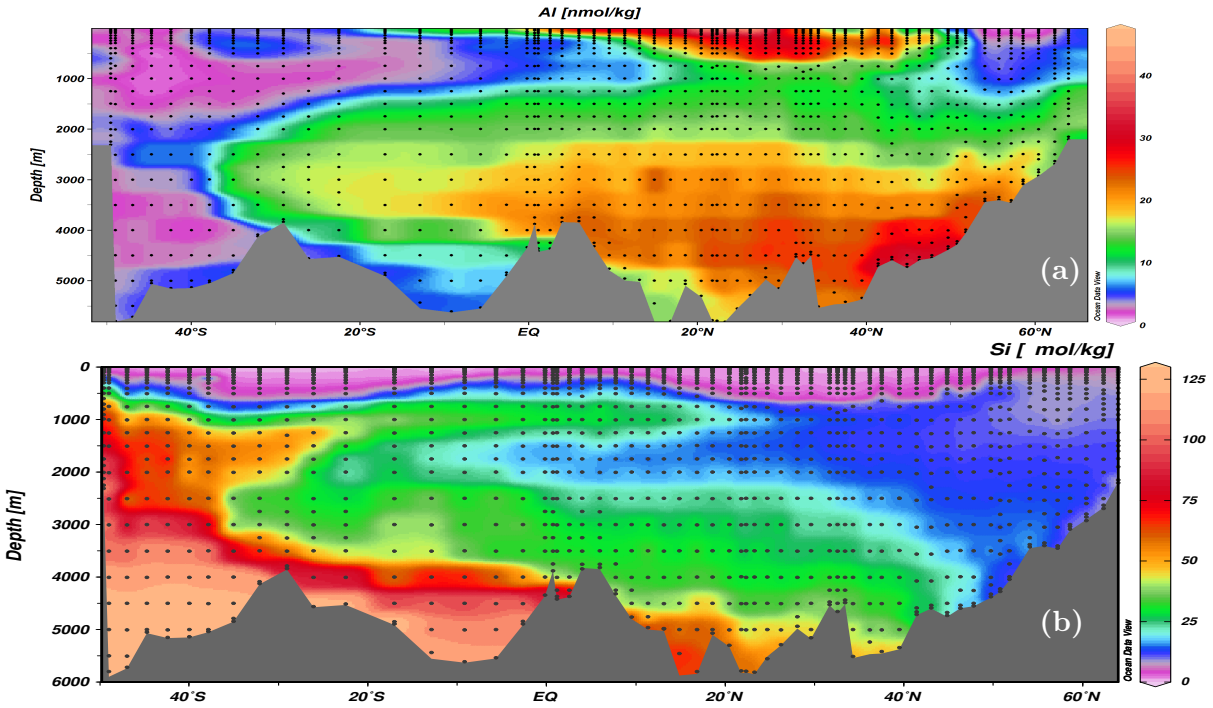

Figure 1.5: Observations of (a) $[Al_{diss}]$ (nM) and (b) $[Si_{diss}]$ (µM) at the West Atlantic GEOTRACES transect [170]. Dots are locations of measurements.

Firstly, how is the structure of the Al_{diss} distribution (Figure 1.5(a)) in the West Atlantic Ocean explained, and why does $[Al_{diss}]$ show a 'mirror image' of $[Si_{diss}]$ (Figure 1.5(b))? In the distributions of both tracers the main water masses can be recognised; chiefly NADW, hence the overturning plays an important role. See Section 1.2.1 and its Figure 1.1 for a description of all water masses. Clearly, a main source of Al is dust deposition and the internal cycling occurs by means of reversible scavenging, mainly by Si_{biog}, and advection and mixing. In Chapter **??** these processes are included in an ocean model and its simulations reasonably reproduce the observations in the upper few km of the ocean. However, at 45–50°N near the sediment in the West Atlantic Ocean, $[Al_{diss}]$ is strongly elevated compared to the ambient seawater. This cannot be easily explained by the just mentioned processes alone. The explaining hypothesis is that sediment is resuspended in this region, and that after resuspension Al dissolves in the seawater. This hypothesis is tested in Section **??**.

Secondly, what is the sensitivity of different sources (or solubilities of the source particles) and model parameters of Al to the ocean Al_{diss} distribution? Specifically, the effects of changes in the solubility of Al in dust particles, in the internal scavenging parameters and in the redissolution of sedimented Al are tested in Chapters **??**, **??** and **??**.

Thirdly, does biological incorporation have an important effect on the Al_{diss} distribution and how big are both the biological incorporation and its effect on $[Al_{diss}]$? If Al incorporated into diatom frustules affects the solubility of the frustules, what kind of effects can we expect? These questions are explored in Chapters **??** and **??**.

Finally, in the same chapters the effects on the Al_{diss} and Si_{diss} distributions of using different dynamics are explored.

For Al, model simulation studies have started with Gehlen et al. [74] and more recently followed up with Han et al. [115], both described in Section **??**. In this thesis comparable, though extended, equations have been implemented in the more evolved model NEMO-Pisces.

The embedded model of aluminium will be described in Chapters **??** and **??**.

1.4.2 Manganese

The secondary focus is Mn, not because it is less important than Al, but because modelling Mn in the world ocean has not been done before and hence the results are very preliminary. In Chapter **??** a model of Mn in PISCES is introduced and compared with observational data. The observations of the West Atlantic GEOTRACES transect is presented in Figure 1.6.

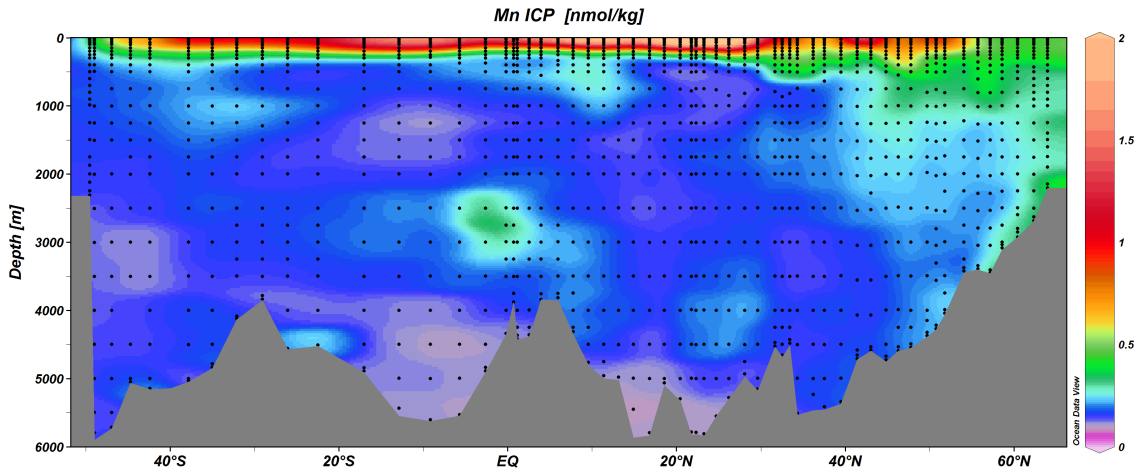

Figure 1.6: Observations of $[Mn_{diss}]$ (nM) at the West Atlantic Ocean GEOTRACES transect (courtecy of Rob Middag). Dots are the locations of the measurements.

It is the first time that an ocean model for manganese is written and assessed. Several questions concerning the distribution of Mn(II) in the ocean are investigated in Chapter **??**, namely:

Firstly, why is there no signal of the Atlantic Meridional Overturning Circulation in the structure of [Mn(II)], as opposed to $[Al_{diss}]$?

Secondly, what makes the distribution of Mn(II) so relatively homogeneous in the inner ocean, except for a few localised features where [Mn(II)] is notably elevated? The elevated local features are located around 2.5 km depth at the Zero Meridian at 50° S (not presented) as well as the West Atlantic Ocean at, and just south of, the equator (Figure 1.6), and at the Denmark Strait overflow. These elevations in [Mn(II)] are hypothesised to be due to hydrothermal activity near those region. Dust deposition and photoreduction explain the high surface [Mn(II)], especially under, and upstream of, dust deposition sites. This leaves the question of the non-zero homogeneous [Mn(II)] 'background' distribution in the rest of the ocean. Even though no unambiguous answer is given in this thesis, Chapter **??** discusses and (partly) tests several hypotheses, among which an *aggregation threshold* of $[MnO_x]$, below which MnO_x is not removed from the model domain, and the possibility of an *oxidation threshold*, i.e. a minimum [Mn(II)] before oxidation takes place. The latter may be interpreted as the existence of Mn ligands, since these keep Mn(II) in dissolution. Other ideas are discussed as well.

Chapter 2

Philosophy of modelling

Science is the ordering and creation of concepts, models, hypotheses, theories and explanations. It is also the enterprise to measure, and to predict and explain phenomena in the universe. All scientific statements, i.e. hypotheses, explanations, predictions and so on, must be testable by means of measurements. Any experiment set up to test a certain hypothesis must be reproducible. There are different ways to learn about reality, but they always involve a combination of the empiricist and rationalist approaches. Modelling changes the focus from empiricism to rationalism, i.e. the focus is more on theorising and less on measuring. At the same time, a new type of empiricism is gaining ground. Models are used as empirically accessible systems on their own, in a similar way as the systems in which we are ultimately interested: the real world or a subsystem thereof.

For instance, an Earth system model[1] is a theoretical construct with the goal to simulate the real Earth. This is not necessarily based purely on fundamental theories, but it is nonetheless typically rationalistic in nature. Model simulations are like laboratory experiments, since 'measurements' are performed by reading variables that the simulation produces. Hence, the model is an experimental set-up that can be used to test hypotheses. This highlights the empiristic nature of model simulation. However, clearly the 'measurements' in model simulations are generally not to be thought of as measurements in the actual Earth system.

This chapter expands on the subject of modelling in science, especially oceanography. By means of a philosophical introduction to science and modelling, several fundamentals of modelling will be highlighted. Furthermore, it will be illustrated how simulations can be validated with respect to observations, but also how they can be misinterpreted. This leads us to a certain level of insight into how far the previously mentioned 'measurement' in model simulation can be regarded as realistic.

2.1 Definition of a model

2.1.1 Models in general

In the literature several consistent and inconsistent definitions of (mathematical) *model* can be found, as well as of *theory*. One definition of model that appears to be consistent throughout several works is the following. A model is a realisation, representation or structure of a theory in which all valid sentences of a theory are satisfied [3 p. 11, 5, 101, 147].[2] This definition is relatively strict in that it only applies to models of theories. Generalised to other domains of

[1] In this chapter a *model* is taken to be a quantitative or *mathematical model*, except when differently qualified (e.g. *conceptual model*).

[2] This is complementary to that a theory is a collection of models, in the semantic view of theories [5, 31, 148].

theories, a model may be a (partial) representation or substructure of a part or any number of theories.

This definition of *model* is still too strict for the purpose of this thesis, even with a loose definition of *theory*. It is strict in the sense that it does not allow for finite *predictive uncertainties* and observational *precision* uncertainties (to be defined in Section 2.5). Hence, here a broader definition, that allows for uncertainties and can be applied directly to observations, is chosen. Henceforth, a *model* is a structure for which at least some sentences of one or more theories, hypotheses or observations are satisfied.

More intuitively, a model is a virtual physical system that follows imposed mathematical equations, derived from *general theory* (in case of a model of a theory) and/or *parameterisations*. Parameterisations can be based on idealisations of theories and concepts, or on metaphores, analogies and other principles, or they are based on observations [155 § 2.3.1]. Often a combination of general theory and parameterisations is necessary, where parameterisations substitute representations of physical processes that cannot be explicitly integrated because of the lack of knowledge of the modelled system and/or computational limitations [155, 152]. In the case of a pure model of a 'complete' and correct theory, i.e. if the objects and structures of these equations refer to the real physical system, the observations will be simulated (in a statistical-mechanical sense, i.e. as long as chaotic behaviour is averaged out). The reverse need not be true. For instance, in the case of a model that includes parameterisations, tuning of parameters is often done to simulate the observations (again in a statistical-mechanical sense); this makes it difficult to independently validate the model. In other words, a correct simulation of observations does not imply the correctness of the model.

For instance, a numerical atmospheric model may generate a temperature field every timestep. Assuming that the model is initialised with the (real or reanalysis) conditions at some moment in the past, the temperature field in the model should be similar to the observed temperature, as long as both the real and modelled temperature is averaged over a sufficiently large temporal and spatial scale. Such averaging is necessary, since models are typically chaotic akin to the real system. Small changes in the initial conditions, or model parameters, can after several days result in large differences in model results, which is very important for weather prediction. In this thesis models are forced by one-year climatologies and run until (quasi-)steady state. It is shown that for most model simulations in this research indeed a (yearly average) steady state is reached. Hence, chaotic behaviour is not relevant for the purpose of this thesis, and not further discussed in this chapter.

2.1.2 Models of theories

Consider a model of a theory,[3] not considering parameterisations at this point. The model might not predict true values T of some variable that we are interested in. This may be the case because there are problems with the implementation of the model, or it is non-linear which calls for an average of an ensemble of simulations, or it is not a good model of the theory, or the theory is not a good description of reality.

A perfect model of a theory is identical to the *formalism* of a theory. When an *interpretation* (including the reference of the model objects to reality) is added to the formalism, the model becomes a theory. For anti-realists this means that a perfect model is identical to a theory. Only for a realist there is a significant difference between a theory and a perfect model of a theory.[4]

[3] Here I use *theory* in a loose sense; it is any mathematical description of the world.

[4] Realism is the view that the world described by science is the real world, including objects that may be part of a theory but are not observable. Anti-realism is the opposite of this and includes many types, including

As an example of such a theory and model, consider Newton's law of universal gravitation. This law states that two masses attract each other with a force that is directly proportional to the product of their masses and inversely proportional to the square of the distance between them. In the form of an equation this is:

$$\mathbf{F} = G\frac{m_1 m_2}{r^2}\mathbf{e} \tag{2.1}$$

where $\mathbf{F}$ is the force, G the universal gravitation constant, m_i the masses, r the distance between the bodies and $\mathbf{e}$ the unit vector directed from the one mass to the other. This equation alone is the formalism of the theory, while the explanation of the symbols is the interpretation. Only the combination of formalism and interpretation is a theory of gravitation.[5] A perfect model of the theory is simply the formalism, i.e. Eqn 2.1. In this specific case, the formalism of the theory is identical to the model, hence the model is a perfect model of the theory.

Of course models are in practice amended with an interpretation as well, but that is not how the term *model* is used here. Adversely, the interpretation is more important for the *conceptual model*, where the formalism is significantly simplified such that it e.g. only contains signs or directions and not actual numbers. The complementary conceptual model to the gravitation model as given by Eqn 2.1 is a picture or a miniature model of the Sun, Earth, Moon etc. From the picture one can determine the directions of the forces, while one needs Eqn 2.1 for the numbers. In other words, a *model* is quantitative, while a *conceptual model* is qualitative.

As another example of a *conceptual model*, consider Figure 1.3, whose caption explains what all terms mean (interpretation). Furthermore, (the dissolution of) dust is clearly a *source* of $\mathrm{Al_{diss}}$, increasing $[\mathrm{Al_{diss}}]$, while adsorptive scavenging is a *sink*, decreasing $[\mathrm{Al_{diss}}]$. However, the quantitative effects of all processes is not displayed in the figure and they cannot be derived from it. Most of the formalism is left out, hence it is only a *conceptual model*.

Another example of a *mathematical model* is the aluminium ocean model described in Section **??**. This is something different from the just mentioned conceptual model. With the mathematical model one can actually make quantitative predictions, while the conceptual model is mostly interpretation and contains little formalism. Contrary to the gravitation model (Eqn 2.1), the model of aluminium is not identical to the formalism of a theory, since the formalism of the underlying theory is much too complex to be implemented. The underlying theory describes a complex interaction between many different types of aluminium and silicon particles. As an example, the effect of organic matter around biogenic silica has an impact on the electric potential between $\mathrm{Al_{diss}}$ and $\mathrm{Si_{biog}}$ particles. This influences the tendency for $\mathrm{Al_{diss}}$ to adsorb onto $\mathrm{Si_{biog}}$. In the used model these effects are ignored (if not important) or parameterised (if important) into a simple equation. In this model, described in Section **??**, two parameters are introduced, a partition coefficient k_d and a first order scavenging rate constant κ. These parameters, and the parameterisation (Eqns **??** and **??**), introduce a parameterisation error, but the idea is that after tuning the model is good enough to reasonably predict the observations. This is illustrated by Figure 2.5(b). While the predictive uncertainty is large, there is a significant overlap with the observational accuracy domain. Furthermore, the model is implemented on a finite-resolution grid which introduces a numerical error. There may be

e.g. *phenomenalism* which is the view that physical objects do not exist in themselves, but only as perceptual phenomena or sensory stimuli; *instrumentalism* which is the view that theories are only useful instruments to understand the world; and *structural realism* which is the view that the structures of the theory are real but not the objects itself.

[5] For simplicity Eqn 2.1 is called the formalism of a theory, but the complete formalism of the theory of gravitation contains some extra equations like $\mathbf{F} = \dot{\mathbf{p}}$ where the momentum $\mathbf{p} = m\dot{\mathbf{x}}$; for the calculation of velocities and locations of masses, these equations, together with the formalism, the boundary conditions and typically for this case the initial conditions, are needed.

problems in the underlying biogeochemical model (PISCES) and the dynamical model (OPA) as well (see Chapter 3). These errors all affect the accuracy of the predictive capability of the aluminium model, i.e. they increase the predictive error. Since this parameterisation only simulates the underlying processes (theory, reality, whatever you wish to call it) by approximation, this model is not identical to the formalism of the theory. Hence, it is an approximate model of the theory, assuming the underlying ideas, like electric potential being a cause of adsorption, are somehow used in constructing the model.

2.2 The need for models

Many systems are outside of our reach of experimental control or are unintelligible if described accurately. For these reasons, scientific modelling is an important tool. Models are often used when theories are too complex to handle. Therefore, models are not a complete representation of such a theory (even though they may utilise several theories at once). It is also possible that there is no theory available, or only an incomplete one. In that case, models may actually complement theories and describe phenomena that lack a good theoretical description [147].

With certain systems, it is very difficult or expensive to perform laboratory experiments. These systems include the very small, like the quark-gluon plasma, and the very large, like galaxies. The Earth is a relatively large system, but experiments can be performed on this system. These include adding carbon dioxide to the atmosphere and painting rooftops white in an attempt to cancel some of the consequences of the first. Of course the first example is not an intended experiment since the addition of CO_2 is a side effect of extracting energy from fossil fuels (Section 1.1). The second example is intentional, but neither of the examples are good scientific experiments. Since there is only one Earth to test our hypotheses on, it is not possible to perform multiple climate experiments under controlled conditions.

For these reasons in many physical sciences modelling is important. For many systems, models are so complex that it is not possible to derive analytical solutions. For the Navier-Stokes equations, e.g., it is not known whether a general analytical solution even exists given any initial velocity field.[6] This is a reason why numerical modelling has become relevant. With such models, hypotheses can be tested in a statistically meaningful way. From the results of numerical models conclusions can be drawn along the lines of *"This simulation based on this hypothesis is consistent with the observations, hence it confirms the hypothesis."* or *"Based on this theory this phenomenon cannot be modelled, so the theory must be wrong."* Even though the hypothesis or theory may seem to be verified or falsified, this may very well be for the wrong reason. In modelling, intuition misleads the modeller into thinking that certain model objects are very similar or functionally the same as objects in a theory or the real world. They are not. They are only abstractions that do not trivially refer to objects in reality. The only thing that a model might 'do' is being 'isomorphic' or similar to some part of a theory or the observations.[7] Or there may be no theory available at all, in which case the model in question is a 'toy model,' a germ from which a theory may or may not grow – most often it does not.[8] This theory may or may not be 'true' – most often it is not. This sounds pessimistic, but this is actually good

[6] Solving this is one of the Clay Millennium Prize Problems.

[7] Models are only structures, to which we add interpretation to make sense of them. There is the possibility that a model is structurally correct but philosophically wrong. It may give the correct answers for this reason but may be still judged as being right for the wrong reason, because the interpretation is wrong.

[8] Such a model may be a fit to a guessed function. Another example is given by one of the solutions to the manganese model issues described in Chapter **??**, where oxidised Mn only settles if the dissolved Mn concentration is above a certain threshold. Even though a scientific hypothesis has been formulated for this model at a later stage, initially that model was not based on any theory or hypothesis. Even with further explanation, such a model is often not very mechanistic and will therefore sometimes be named a *toy model*.

science. The job of the scientist is to try to falsify hypotheses, sometimes even whole theories, and certainly and always models. Models are often wrong and misleading (e.g. because of wrong parameterisation or other incorrect assumptions). For this reason, they need to be critically examined to find out whether they actually fulfil their purpose. They also need to be checked for correctness: *Do the objects and processes in the model refer to reality in a reasonable way?* Field and laboratory studies must be used for this. Models are not only validated in this way, but also model development must be done in close collaboration with such studies.

Even though models may be wrong in a strict sense, they can be very useful. Models can give insight and, if formulated and interpreted very carefully, may help further science.

2.3 Reproducibility and development

I have argued for the usefulness of models. Of course they must be written and implemented correctly, and the simulations must be performed and interpreted carefully. However, there are other issues to consider as well as a modeller. As noted in Section **??**, experiments must be reproducible since that is the only way to verify or falsifiable a result, a central principle in the scientific method. For this a full description of an experiment must be given, such that modellers can not only reproduce the results but also do derivative work that he or she should be able to share with the community. In the case of models this amounts to the publication of the source code as free software, such that it can be used, modified and redistributed without restrictions.

There are other important aspects for reproducibility and effective development of models. These include that model code should be clearly written, portable, modular, object oriented, adhering to standards (e.g. the Fortran 95 standard) and accompanied with documentation, and there should be version control. Petersen [155 p. 30–2] gives a short overview on these issues. Nowadays many of these elements are incorporated in model development, but it is still too common that the code is not available as free software. Therefore I will give in this section the definition of free software and set out the central arguments for models to not only be released, as has often been argued by for instance Galison [52], Ince et al. [150], but released as free software.

For software to be free, its users must have these four essential freedoms [156]:

- The freedom to run the program, for any purpose (freedom 0).
- The freedom to study how the program works, and change it so it does your computing as you wish (freedom 1). Access to the source code is a precondition for this.
- The freedom to redistribute copies so you can help your neighbour (freedom 2).
- The freedom to distribute copies of your modified versions to others (freedom 3). By doing this you can give the whole community a chance to benefit from your changes. Access to the source code is a precondition for this.

To enforce these four freedoms to a program, the program must be released either under a free licence or in the public domain (though the latter is not possible in many jurisdictions). A widely used example of a licence giving the user the four freedoms is the GNU General Public License (GPL). There are two optional requirements that can give protection to the work and author without the need to impede on the above freedoms. The first is *copyleft*, imposed by the GNU GPL, which amounts to giving users of derivative software the same four freedoms by releasing all derivative work under the same or compatible licence. The second is *attribution*, giving credit to the author.

The scientific modelling process is the translation from theory or concepts to model code. Many steps are involved in this process, starting with the translation from the theoretical concepts, often represented in a conceptual model, to a mathematical model. Often the equations are approximated in this process. After this step, further simplification (like parameterisation) and discretisation is needed before the model is implemented in computer code [155 p. 30]. The mathematical model is always presented in the scientific literature in more or less detail. However, most literature in ocean and climate modelling does not publish the computer code, and this is a problem.

Assuming that the description of the mathematical model is detailed enough for a good understanding of the model, a fellow scientist can reimplement the model and he should be able to reproduce the results of the simulations presented in the literature. However, this is often not done for at least two reasons. Firstly, it is very time consuming to reimplement the model, while reusing the code would be much more time efficient. Secondly, even if the time is invested in reimplementing the model, it is often not possible to reproduce the results. If you do not have the original code, it may be impossible to determine where the problem lies. This may be, for instance, because of several types of ambiguity in the model description, or configuration details in the software environment [150].

Since there are many steps involved where things can go wrong from the theoretical concepts to running the model, one must be able to verify every step. The most essential part of this, which is often ironically left out of publications, is the source code of the model. Some climate scientists argue that "anything less than the release of source programs is intolerable for results that depend on computation" [150]. Furthermore, using, studying and changing the model must not be restricted in either technical or legal way, hence freedoms 0 and 1 are central to this argument. Auxiliary programs and scripts used for compiling the model and doing complicated analyses are desirable to be published as well, alongside the model code, since this is part of the chain of conceptualising real-world processes to the point of analysing the simulation output.

The arguments in this section go further and include freedoms 2 and 3 who ascertain that the model can be developed by the community. This also implies that many more people can analyse the code and model simulations. Software freedom may be seen as a moral obligation, but there are also direct practical advantages, such as the higher probability that bugs are found in the implementation. In this sense climate scientists can learn a lot from the free software community, where software freedom is often a requirement in the social contract or guidelines of the community.[9] A similar requirement should also be present within the modelling community. To stimulate this, science funding agencies and journals may add this as a condition. Also the use of copyleft is a method to enforce software freedom.

The model used in this work (NEMO-Pisces, see Chapter 3) is an example of free software that gave rise to this work and other derivative models [e.g. 166], which in turn are also released as free software. Also the source code of the aluminium and manganese model in this thesis has been published, and, because of copyleft, under a free licence equivalent to that of NEMO. However, not all code based on NEMO and other free software are released. Studies have been published using extensions of the model that are only described with the help of prose and (often incomplete) equations. Even though this practice is probably compatible with any free software licence since the licences only concern the code of the program and not the equations on which it is based or the simulation output, it is undesirable because the results are much harder to verify [e.g. 150].

To conclude, models can be useful, and they are of much greater use when they are free software than when they are not. Hence, it is commendable that all relevant source code should

[9] An example of such guidelines is the Debian Free Software Guidelines (DFSG), which is used as a basis for the development of Debian GNU/Linux.

accompany the publication of a model or publications based on that.

2.4 General circulation model

One type of numerical model is the General Circulation Model (GCM). This can be regarded as a specific type of box model [14 pp. 15–22, 275–7, 102 pp. 10–5] with typically a very large number of boxes ($> 10^5$), and hence computationally intensive [64 § 2.1.1, 102 pp. 215–21]. Such models may simulate geophysical fluids like the ocean and the atmosphere. General Circulation Models are discretised versions of the Navier-Stokes equations, classical mechanics generalised to fluids, together with several other equations for thermodynamics and radiation [138 pp. 77–82].[10]

Analytical steady-state solutions of the Navier-Stokes equations exist only for a few artificial systems. Therefore, these equations are either approximated to equations that can be solved analytically (e.g. reducing the equations to the Eady model for which bottom friction is neglected and the f-plane approximation is applied ($\beta = 0$), or they are solved numerically (i.e. within GCMs). In the first case, an approximation of the equations is solved exactly, while in the second case, the full equations are solved approximately, hence in both cases the solutions are approximations. Because of computational limitations, the Navier-Stokes equations are typically also approximated when they are solved numerically. For instance, in ocean models the Boussinesq approximation is applied. After these kind of approximations, the equations need to be discretised, since computers are discrete as well and there is only finite memory and computational power in a computer [1]. This goes together with a number of assumptions. There are no hard and fast rules for writing and implementing such a model: it is more of an art than sound craftsmanship.

One of the most difficult issues in writing a GCM is the handling of subgrid processes. At any finite resolution, be it 1000 km or 1 m, there will always be processes not described by the model. One of the quantities that cannot be calculated correctly from any GCM is the kinetic energy. There will be more kinetic energy at smaller and smaller scales until viscosity gets important where energy dissipates (energy cascade). This occurs at the Kolmogorov length scale (less than 1 mm). At that scale turbulence converts kinetic energy into heat [118 pp. 89–94]. However, on the resolution where this takes place, no geophysical fluid model exists since that is computationally unfeasible.

The difficulty is that in a model with a finite resolution, climate variables are not calculated on subgrid scales even though they may be significant for processes on supergrid scales. This calls for parameterisations (Section 2.1). Typically, parameterisations express unresolved processes through (large-scale) modelled quantities [e.g. 155 p. 24]. Eddy diffusion is introduced as a parameterisation that accounts for subgrid dynamics. The introduced parameters, the eddy diffusivities (or eddy diffusion coefficients), replace molecular diffusivity in the equations. Molecular diffusion is of no relevance for modelling geophysical fluids. The coefficients for (eddy) diffusion depend on the spatial scale and hence the values of the horizontal and vertical diffusion are different from each other.

The resulting GCM, including these subgrid parameterisation, should be something that works, if the art is done well. This means that observations can be reproduced sufficiently well

[10] To be more precise, the Navier-Stokes equations are the combination of Newton's second law ($\mathbf{F} = \dot{\mathbf{p}}$) and the postulate that the fluid's stress is the sum of a diffusing viscous term and a pressure term. When interpreting every term in the equations as objects in the real world (e.g. "$\mathbf{p}$ represents the rate of change of momentum, where momentum represents the mass (resistance of being accelerated) times the rate of change of the position.") one arrives at a theory of fluid dynamics. The mentioned equations are a perfect model of this theory. We see that the Navier-Stokes equations utilise only part of classical mechanics, and there are extra assumptions needed. We say that the Navier-Stokes equations are a model of classical mechanics applied to fluids. But it is also a *idealised model* of statistical mechanics [155 pp. 23–4].

for the purposes of the research.

The model may be run with different sets of boundary conditions. Boundary conditions include initial conditions and (variable) forcings. Consider for example an atmospheric GCM, or coupled model, to project future climate. Initial conditions, ideally based on current observed climate variables, are important for at most the first several decades [111]. Beyond that timescale the initial conditions are no longer relevant for prediction. Rather other boundary conditions and model uncertainty are more important [121]. Among such boundary conditions are solar radiation and the average concentration of carbon dioxide in the atmosphere (forcings). Other boundary conditions include those at the ocean–atmosphere interface, the land–atmosphere interface and the top of the atmosphere. The latter is defined in an arbitrary but practical way; this is part of the art of modelling. On longer timescales variability in the deep ocean is important, which calls for the coupling of the atmosphere with an Ocean GCM (OGCM). This implies the need for boundary conditions at the ocean–sediment boundary. On even longer timescales a sediment model may be included, in which case a deeper boundary within the sediment is defined.

All this depends on the amount of complexity that you need to do a future climate projection, and the timescale on which you want to do the projection. Of course a limiting factor is also our lack of knowledge about parts of the Earth system. If carbon dioxide would not be prescribed, one would need a full carbon cycle and socioeconomic model as part of the system. In that case, long-term climate projections would become climate forecasts. However, reliable models of that kind do not exist at the moment and will probably not be developed in the near future, since human behaviour is effectively unpredictable.

2.5 Errors in observations and models

In this section I will set out how to judge how well a model performs with respect to the observations (how reliable [155] it is), and how this relates to the accuracy of the measurements and the predictive error of the model.

If some modelled variable and the corresponding measured variable coincide sufficiently (Section 2.5.2), the model may be reliable, but it may also give the right results for the wrong reasons. This means that in principle such a result does not say anything about the intrinsic[11] goodness of the model, but it does say something about the reliability of the model, or how well it performs within the context where it is used.

If the model simulation output and the observations are not sufficiently similar, the model is not reliable.[12] In that case, if the model is based on a theory, most likely it is not a good model of the theory. However, if it is a good model of the theory (for instance when the model is isomorphic to the formalism), either the theory or the observations are wrong. If in that case the observations are correct, the model provides evidence for the falsity of the theory.

Section 2.5.1 introduces the concepts precision and accuracy and illustrates them with Al and Mn data. Section 2.5.2 presents a statistical measure of goodness of fit of the model simulation compared to the observations.

2.5.1 Observations

The measured value of an observable (shortly: measurement) is never equal to the real value of the observable (shortly: true value). The observational error consists of at least a random

[11] Realists and structural realists would say *ontological*, while empiricists and the like would probably not care.

[12] In the case of chaotic behaviour, an average of an ensemble of simulations with small variations in the internal state or boundary conditions of the model may be taken to compare with the observations.

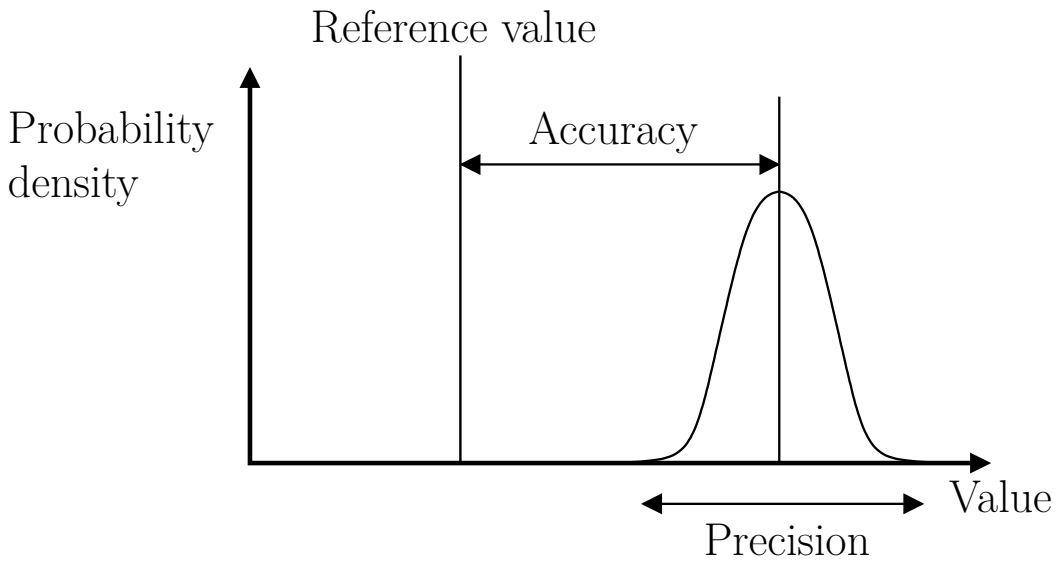

Figure 2.1: Accuracy is the proximity of measurement results to the reference value. Precision is the reproducibility of the measurement (based on `http://commons.wikimedia.org/wiki/File:Accuracy_and_precision.svg`).

error and potentially a systematic error (also named *bias* or *accuracy*):

$$\text{measurement} = \text{real value} + \text{bias} + \text{random error} \,. \tag{2.2}$$

Figure 2.1 presents a hypothetical measurement, or average of several measurements, with a probability distribution around that value. The typical spread of this distribution is the *precision* or *reproducibility* of the measurement. The random error lies, with a high probability, within the precision. Another value in the figure is denoted as *reference value*. The difference between this value and the measured value is the accuracy of the measurement. Ideally the reference value is equal to the 'truth' or 'real value', but that is empirically inaccessible.

In the case of recent oceanographic programmes like GEOTRACES, so called 'reference samples' were taken, of which subsamples were sent to different laboratories. There the values were determined with the methods used by the respective laboratories. An independent referee derived 'consensus values' from these samples are derived. These consensus values are used as reference values. Henceforth, both *truth* and *consensus value* may be used for the reference value, and the difference between these terms is of no further use for the goals of the rest of the thesis.

The dissolved Al data at the Bermuda Atlantic Time-series Study (BATS) from the GEOTRACES cruises by Royal Netherlands Institute for Sea Research (NIOZ) were checked for accuracy by comparison with the consensus values calculated from an independent referee. This lab had received seven reference values from the cross sections of seven different cruises, including the values that were determined by NIOZ. Of these cruises one reference value was removed, leaving six values. These reference values were averaged, resulting in a consensus value, which is here considered as the true value. These values are listed in Table 2.1, together with the values determined by NIOZ. The observations by NIOZ have accuracies (compared to the reference values) that are smaller than the precisions of both the consensus and NIOZ values. Furthermore, the profile at the BATS shows a good comparison with another cruise (Figure 2.2). The differences between the two are notable, but this is because of variability (at a timescale of seasons or more).

$[Al_{diss}]$ (nmol kg^{-1})	Consensus	Middag et al.
SAFe S	1.67 ± 0.10 ($n = 6$)	1.68 ± 0.03 ($n = 4$)
GEOTRACES S	27.5 ± 0.2 ($n = 6$)	27.4 ± 0.3 ($n = 12$)
GEOTRACES D	17.7 ± 0.2 ($n = 6$)	17.5 ± 0.3 ($n = 21$)

Table 2.1: Consensus values of $[Al_{diss}]$ in the SAFe and GEOTRACES reference samples as of November 2011 and the according values of those determined by NIOZ (Middag et al.).

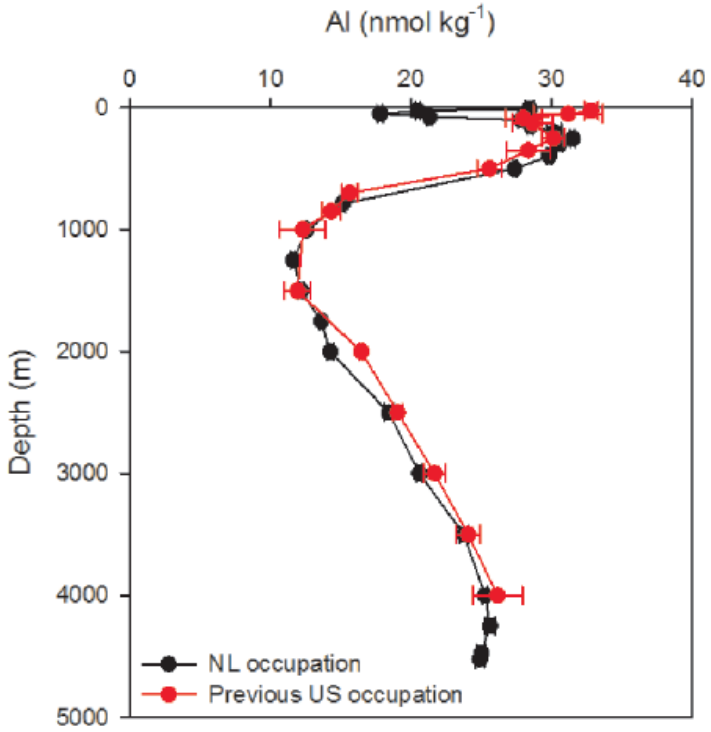

Figure 2.2: $[Al_{diss}]$ at the NL 2010 (Bermuda) station: good agreement with US 2008. Al_{diss} data by Middag [135] and Brown and Bruland [112]. Redrafted after Cutter and Bruland [146].

This has also been done for dissolved Mn, but with more than six samples (Table 2.2). Again, the BATS intercomparison or cross-over station showed excellent agreement between sampling and processing systems used by NIOZ. In this case the distributions of the measurements from NIOZ lie within the precision of the consensus values. In other words, the accuracy is smaller than the precision of both the consensus and NIOZ values, i.e. the reference value lies within the bell curve of Figure 2.1.

[Mn(II)] (nmol kg^{-1})	Consensus	Middag et al.
SAFe D2	0.35 ± 0.05	0.33 ± 0.01 ($n = 24$)
GEOTRACES S	1.46 ± 0.14	1.47 ± 0.03 ($n = 10$)
GEOTRACES D	0.21 ± 0.03	0.18 ± 0.01 ($n = 5$)

Table 2.2: The BATS intercomparison or cross-over station used by the NIOZ (Netherlands).

Besides the good agreement with the consensus values, the measurements also agreed well with an independent lab. The profiles of both laboratories at BATS are presented in Figure 2.3. The difference between the two profiles is significant mostly in the mixed layer. Furthermore, these Mn profiles are also consistent with the profiles determined by Landing et al. [e.g. 48].

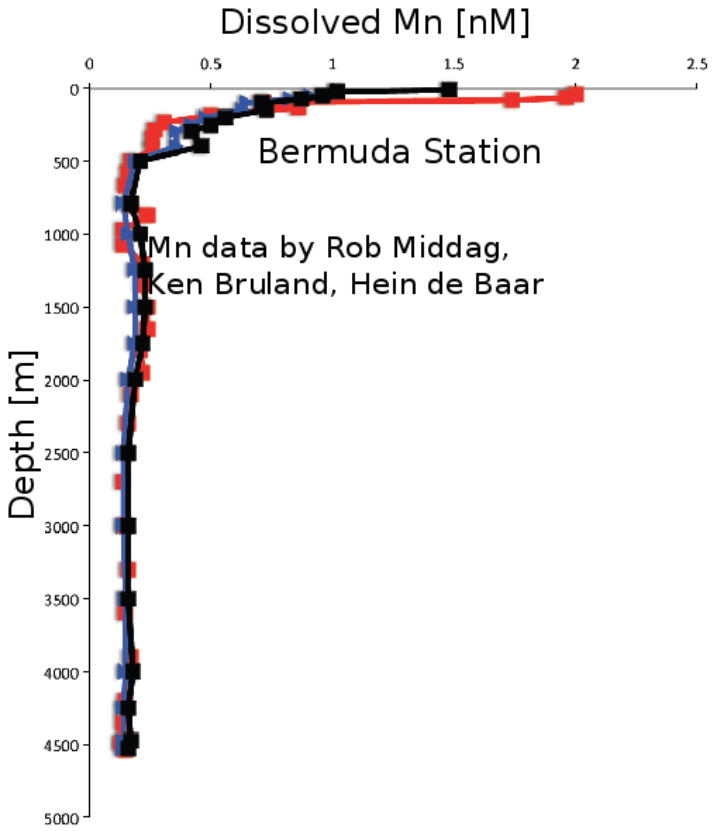

Figure 2.3: [Mn(II)] at the NL 2010 (Bermuda) station: good agreement two different methods of two labs with independent primary lab standards prepared by Rob Middag at NIOZ and Geoffrey Smith at UCSC. Samples were analysed by Rob Middag both at sea (FIA NIOZ) and in the lab (ICPMS UCSC).

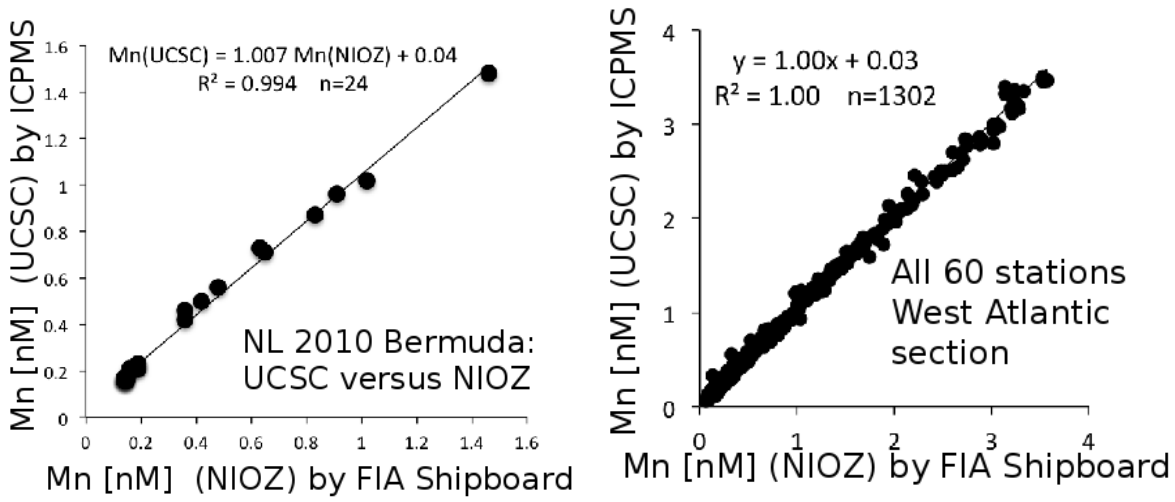

Figure 2.4

Figure 2.4 shows the correlation between the two methods of analysis for the determination of [Mn(II)], shipboard and laboratory measurements, by NIOZ (courtesy of R. Middag). There is a very good agreement between the shipboard and mass spectrometer analyses, which strongly suggests a high observational accuracy.

`NOTE MvH: The seawater can be contaminated, though!`

2.5.2 Model validation

A model can make predictions of variables in a system. How these predictions relate to observations and the true state of the system is depicted in Figure 2.5. This figure describes all, if not more, quantitative aspects of the reliability of a model simulation relevant for the purposes in this thesis. For a wider typology of uncertainties, refer to Petersen [155].

The reference value T (or truth) is represented by the green circle, and the measured value O (or observation) by the blue circle. The dotted circles around observation O and prediction P represent the typical spread in the measurements. More precisely, they represent levels of constant probability density of P and O, respectively, e.g. such that the integrated density outside their circles are 5 %. The observation-related objects on the figure are identical to those in Figure 2.1.

The observation O should be close to T. The distance between O and T is the *accuracy* of the observation. Of course, T and hence the accuracy and the predictive error are not known. If there is no systematic error in the method of measurement, the truth T lies within the observational *precision*. The precision is also referred to as *reproducibility* and is equal to the standard deviation of several measurement of a certain reference sample.

A modelled value P (prediction) of a variable should be as close as possible to the true value T. The smaller the difference between P and T, the more predictive the model is. Therefore this distance is simply called the *predictive error*. This error consists of structural errors, including the errors of the underlying model structure and its parameters. Also numerical errors, ideally negligible, are part of the (implemented) model structure, hence they are part of the predictive error. As with observations, models know a sort of reproducibility, which is here referred to as *predictive uncertainty*. This uncertainty includes internal variability and other chaotic behaviour. In the Al and Mn models in this thesis (Chapters **??**, **??** and 7) interannual variability and chaotic behaviour from the model's dynamics do not occur because the dynamics

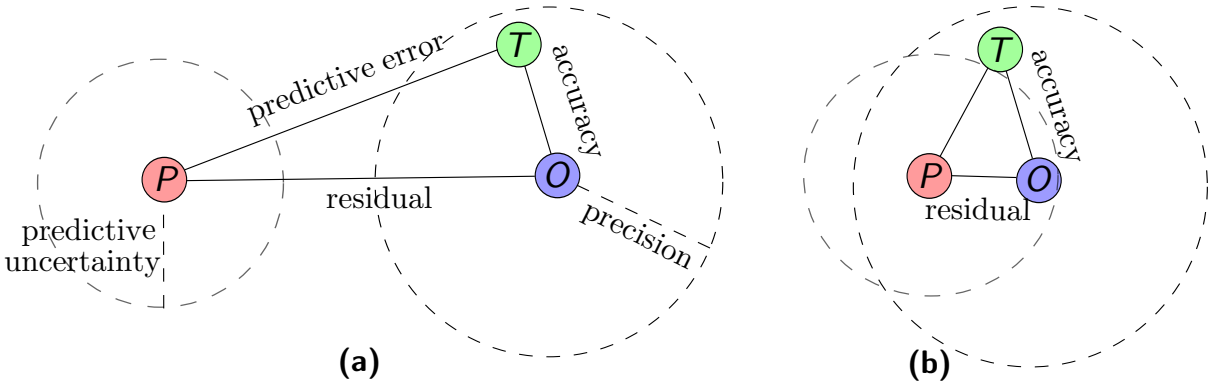

Figure 2.5: Accuracy, precision, residual, predictive error and predictive uncertainty. The green circle represents the true value of a variable (T), the blue circle is the observation (O) and the red circle is the prediction (P) by the model. The random error of the observation is the *precision* and the error of the model is the *predictive uncertainty*. They are represented by the large dashed circles around O and P. The distance between the observation and the truth is the *accuracy*. The *residual* is defined by the distance from the prediction to the observation, while the distance to the truth is called the *predictive error*. In **(a)** there is no overlap between the domain of predictive uncertainty around P and the domain of precision around O, which signifies a wrong prediction, while there is a big overlap in **(b)**, hence in that case the prediction is relatively good. This figure is loosely based on Stow et al. [126], though the terminology is different from theirs.

are prescribed by a climatology of one year (Chapter 3), and the trace metal models are linear and do not feed back to the underlying model, and the model simulations are ran to a steady state. There is a seasonal cycle of Al and Mn in the model, but it is small. This type of model (and the way its output is analysed) amounts to a predictive uncertainty of zero. The only probabilistic quantities left are the predictive error and the residual. Furthermore, numerical errors are assumed to be small. Hence, the predictive error only concerns the free range of possibilities in choice of parameters and the correctness of the model. Those are not probed, except for a small number of sensitivity simulations in the core parameters of the Al and Mn model (not the underlying NEMO-Pisces model). Besides that, to some extent the parameters are tuned such that the model better reproduces the measurements, i.e. minimises the residual (and generally with that the residual). This does not mean, however, that the predictive error can always become zero; the total degrees of freedom of the 3-D model (taking only the yearly average of a quasi-steady-state year) is much higher than the number of tunable parameters.

As long as the precision and accuracy are small compared to the predictive error, one can decrease the predictive error by decreasing the *residual*, i.e. the difference between the prediction and the observation. This is important, since the observations are known, while the truth is empirically inaccessible. The goodness of fit measures the performance of a model. It is defined as some function of the residuals, and modellers typically try to optimise the goodness of fit.

In Section **??** several goodness of fit functions are introduced. In Figure 2.5(a) there is no overlap between the domain of predictive uncertainty around P and the domain of precision around O, which signifies a wrong prediction and should correspond to a low goodness of fit, while there is a big overlap in Figure 2.5(b), corresponding to a high goodness of fit, hence in that case the prediction is relatively good.

2.5.3 Models of observations

Let us go back to our original definition of *model*: a structure in which at least *some* sentences of a theory, hypotheses or observations are satisfied. Consider again the aluminium ocean

model. Imagine that the dissolved aluminium concentration A_{diss} of 1.00 ± 0.01 nM is observed (the 1.00 nM being the measurement and 0.01 nM the precision) at coordinates $(\mathbf{x}, t)$, while the model predicts a $A_{\text{diss}}(\mathbf{x}, t)$ of 0.90 ± 0.05 nM (the 0.90 nM being the prediction and 0.05 nM the predictive uncertainty). This corresponds to Figure 2.5(a), where the two circles are disjunctive. In other words, the predicted sentence "$A_{\text{diss}}(\mathbf{x}, t) = 0.90\pm0.05$ nM" is clearly wrong with respect to the measurement. However, this does not imply that the model is useless. The demand is that there are *at least some* sentences true. So if the model also predicts that $A_{\text{diss}}(\mathbf{x}', t') = 7.0\pm0.5$ nM, and the observations contain the sentence "$A_{\text{diss}}(\mathbf{x}', t') = 7.2\pm0.1$ nM", there is such a good overlap (the observational accuracy is even encapsulated by the predictive uncertainty) that one may say that the model satisfies this sentence.

The main point here is that even though there are uncertainties in both the model simulation results (which may be an ensemble average to account for chaos) and the observations, a model may reproduce observations to a sufficient degree. And even if some observations are not reproduced, this does not mean the model is not useful. Of course, one should define a goodness of fit function for A_{diss} on the whole model domain, or a useful subset of it, as is done in Section **??** for the Al model. Only then one can decide how useful the model is.

2.6 Epilogue

Besides projecting future climate, models are used to test our knowledge of the real world. If base assumptions about the Earth are put into the model, the phenomena in the real world should be seen in the models as well. If that is not the case, the model or our understanding of the world is wrong. This approach will be applied in Chapters **??**, **??** and **??**.

Instead of trying to model the real world, it is also possible to do sensitivity simulations in which boundary conditions or internal variables of a model are changed. The effect on the system (e.g. the change in surface temperature or the effect of pollution on certain plants) may then be quantified relative to the perturbation in the boundary condition or internal variable. This is a way to find out what the most important processes in a model are. This approach will be applied in Chapters **??**, **??** and **??**. If the model shows a high goodness of fit with observations, these processes may be the most important ones in the real system. These processes should be looked at most carefully when modelling the Earth or when changing things on our Earth.

Chapter 3

The model

For the studies in this thesis, the three-dimensional distribution of dissolved Al and dissolved Mn have been simulated with numerical models. These models are embedded in the biogeochemical model NEMO-PISCES [96, 100]. This chapter sets out the relevant details of NEMO and PISCES, while the Al and Mn models are described in the subsequent chapters. A definition and philosophical remark on modelling is given in Chapter 2. This model has been employed for many other studies concerning trace metals, as well as large scale ocean biogeochemistry [e.g. 96, 106, 119, 120, 137]. In the simulations described here, PISCES has been driven by climatological (i.e. for a typical or average year) velocity, temperature and salinity fields obtained from the general circulation model called *Nucleus for European Modelling of the Ocean* (NEMO). This is also referred to as running PISCES *off-line*, while running it coupled to the dynamical part of NEMO, including possible feedbacks from the biogeochemistry to the dynamics, is referred to as an *on-line* simulation (not done in this thesis).

NEMO is a framework for ocean models [116].[1] Its seawater and sea ice (thermo)dynamics components are Océan PArallélisé (OPA) and Louvain-la-neuve Ice Model (LIM), respectively. Furthermore, Tracer in the Ocean Paradigm (TOP) models the biogeochemistry. TOP contains both transport (TRP) and sources minus sinks (LOBSTER, PISCES).[2] The framework NEMO is intended to be a flexible tool for studying the ocean and its interactions with the other components of the Earth's climate system (atmosphere, sea ice, biogeochemical tracers, ...) over a wide range of space and time scales.

Besides these general considerations, NEMO-PISCES has been used with ORCA2, one of its standard configurations. This configuration resolves all dominant water masses and has a high enough resolution to resolve the relevant processes studied in this thesis. Its resolution is similar to that of an observational dataset that is intensively used in this work. In both the resolution and the modelled tracers, this model is flexible enough for our purposes of modelling trace metals, but at the same time it does not introduce too many degrees of freedom. That would complicate matters in the sense of underdetermination of the model parameters, and computational integration time.

3.1 Configuration

All model fields are defined on the ORCA2 coordinate frame (or grid), an irregular grid covering the whole world ocean with a nominal resolution of $2^\circ \times 2^\circ$, with the meridional resolution

[1] NEMO and its components are released under the CeCILL (CEA CNRS INRIA Logiciel Libre) licence, an international free software licence that is explicitly compatible with the GNU GPL. Its source code can be downloaded from `www.nemo-ocean.eu`.

[2] In this thesis only PISCES is used, not LOBSTER. Neither LOBSTER nor PISCES are acronyms.

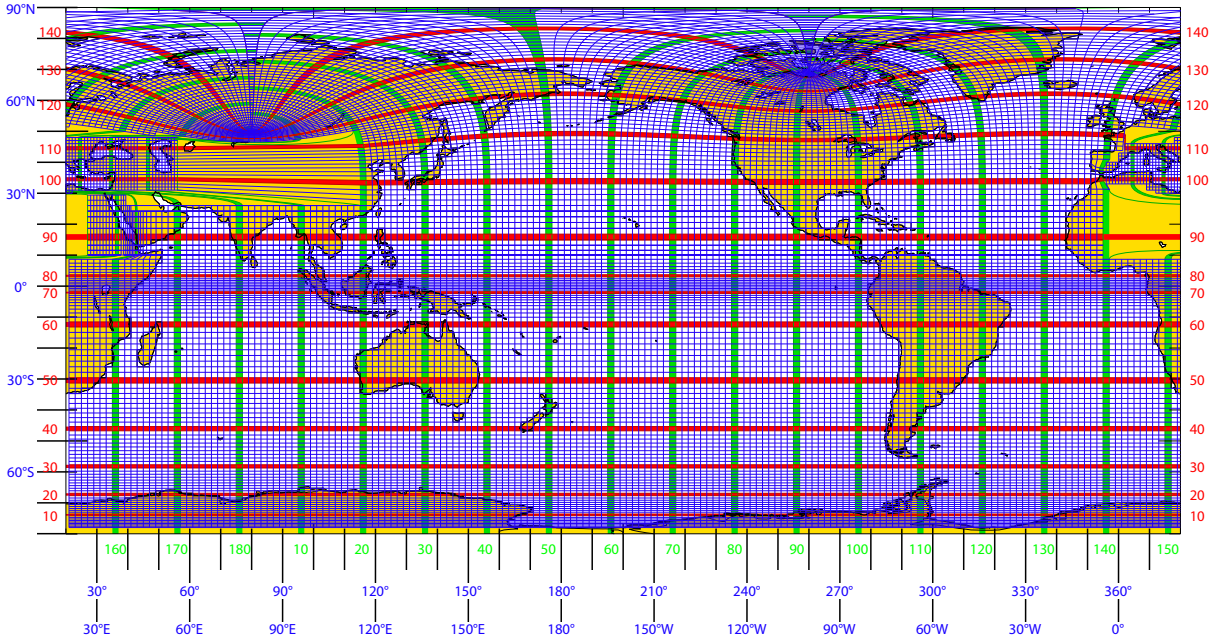

Figure 3.1: The ORCA2 coordinate frame. The nominal resolution is 2°×2°, with the apparent singularity at the north pole removed, and increase in resolution near the equator, near Antarctica and in several large seas. This grid is the same at all model depth levels [56, 55].

increased near the equator and Antarctica, and both the meridional and zonal resolutions in the Mediterranean, Red, Black and Caspian Seas. On the northern hemisphere, it has two coordinate singularities, one in Canada and the other in Russia. More usual grids, like the commonly used geographic projection and the Mercator projection, have their singularity at the geographic north pole. The problem with this is that the north pole happens to be in the sea (the Arctic Ocean). Hence, it is not possible to integrate the primitive equations near the north pole on a geographical projection. Since a coordinate singularity is an *apparent singularity*, it can be removed by choosing a different coordinate frame. One such a frame is the ORCA2 grid that has removed the coordinate singularity from the geographic north pole to points on land which lay outside the effective model domain. The grid has no singularity on the southern hemisphere, since it is not defined south of 78.2° S. Figure 3.1 presents the ORCA2 grid laid over the geographical grid. The vertical resolution of the ORCA2 grid is 10 m in the upper 100 m, increasing downwards to 500 m, such that there are 30 layers in total and the ocean has a maximum depth of 5000 m [56, 55].

3.2 Dynamical model: OPA

The dynamical component of NEMO is OPA, optionally coupled with the sea ice component LIM. The OPA model is a General Circulation Model (GCM) that numerically solves the primitive equations on a rotating sphere (the Earth). These equations consist of approximations of the Navier-Stokes equations (conservation of momentum), the continuity equation (conservation

of mass) and the equation of state (relating temperature, salinity and density). In all Ocean GCMs (OGCMs), including OPA, several approximations are made. Firstly, the geometry of the ocean is assumed to be spherical and thin compared to the radius of the Earth. Secondly, the effect of density variations are neglected, except when they give rise to buoyancy forces (Boussinesq approximation) and assuming incompressibility. Thirdly, parameterisations are introduced (simulating subgrid processes using the turbulent closure hypothesis and convection assuming hydrostatics) [64 pp. 36–44, 138 pp. 77–92, 153 pp. 12–14]. The next subsection gives the equations (details are to be found in Madec et al. [153]).

3.2.1 Model equations

The development of any conservative tracer $\mathcal{T}$ follows the tracer conservation equation, which is given by:

$$\frac{\partial \mathcal{T}}{\partial t} = -\nabla \cdot \mathbf{v}\mathcal{T} + \nabla \cdot (\mathbf{D} \cdot \nabla \mathcal{T}) \,, \tag{3.1}$$

where t is the time, and the first term on the right-hand side is advection with $\mathbf{v}$ the 3-D advection velocity. The second term represents diffusion, where $\mathbf{D}$ is the diffusivity tensor.

It will be assumed that the fluid is incompressible ($\nabla \cdot \mathbf{v} = 0$), hence advection is simplified to $-\mathbf{v} \cdot \nabla \mathcal{T}$. Furthermore, molecular diffusion is negligible and here the diffusion term is rather *eddy diffusion* or *turbulence*, parameterising subgrid processes. This term can be presented by one scalar for the horizontal diffusion and one for the vertical (assuming the fluid is Newtonian, incompressible and isotropic). Hence, (eddy) diffusion is simplified to $\mathcal{A}\nabla_H^2 + \nu_E \partial^2/\partial z^2$, with ∇_H the horizontal divergence, and where $\mathcal{A}$ and ν_E are the horizontal and vertical eddy diffusivity coefficients, respectively. An eddy-induced velocity $\mathbf{v}_{\mathrm{GM}}$ is calculated, following the Gent-McWilliams eddy parameterisation scheme [34, 46].

Since all tracers are advected and mixed according to the same equations, these effects may be put together in a generic operator Γ, following Sarmiento and Gruber [102 p. 115]:

$$\Gamma := \frac{\partial}{\partial t} + (\mathbf{v} + \mathbf{v}_{\mathrm{GM}}) \cdot \nabla - \mathcal{A}\nabla_H^2 + \nu_E \frac{\partial^2}{\partial z^2} \,. \tag{3.2}$$

Γ may be interpreted as all conservative 'transport' processes, where 'transport' includes both advection by the velocity field, and eddy diffusion. The Γ-notation is used for convenience since we are primarily interested in the biogeochemistry, and advection and eddy-diffusive mixing applies to all tracers in the same way. The result is that the conservation equations for the dynamical tracers reduce to:

$$\Gamma(\mathcal{T}) = 0 \,, \tag{3.3}$$

where boundary fluxes are not included.

The primitive equations, including boundary fluxes, are

$$\frac{\partial \mathbf{v}_h}{\partial t} + \left[(\nabla \times \mathbf{v}) \times \mathbf{v} + \frac{1}{2} \nabla \mathbf{v}^2 \right]_h = -f\mathbf{k} \times \mathbf{v}_h - \frac{1}{\rho_0} + \mathbf{D} + \boldsymbol{\mathcal{F}_v} \tag{3.4a}$$

$$\frac{\partial p}{\partial z} = -\rho g \tag{3.4b}$$

$$\nabla \cdot \mathbf{v} = 0 \tag{3.4c}$$

$$\Gamma(T) = \mathcal{F}_T \tag{3.4d}$$

$$\Gamma(S) = \mathcal{F}_S \tag{3.4e}$$

$$\rho = \rho(T, S, p) \,, \tag{3.4f}$$

where $\mathbf{v}$ and $\mathbf{v}_h$ are respectively the three- and horizontal velocities, z is the vertical coordinate, ρ is the *in situ* density given by the equation of state (last equation), ρ_0 is a reference density, p the pressure, f is the Coriolis acceleration, and g is the gravitational acceleration. $\boldsymbol{\mathcal{F}_v}$, $\mathcal{F}_T$ and $\mathcal{F}_S$ are the surface forcing terms [153], which are described in the next subsection.

3.2.2 Boundary conditions

Precipitation, evaporation, river runoff and solar radiation have an effect on salinity and temperature, and hence the density of seawater (equation of state), which feeds through the pressure gradient into the Navier-Stokes equations (or primitive Eqns 3.4 in the model). All mentioned forcings also affect mixing, which has an influence on the currents as well. River inflow is specified as a fresh water flux at the river mouth. At the solid boundaries (sediment and coastlines) the seawater flow is parallel to the boundary, and heat and salt fluxes are neglected. At the interface between sea ice and the ocean, heat, salt and fresh water are exchanged, and temperature and salinity in the upper model layer are calculated.

In this thesis climatologies from simulations with two different air-sea boundary conditions have been used. Both use the ORCA2 configuration and solve the same primitive equations, and both sets of boundary conditions were derived from observations (satellite-derived data and re-analyses). Both model simulations are forced at the surface by heat and freshwater fluxes obtained from bulk formulae that are functions of wind, sea surface temperature, and evaporation minus precipitation. The differences between the forcings are described next.

Dynamics I

Daily wind stress based on European Remote Sensing (ERS) satellite data is used for the tropics, and NCEP/NCAR re-analysis data for the polar regions [54, 69]. Surface salinity is restored with a timescale of 60 d towards the seasonal Polar Science Center Hydrographic Climatology (PHC) dataset to avoid model drift [92]. The last year of this simulation is used as our one-year 'climatology' with a resolution of five days of the dynamics. Henceforth this climatology is referred to as *Dynamics I*, since it corresponds to the earlier Al simulations performed in this thesis, especially Chapter **??**, as well as the Mn simulations (Chapter 7).

Dynamics II

The other climatology is based on DFS3, a forcing dataset based on uncorrected surface atmospheric state variables of ERA-40 extended in time until 2007 with fields of the ECMWF operational analysis, and the radiation and precipitation products proposed by Large and Yeager [79], Uppala et al. [93]. The wind velocities are taken from ERA-40, the Re-Analysis performed by ECMWF of the global atmosphere and surface conditions for 45 years, over the period from September 1957 through August 2002 [93]. The model was initialised from the ocean conditions in 1958 from Levitus et al. [61]. A more detailed description of the creation of this dynamics can be found in Brodeau et al. [128]. From this simulation years 1959 to 1972 were averaged to obtain a monthly climatology with a reasonable Atlantic overturning (next section). This climatology will be referred to as *Dynamics II* and corresponds to the later simulations of aluminium in this thesis, especially in Chapter **??**. Chapter **??** utilises both dynamics, and only when relevant for the simulation it will be noted which dynamics is used.

3.2.3 General characteristics

Surface currents

Figure 3.2 presents the annually averaged surface velocity field of the OPA output, for both dynamical forcing fields. Both show the main features of the ocean circulation such as the equatorial current systems, the western boundary currents (among which the Gulf Stream and Kuroshio) as well as the Antarctic Circumpolar Current. There are minor differences between the two dynamics. For instance, the equatorial currents are weaker in Dynamics II.

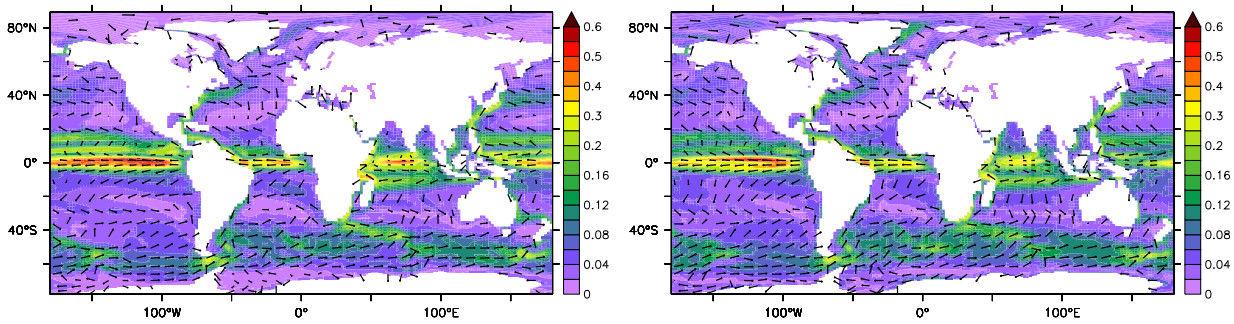

(a) Dynamics I (b) Dynamics II

Figure 3.2: Modelled velocity at the surface, yearly average. The colour indicates the speed in m/s, while the vectors represent the direction of the flow. Vectors are plotted at every fifth gridpoint.

Meridional overturning circulation

Figure 3.3 presents the Overturning Stream Function (OSF) of the Atlantic Ocean for both dynamics. The OSF is defined as the zonally (through the basin) and vertically (from the surface downwards) integrated meridional current speed. It is used as a measure for the Atlantic Meridional Overturning Circulation (AMOC, Section **??**). The upper overturning cell has a strength of about 14 Sv (1 Sv $= 10^6\ \mathrm{m^3\,s^{-1}}$) in both dynamics. Observations suggest higher values of about 19 ± 5 Sv [75, 105, 142].

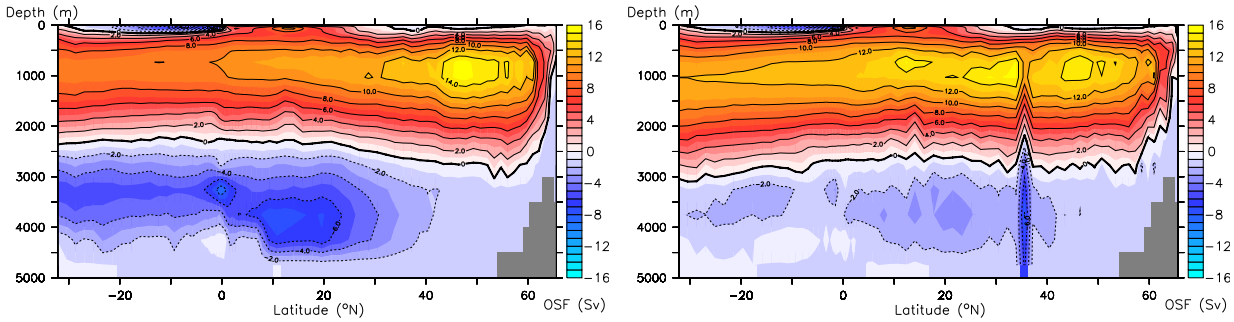

(a) Dynamics I (b) Dynamics II

Figure 3.3: Atlantic Overturning Stream Function (OSF), a measure for the AMOC in Sv (1 Sv $= 10^6\ \mathrm{m^3\,s^{-1}}$). The erratic behaviour at 36°N is an artefact from cross-land mixing through the Strait of Gibraltar. This is a model parameterisation that attempts to resolve the problem that the Strait of Gibraltar is significantly smaller than the model resolution, while the fluxes between the Atlantic Ocean and the Mediterranean Sea are important for the world ocean.

Even though both dynamics reproduce the AMOC, there are pronounced differences between them. Firstly, the maximum southward flux is at 2 km depth in Dynamics I, while this is deeper for Dynamics II. Secondly, the lower cell is much stronger in Dynamics I compared to Dynamics II. The value of 3 Sv in Dynamics II is more realistic than the 7 Sv of Dynamics I [75, 142]. This has significant consequences for biogeochemical tracers, among which dissolved aluminium (Al_{diss}) and silicic acid (Si_{diss}). The effect on [Si_{diss}] is presented in Section **??** and the effect on [Al_{diss}] is discussed in Section **??**.

3.3 Biogeochemical model: Pisces

The model Pisces simulates the cycles of carbon, the major nutrients (nitrate, phosphate, ammonium, silicic acid) and the trace nutrient iron, along with two phytoplankton types (nanophytoplankton and diatoms), two zooplankton grazers (micro- and mesozooplankton), two classes of particulate organic carbon (small and large) with differential settling speeds, as well as calcite and biogenic silica. The Pisces model distinguishes three silicon pools: the silicon content of living diatoms (Si_{diat}), the silicon content of dead settling diatoms (Si_{biog}), and dissolved silicic acid (Si_{diss}). In the model, Si_{diss} and other nutrients are supplied to the ocean by means of atmospheric dust deposition and rivers, while iron enters the ocean additionally through sediment remobilisation [96].

In this section several details important for trace metal modelling will be discussed. These details include how the Pisces tracers behave in general (Section 3.3.1), the sources of the tracers which are important for both the major and the trace nutrients (Section 3.3.2), and the characteristics of specific Pisces tracers (Section 3.3.3). For a more detailed description of Pisces see Aumont and Bopp [96] and Aumont [169].

3.3.1 Model equations

At any location in the ocean away from the boundaries, every tracer $\mathcal{T}$ is conserved, except for internal chemical and biological conversions, often referred to as the internal Sources Minus Sinks (SMS). The tracer conservation equation has the form:

$$\Gamma(\mathcal{T}) = -\frac{\partial}{\partial z}(w_{\mathcal{T}} \cdot \mathcal{T}) + SMS_{\mathcal{T}} + f_{\mathcal{T}} \cdot \mathcal{F}_{\mathcal{T}} \,, \tag{3.5}$$

where the dynamics are included in Γ. The first term on the right-hand-side represents settling of heavy particles through the water column with z the depth (negative downwards) and $w_{\mathcal{T}}$ the settling speed of tracer $\mathcal{T}$. In Pisces this is simplified to two different settling velocities, one for small and one for big particles (and, in principle, one where $w_{\mathcal{T}} = 0$ for dissolved substances and colloids). The second term is the SMS, and the third term presents the forcing fields (Section 3.3.2).

Settling of particles is, similar to advection and mixing, a purely physical process and hence conserves the tracer. Nonetheless, this term is not included in Γ for several reasons. Firstly, the settling speed is *not* the same for all tracers. Secondly, it is not part of the material derivative since settling is transport *through* seawater. Thirdly, settling is a term that relates strongly to the biological and chemical processes (SMS), so it should be explicit in the notation of the equations.

Specific cases include drifting tracers (dissolved particles and colloids) where $w_{\mathcal{T}} = 0$ and hence $\Gamma(\mathcal{T}) = SMS(\mathcal{T})$; conservative tracers (no biology/chemistry) such that $\Gamma(\mathcal{T}) = \partial(w_{\mathcal{T}} \cdot \mathcal{T})/\partial z$; and drifting, conservative tracers for which $\Gamma(\mathcal{T}) = 0$. All this is valid as long as $\mathcal{F}_{\mathcal{T}} = 0$, i.e. away from the boundaries.

The standard version of PISCES accounts for 24 tracers. They can chemically or biologically transform from one state to another (SMS) as long as the two states concern the same chemical element (conservation of atoms). E.g., iron in small particles can form iron in big particles, but they cannot transform to any tracer of nitrogen.

As an example, consider the equation for carbon fixed in phytoplankton (C_{phy}):

$$\Gamma(C_{\text{phy}}) = (1-\delta)\mu_{\text{phy}}C_{\text{phy}} - m_{\text{phy}}\frac{C_{\text{phy}}}{K + C_{\text{phy}}}C_{\text{phy}} - w_{\text{aggr}}C_{\text{phy}}^2 - g_{\text{zoo}}C_{\text{phy}}C_{\text{zoo}} \ , \tag{3.6}$$

where the first term on the right-hand side is the production term of phytoplankton, with δ the excretion of Dissolved Organic Carbon (DOC) and μ_{phy} the rate of photosynthesis (see below). The second term simulates mortality, with m_{phy} the phytoplankton mortality rate and K the half-saturation constant for mortality. This means that for small phytoplankton concentration ($C_{\text{phyt}} \ll K$) mortality is quadratic, while for large phytoplankton concentration ($C_{\text{phyt}} \gg K$) mortality is proportional to C_{phyt}; relative mortality halves when $C_{\text{phyt}} = K$. The third term on the right-hand-side represents aggregation, with w_{aggr} the phytoplankton aggregation term, which depends on the shear rate, as the main driving force for aggregation is the local turbulence. The fourth term models grazing by zooplankton, with g_{zoo} is the grazing rate and C_{zoo} is carbon in zooplankton. All these terms together form the SMS for phytoplankton. This equation applies to both functional classes of phytoplankton in PISCES, namely nanophytoplankton and diatoms.

The rate of photosynthesis μ_{phy} can be modelled as a Monod function [2]. Diatoms, for instance, can be Si limited. In that case, μ_{phy} is proportional to the Monod function of the Si_{diss} concentration S:

$$\mu_{\text{phy}} \ \propto \ \frac{S}{K_{\text{Si}} + S} \ , \tag{3.7}$$

where K_{Si} is the Si_{diss} concentration for which μ_{phy} is half the maximum photosynthesis rate (rate is maximal when $S \to \infty$). If iron (Fe) is limiting as well, the rate of photosynthesis is modelled as the minimum of two Monod functions [102 p. 132]:

$$\mu_{\text{phy}} \ \propto \ \min\left(\frac{S}{K_{\text{Si}} + S}, \frac{F}{K_{\text{Fe}} + F}\right) \ , \tag{3.8}$$

where F is the Fe_{diss} concentration.[3] This example illustrates the influence of nutrients on photosynthesis and hence diatom growth. Of course, also other factors like temperature and acidity have an effect on the diatom growth rate, but these influences are neglected in this model.

The equation for particulate organic carbon (C_{det}) is given by:

$$\Gamma(C_{\text{det}}) = m_{\text{phy}}\frac{C_{\text{phy}}}{K + C_{\text{phy}}}C_{\text{phy}} + w_{\text{aggr}}C_{\text{phy}}^2 + \text{other terms} - w_{\text{det}}\frac{\partial C_{\text{det}}}{\partial z} \ . \tag{3.9}$$

Since this is a heavy tracer, the settling term is not zero ($w_{\text{det}} > 0$). 'Other terms' includes SMS from the two zooplankton carbon tracers and DOC. The rest of the terms are defined before. When adding the different equations for carbon, the result is $\Gamma(C) = 0$, hence carbon is conserved. This stands in contrast to the individual tracers, like fixed carbon (C_{phy}), which are non-conservative.

[3] The choice of a minimum is relatively arbitrary. It can also be modelled as the product of two Monod functions, which more accurately represents the idea of co-limiting nutrients. In such a model, addition of Fe can partly neutralise Si limitation, or vice versa. In that case, if $S = K_{\text{Si}}$ and $F = K_{\text{Fe}}$, and F were to be halved, then S must be multiplied with 3 to get back to the original rate of photosynthesis. Proof: We must solve $1/4 = (x/(1+x)) \cdot 1/3$ for x, in case of $S = x \cdot K_{\text{Si}}$. Its solution is $x = 3$. Thus, beginning from the half-saturation concentrations for both the silicic acid concentration S and the dissolved Fe concentration F, decreasing one of the concentrations, the other must disproportionally increase to keep the production rate the same. However, in the PISCES model either Si or Fe is limiting, depending on which term is smaller.

3.3.2 Boundary conditions

Besides the transport and internal SMS of tracers within the ocean, they are added to and removed from the oceans at its boundaries (last term in Eqn 3.5). As long as the model is not coupled to other models at the boundaries (e.g. an atmospheric model), the tracer flux is prescribed by forcing fields, and tracers are removed according to the internal state of the model. Both sources and sinks are modelled as a concentration change of the tracer at the boundaries (sea surface, coast, sediment and mid-ocean ridges). Since most of these input fluxes are only used for the manganese ocean model in this thesis, the equations are given in the respective Section 7.2.2.1.

Figure 3.4 shows the four source fields of PISCES, and Table 3.1 lists the relative input of the different basins for each of these sources.

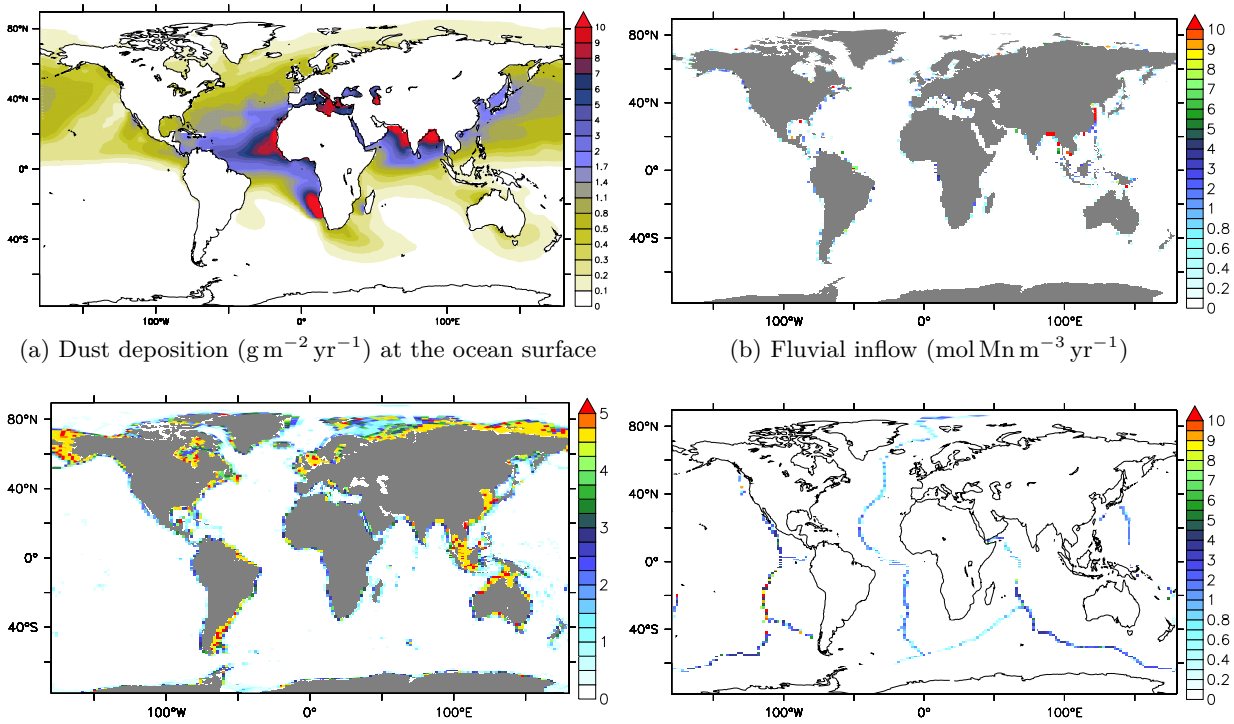

(a) Dust deposition ($\mathrm{g\,m^{-2}\,yr^{-1}}$) at the ocean surface

(b) Fluvial inflow ($\mathrm{mol\,Mn\,m^{-3}\,yr^{-1}}$)

(c) Inflow from reducing sediments ($\mathrm{mmol\,Mn\,m^{-2}\,yr^{-1}}$)

(d) Hydrothermal input ($\mathrm{mol\,{}^3He\,m^{-2}\,yr^{-1}}$)

Figure 3.4: Sources of Mn(II) to the ocean. Three-dimensional fields are vertically integrated.

Basin	Dust	Sediment	Fluvial	Hydrothermal
Atlantic Ocean	47.9	18.1	32.2	13.8
Pacific Ocean	20.3	27.9	44.0	62.2
Indian Ocean	21.8	7.4	20.8	20.1
Southern Ocean	0.12	11.4	0.0	3.1
Arctic Ocean	0.55	22.8	3.3	0.8
Mediterranean Sea	6.6	3.6	1.8	0.0
total	100.0	100.0	100.0	100.0

Table 3.1: Relative amount of yearly dust, sediment, river and hydrothermal input into each basin (%). The Southern Ocean is defined as the ocean south of 59°S.

Removal occurs near the sediment by burial of particles that are heavier than water, and

by equilibration of gases between the ocean surface and the atmosphere. Input of tracers is modelled as an external flux at the interface, i.e. not as a consequent of a pressure difference as is the case with CO_2. In general this is given by $\partial\mathcal{T}/\partial t = f_{\mathcal{T}} \cdot \mathcal{F}_{\mathcal{T}}$, where $\mathcal{F}_{\mathcal{T}}$ is a forcing field that may need to be scaled by measures of the corresponding gridbox and/or conversion between elements ($f_{\mathcal{T}}$).

Further details on the PISCES model can be found in the supplementary material of Aumont and Bopp [96], Aumont [169] and the source code of the model, to be found at `http://www.nemo-ocean.eu/`.

3.3.3 Characteristics of the output fields

This section presents and discusses the modelled behaviour of silicic acid and iron in our specific simulation by PISCES, that are relevant for the rest of this thesis. A more concise presentation of the general characteristics of chlorophyll, nitrate, silicic acid, oxygen, Dissolved Inorganic Carbon (DIC), alkalinity and iron is given by Aumont [169] and references therein.

Silicic acid

Figure 3.5 presents modelled [Si_{diss}] for both dynamical fields, with measured [Si_{diss}] as coloured dots. Clearly Figure 3.5a, corresponding with Dynamics I, presents a strongly overestimated

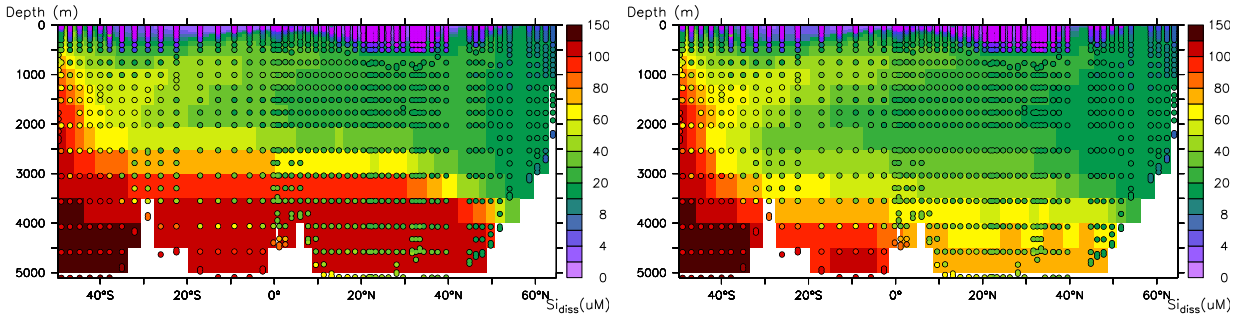

(a) Dynamics I (b) Dynamics II

Figure 3.5: The modelled silicic acid concentration at the West Atlantic GEOTRACES section. Coloured dots are measurements. Both simulated and observed concentrations are in µM (on a non-linear scale).

[Si_{diss}] in the deep ocean, while this overestimation is significantly reduced in Figure 3.5b (Dynamics II). The reason for this is that in Dynamics II less Si_{diss} is transported northwardly with the AntArctic Bottom Water (AABW) than in Dynamics I (Figure 3.3). This means that the more realistic deep overturning cell in Dynamics II results in a more realistic simulation of [Si_{diss}] in the deep Atlantic Ocean.

A statistical comparison of the effects of the two dynamics on [Al_{diss}] and [Si_{diss}] is given in Section **??**.

Iron

There is insufficient knowledge about the cycling of most trace elements, which makes modelling them difficult. Nonetheless, iron is the most important micronutrient [e.g. 36, 80, 85, 86, 107, 113, 127, 143, 157], hence in standard PISCES iron is modelled (as the only trace element).

Figure 3.6 presents the modelled and measured dissolved iron (Fe_{diss}) concentrations at the West Atlantic GEOTRACES cruise section. This simulation is based on Dynamics II. General properties of the iron distribution are captured by the model. These include the depletion at

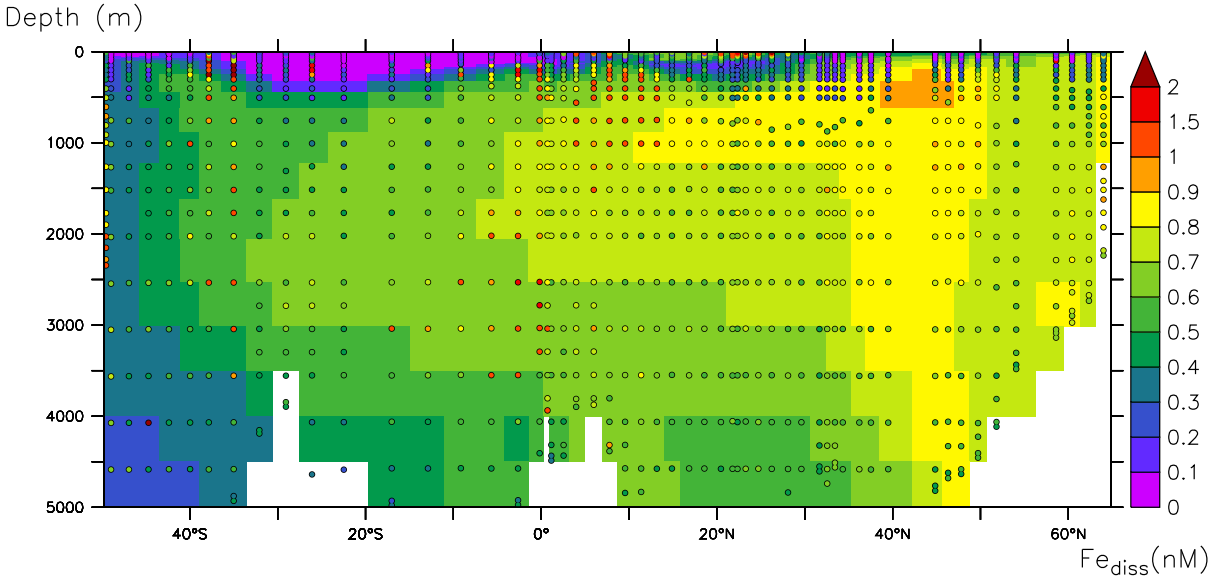

Figure 3.6: Modelled [Fe_{diss}] (nM) at the West Atlantic GEOTRACES cruise track, based on Dynamics II. Measurements of [Fe_{diss}] are taken during the GEOTRACES cruises (M. Rijkenberg) and are presented as coloured dots (same non-linear scale).

the ocean's surface and the subsurface minimum at 10–30°N. However, there are important deviations from the measurements. Around 10°N at 300–1000 m depth [Fe_{diss}] is elevated in the measurements (coloured dots in the figure). This is probably from remineralisation since it coincides with the Oxygen Minimum Zone (OMZ). The model does not reproduce this, even though an OMZ is present in the model. The high measured concentrations deeper than 2.5 km are probably due to hydrothermal vents, which are not included in this model simulation. All measurements are described by Rijkenberg et al. [171] in more detail. Since PISCES 3.1 [96] there have been improvements in simulating iron (A. Tagliabue, personal communication, 2013; Tagliabue and Völker [145]). Results from more recent versions of PISCES have not been included, since for consistency all simulations in this thesis are based on PISCES 3.1.

3.4 Epilogue

This chapter gave a succinct description of NEMO-PISCES, which is the underlying model used in this thesis. In this thesis two new trace elements are added to the model. One of these trace elements is aluminium, which will be described in Chapters **??** and **??**. This element interacts with the silicon cycle and can also be used as a tracer for dust deposition. The second new trace element is manganese, described in Chapter **??**. This is one of most important trace nutrients after iron [e.g. 32 pp. 724-5].

Chapter 7

Manganese in an ocean general circulation model

7.1 Introduction

In the ocean manganese (Mn) exists in low concentrations (0.1–25 nM), and in many forms, among which incorporated in organisms and particles. From a chemical oceanographic perspective two phases are the most important. One is dissolved Mn, Mn(II), available for uptake by autotrophs. The other is oxidised Mn, MnO_x, not bioavailable and subject to adsorptive scavenging [e.g. 45].

Manganese is an essential nutrient for all life. One important function of Mn for phytoplankton is its role in photosynthesis, namely photolysis in photosystem II [18, 36], represented as *growth* in Figure 1.4. Photosystem II is the first protein complex in the light reaction (see p. 12) where photons are captured and transformed into the chemical energy of ATP and NADPH [32 pp. 209–19].

Furthermore, Mn is needed for superoxide dismutase enzymes in diatoms [82, 104]. Superoxide dismutase destroys reactive oxygen species. Under Fe deficient conditions the efficiency of photosystem II decreases, which results in an increased formation of reactive oxygen species [82]. Therefore Mn availability is especially important under low (bioavailable) Fe conditions [135 p. 16, and references therein]. This is also referred to as co-limitation of Fe and Mn. In other words, when too little Fe is present, Mn can compensate this deficit for a large part. In that case more Mn must be available than in the case of sufficient iron availability [162].

Another important export mechanism is *oxidation* of dissolved Mn(II) to Mn(IV) (and possibly other oxidation states), and the subsequent aggregation and adsorptive scavenging by particulate matter [45]. Since Mn(II) is unstable, oxidation occurs everywhere in the ocean where oxygen is available [29]. This process can be strongly accelerated by Mn(II)-oxidising microorganisms, primarily bacteria and fungi [91]. The reverse process is *reduction*, reducing MnO_x to Mn(II). This process is significantly faster under the influence of sunlight, then referred to as *photoreduction*. This is the most important reason why the Mn(II) concentration is relatively high at the ocean surface. The relative speed of photoreduction compared to oxidation is important for dissolved Mn availability. A higher oxidation rate means more scavenging, hence more Mn export.

Manganese enters the ocean by several means. The first of these sources, dust deposition, is a second reason for high surface [Mn(II)]. Especially in the central/north Atlantic Ocean surface dust input is high from the Sahara [24, 47, 44, 97, 108]. Rivers are another source of Mn to the ocean [8, 95]. Anoxic or suboxic shelves are a diffusive source of Mn(II), because sediment microorganisms reduce MnO_x if there is no more oxygen (or nitrate) left [12, 20, 110]. Finally,

hydrothermal sources show pronounced localised elevations in [Mn(II)] [13, 19, 21, 70, 140, 141].

7.2 Methods

7.2.1 Model framework

In order to model the three-dimensional distribution of dissolved Mn, the biogeochemical model PISCES has been used [96, 100]. This model has been employed for many other studies concerning trace metals, as well as large scale ocean biogeochemistry [e.g. 96, 106, 119, 120, 137, 158 or Chapter **??**, 167 or Chapter **??**]. In the simulations described here, PISCES has been driven by climatological velocity fields obtained from the general circulation model called *Nucleus for European Modelling of the Ocean* (NEMO) [116], of which the dynamical component is called *Océan PArallélisé* (OPA) [62].

The model PISCES simulates the cycles of carbon, the major nutrients (nitrate, phosphate, ammonium, silicic acid) and the trace nutrient iron, along with two phytoplankton types (nanophytoplankton and diatoms), two zooplankton grazers (micro- and mesozooplankton), two classes of particulate organic carbon (small and large) of differential settling speeds, as well as calcite and biogenic silica. PISCES distinguishes three silicon pools: the silicon content of living diatoms (Si_{diat}); the silicon content of dead, settling diatoms (Si_{biog}) and dissolved silicic acid (Si_{diss}). In the model, Si_{diss} and other nutrients are supplied to the ocean by means of atmospheric dust deposition and rivers. For iron an additional source is sediment remobilisation [96]. The standard version of PISCES accounts for 24 tracers. For a more detailed description of PISCES refer to Chapter 3.

In this study PISCES is run off-line forced by a climatological year of monthly physical fields including turbulent diffusion. All model fields are defined on the ORCA2 grid, an irregular grid covering the whole world ocean with a nominal resolution of $2^\circ \times 2^\circ$, with the meridional (south–north) resolution increased near the equator. It has two 'north poles' in Canada and Russia to eliminate the coordinate singularity in the Arctic Ocean. Its vertical resolution is 10 m in the upper 100 m, increasing downwards to 500 m, such that there are 30 layers in total, and the ocean has a maximum depth of 5000 m.

7.2.2 Manganese model

tracer:	concentration:	biochemical form:
Mn(II)	M_{diss}	dissolved Mn(II): Mn^{2+}
MnO_x	M_{ox}	Mn(III,IV,...) oxides: MnO_x
Mn_{react}	M_3	hydrothermal Mn
Mn_{phyt}	M_{phyt}	nanophytoplankton incorporated Mn
Mn_{pbiog}	M_{pbiog}	dead nanophytoplankton Mn
Mn_{diat}	M_{diat}	diatom incorporated Mn
Mn_{dbiog}	M_{dbiog}	dead diatom Mn

Table 7.1: Manganese tracers in PISCES: name of tracer referred to in text, mathematical notation for its concentration and the description.

Figure 7.1 presents the model scheme. The tracers presented there are explained in Table 7.1. In this section all sources and processes (the arrows) are discussed and quantified. We assume that there already is a biogeochemical carbon cycle in the underlying model, including at least one type of phytoplankton and sediment, hydrothermal, fluvial and dust sources of

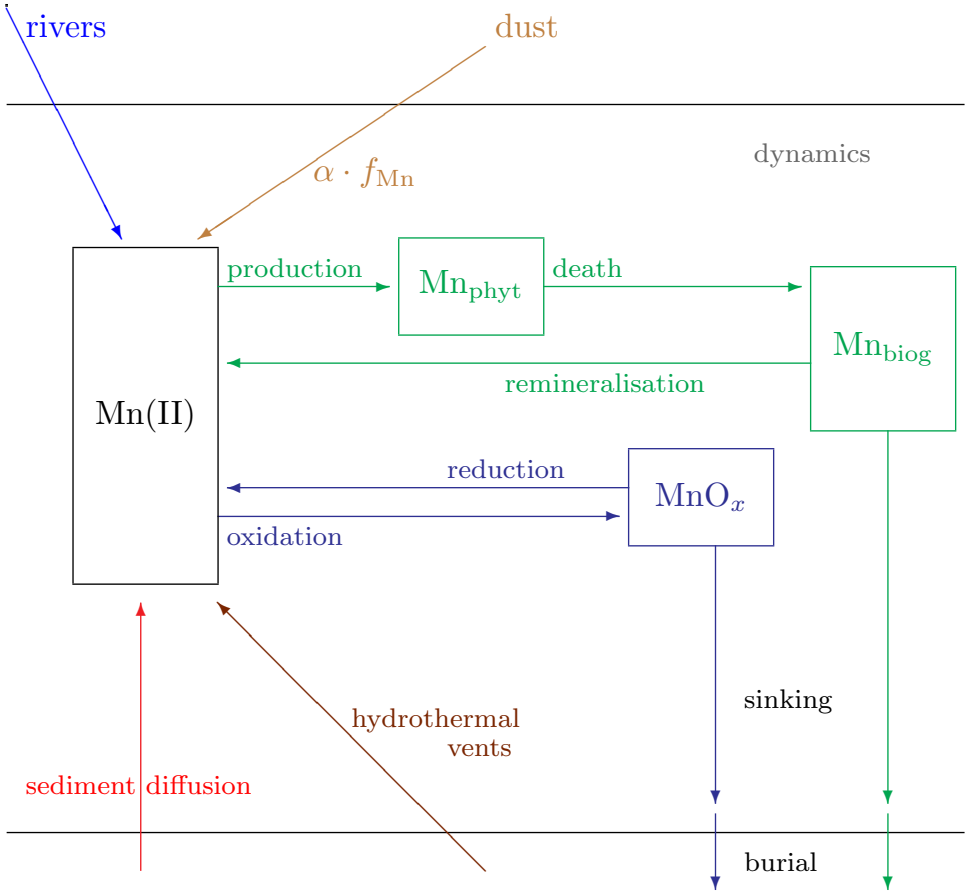

Figure 7.1: Model scheme. Biology in green; redox and scavenging in blue; dynamics in grey; and the sources dust, rivers, hydrothermal and sediment are in light brown, light blue, dark brown and red, respectively. Symbols are explained in Table 7.1.

iron. They can then be converted by the respective empirically determined Mn/Fe conversion factors. Furthermore, a climatological forcing of the ocean dynamics must be available if the biogeochemical model is run offline. Our model can be implemented in any such biogeochemical ocean model, among which PISCES (Section **??**).

7.2.2.1 Sources

Manganese enters the ocean mostly by dust deposition, but over large shelf and slope regions (e.g. polar oceans) the flux of Mn(II) from the shelf and slope regions is of the same order as or larger than the dust deposition flux [140, 162]. Also rivers are important. Finally, in the deep ocean hydrothermal vents play an important role in Mn addition. This section describes how these sources are modelled.

Atmosphere. From observations in the Atlantic Ocean dust deposition appears an important source of Mn, since in the surface of the Atlantic Ocean large amounts of Mn are present (data from R. Middag). The high dissolved Mn concentration is strongly enhanced by photoreduction. This is and important process that keeps the [Mn(II)] in the photic layer notably higher compared to the aphotic zone [45]. The dust deposition field used in this model is taken from Hauglustaine et al. [77]. Figure 3.4a presents the average of the twelve-month climatology. The total dust deposition is 599 $\mathrm{Tg\,yr^{-1}}$.

The average mass fraction of Mn in the Earth's upper crust is known to be 527 ppm [50]. However, the fraction measured in Saharan dust is 880 ppm [134], consistent with Guieu et al. [44] and Statham et al. [63]. Since most of the dust deposition in the Atlantic Ocean originates from the Sahara and our focus is the Atlantic Ocean, here the value of 880 ppm is used.

Solubility of Mn from dust is uncertain and relatively high compared to most other trace metals. Here $\alpha_{\mathrm{Mn}} = 30\,\%$ of the Mn in dust is assumed to be dissolved, largely consistent with the values reported by Guieu et al. [44], Jickells [47], Baker et al. [97], De Jong et al. [108], Buck et al. [130]. Several studies report even higher values ($> 50\,\%$) which are, however, mainly from anthropogenic or otherwise manipulated dust, while the lower reported values ($< 50\,\%$) are from natural dust, mainly of Saharan origin.

Manganese in dust is added to the pool of Mn(II) in the upper model layer:

$$\frac{\partial M_{\mathrm{diss}}}{\partial t}\Big|_{z=0} = \frac{\alpha_{\mathrm{Mn}} \cdot f_{\mathrm{Mn}}}{m_{\mathrm{Mn}} \cdot \Delta z_1} \cdot \Phi_{\mathrm{dust}} \,, \tag{7.1}$$

where M_{diss} is [Mn(II)], $z = 0$ denotes the upper model layer, m_{Mn} is the atomic mass of Mn, Δz_1 the upper model layer thickness and Φ_{dust} is the total dust deposition flux (mass per area per time), and α_{Mn} is the dissolution fraction.

Rivers. Rivers are another source of Mn to the ocean, which is important for marine primary production [151 and references therein]. Manganese enters the coastal area both in dissolved and particulate form, but upon entering the open ocean, much of both forms is scavenged [151]. Scavenging in estuaries and margins is not taken into account here, since it is not part of global ocean models (coarse resolution).

We assume the presence of a fluvial source of iron in the underlying model. The relative input into the ocean by rivers is given by Figure 3.4b. The effective inflow of Fe into the open ocean is corrected for scavenging that is not resolved by the model. Furthermore, we assume that Mn near the boundaries is scavenged with the same relative rate as Fe, using an average fluvial concentration ratio between dissolved Mn and Fe. River concentrations are [$\mathrm{Fe_{diss}}$]=700 nM and [Mn(II)] =150 nM [102 p. 2], resulting in a ratio $f^{\mathrm{riv}}_{\mathrm{Mn:Fe}} = 0.214$, much higher than the crustal ratio which is about 0.0205. Even though the measurements are not recent and do not need to represent a good average over the important world rivers, it is certainly more reasonable to use this value instead of the crustal ratio. The concentration change of Mn(II) due to river input becomes:

$$\frac{\partial M_{\mathrm{diss}}}{\partial t}\Big|_{\mathrm{rivers}} = f^{\mathrm{riv}}_{\mathrm{Mn:Fe}} \cdot \frac{\partial F_{\mathrm{diss}}}{\partial t}\Big|_{\mathrm{rivers}} \,, \tag{7.2}$$

where F_{diss} is the dissolved iron concentration. This fluvial concentration change only takes place in the upper gridbox nearest to the river outflow.

Shelves. A third important source of Mn to the ocean are shallow sediments, mostly found on the shelves (presented in red in Figure 7.1) [110, 141]. The underlying process for this flux of Mn(II) out of sediments is the reduction of MnO_x in the anoxic environment in the sediment and subsequent diffusion into the bottom water. This process is the same as for sediment diffusion of dissolved Fe, which is present in the underlying model [96]. Hence we will base the Mn source on the parameterisation of that of Fe. Iron diffusion out of the sediment has been modelled as a function of bathymetry. This accounts, in first order, for the degree of oxygenation of the sediments.

This simple parameterisation is a big improvement to several of the other attempts to model this highly unknown source. Moore et al. [81] used a step function setting the iron flux to $2\,\mu\mathrm{mol\,Fe\,m^2\,d^{-1}}$ for depths of less than 1100 m and 0 in the deep ocean. They note

that "[i]nputs are likely too low in shallow, highly productive regions and too high in deeper areas underlying lower productivity waters. However, even this simple parameterization notably improves the model results in several regions." Arguably, Aumont and Bopp [96] improved this parameterisation further by making Fe input relatively large in the upper 200 m and much smaller below 500 m. Further improvements have been made by Moore and Braucher [117].

For Mn the same approach is used. However, manganese reduction results in a higher free energy reduction than Fe reduction, so that Mn reduction takes place more easily and thus before Fe oxides are reduced [102 pp. 232–236]. There are further uncertainties, among which the amount of Mn oxides available in the sediment. Therefore, we simply model Mn addition from the shelves proportional to Fe addition, weighed with the crustal ratio $f^{\text{sed}}_{\text{Mn:Fe}}$:

$$\frac{\partial M_{\text{diss}}}{\partial t}\Big|_{\text{sediments}} = f^{\text{sed}}_{\text{Mn:Fe}} \cdot \frac{\partial F_{\text{diss}}}{\partial t}\Big|_{\text{sediments}} . \tag{7.3}$$

The (redox) reactions in the sediment are not explicitly modelled, since the sediment is not part of our model domain. Therefore, addition from the sediment is modelled as a prescribed source, which is presented by Figure 3.4c. When integrating the yearly manganese flux ($\text{mmol}\,\text{m}^{-2}$), one gets a total Mn input of 162 $\text{Gmol}\,\text{Mn}\,\text{yr}^{-1}$.

Alternatively to using the crustal ratio, actual pore water concentrations of dissolved Fe could be compared with Mn(II). Using the concentrations in the top 5 cm of the sediments studied by Bortleson and Lee [7], an average concentration of Mn and Fe of respectively 1.94 and 59 mg/g has been derived. Its ratio is 0.0328, about 50% higher than the crustal ratio.

Hydrothermal. This source can be modelled in the same way as ^{3}He [e.g. 66, 76] and iron [26, 71, 137]. The ^{3}He source is presented in Figure 3.4d. Tagliabue et al. [137] used a dissolved Fe/^{3}He molar ratio of $4.5 \cdot 10^8$ and assumed that 0.2% enters the open ocean. The rest (99.8%) is scavenged [41] and not modelled explicitly. We used an upper crustal concentration of Mn 580 ppm [50] to arrive at the effective Mn/Fe input ratio. Again it is assumed that scavenging of Mn occurs with the same rate as that of Fe.

Instead of adding Mn from hydrothermal vents to the Mn(II) pool, it was decided to include this in a separate pool. This pool is named here Mn_{react}, of which its concentration is referred to as M_3. The added Mn_{react} is removed from the model domain according to

$$\frac{\partial M_3}{\partial t}\Big|_{\text{hydroth}} = \lambda_{\text{Mn}} \cdot M_3 \ , \tag{7.4}$$

where λ_{Mn} is the decay rate. There is no interaction between Mn_{react} and the other tracers in the model. The rationale for modelling this tracer separate from the rest of the model is the fact that the region around hydrothermal vents is highly reactive.

Modelling this source as a simple addition to the Mn(II) pool results in a notable overestimation of [Mn(II)] everywhere in the Southern Ocean (results not presented). Observations of Bruland et al. [43] show that in the deep central North Pacific Ocean the ratio $[\text{Mn}_{\text{part}}]/[\text{Mn}_{\text{diss}}]$ is around 0.2. The reduction rate in the aphotic zone $k^{\text{AZ}}_{\text{red}}$ is chosen such that $k_{\text{ox}}/k^{\text{AZ}}_{\text{red}} = 0.2$ (see Section 7.2.2.2). In the model we assume that this is valid at any location in the aphotic zone of the ocean. It appears that at least near hydrothermal vents this assumption is false. Consider the idealised model of Lavelle et al. [41] to get to this conclusion. In this study Mn is partitioned into three size classes with different settling velocities. In equilibrium their dissolved Mn T_d and small Mn particles T_p are partitioned such that $T_p/T_d = 0.3$, while small and big particles T_s are partitioned as $T_s/T_p = 1$. Hence, all particles versus dissolved is $(T_s + T_p)/T_d = 0.6$, which is three times the value derived from Bruland et al. [43]. Small particles in the model of Lavelle et al. [41] settle with a small velocity of $0.1\,\text{m}\,\text{d}^{-1}$ and large particles with a large

velocity of the order of $100\,\mathrm{m\,d^{-1}}$. Even if the small particle pool is added to the dissolved pool, there the particulate/dissolved fraction would still be 50 % higher than that found by Bruland et al. [43] and the settling velocity of the (big) particle pool is 87 times as high! In other words, the biogeochemistry appears different near hydrothermal vents compared to the central North Pacific Ocean.

Biology probably plays an important role in this. For instance, $\mathrm{Mn_{react}}$ may include an intermediate product between Mn(II) and MnO_x, namely Mn(III) [84, 94]. Furthermore, scavengers and bacteria help removing Mn(II) near hydrothermal vents. These processes are too detailed and too uncertain to model explicitly. Hence the extra tracer M_3 is introduced.

7.2.2.2 Internal processes

Redox. Reduction of manganese oxides (MnO_x), presented in blue in the model scheme (Figure 7.1), is a combination of several processes. Firstly, MnO_x is subject to non-biological reduction, significantly stimulated by sunlight [e.g. 45]. Furthermore, the rate of oxidation is also mediated by microbes (certain bacteria and fungi) [45, 91], and it depends on the $\mathrm{O_2}$ concentration and pH. This is observed in the North Pacific Ocean [53 and references therein]. However, measurements from the West Atlantic Ocean and Zero Meridian Southern Ocean GEOTRACES cruises do not show a clear minimum of [Mn(II)] between the photic and oxygen minimum zones. This gives motive for not adding the dependency on $[\mathrm{O_2}]$ to the model for a first approximate simulation of [Mn(II)]. Hence, here we chose to model Mn following pseudo-first-order reactions where k_{ox} and k_{red} are pseudo-first-order rate constant (conventional primes omitted, e.g. Stone and Morgan [37]):

$$\begin{aligned} \frac{\partial M_{\mathrm{diss}}}{\partial t}\Big|_{\mathrm{redox}} &= -k_{\mathrm{ox}} M_{\mathrm{diss}} + k_{\mathrm{red}} M_{\mathrm{ox}} \\ \frac{\partial M_{\mathrm{ox}}}{\partial t}\Big|_{\mathrm{redox}} &= k_{\mathrm{ox}} M_{\mathrm{diss}} - k_{\mathrm{red}} M_{\mathrm{ox}} \ , \end{aligned} \tag{7.5}$$

where

$$k_{\mathrm{red}} = \begin{cases} k_{\mathrm{red}}^{\mathrm{PZ}} & \text{in the photic zone} \\ k_{\mathrm{red}}^{\mathrm{AZ}} & \text{elsewhere} \end{cases} \tag{7.6}$$

Other causes for reduction or oxidation may also play a role (e.g. Mn-oxidising bacteria, Sunda and Huntsman [45], Von Langen et al. [59]), but for now we assume these to be included in the redox rate constants. These constants are tuned to get the correct ratio between the particulate (assume: oxidised) Mn and dissolved Mn [43] concentrations. If we want the redox rate constants to depend on inhomogeneously distributed quantities like bacterial distribution or oxygen concentration, the equations may need to be modified.

We assume that the process of oxidation is strongly mediated by adsorption onto particles. Adsorption and desorption are not modelled explicitly either. Rather, we assume that the MnO_x is instantaneously adsorbed onto a homogeneous omnipresent pool of particles. Instead, $\mathrm{Mn_{ads}}$ can be modelled implicitly by changing the settling speed (Section 7.3.4).

Production and remineralisation. The model's biology is presented in Figure 7.1 in green. Manganese is incorporated into phytoplankton during growth (henceforth, *production*). Incorporation of Mn can be modelled proportional to the change in phytoplankton carbon concentration. In the following model equations, the terms *prod, resp, mort, graz* and *diss* stand respectively for the change of the carbon pool due to production, respiration, death, grazing and dissolution of each of the modelled phytoplankton functional types and its detrital products. Assuming that grazed Mn is instantaneously excreted as Mn(II) and the Mn/C ratio is

Process:	Parameter:		Value:	Sources:
Dust deposition	Mn fraction	$f_{\mathrm{Mn}}^{\mathrm{dust}}$	696–**880** ppm	Wedepohl [50], Mendez et al. [134]
	solubility	α_{Mn}	10–70 (**30**) %	Baker et al. [97]
Sediment diffusion	Mn/Fe ratio	$f_{\mathrm{Mn:Fe}}^{\mathrm{sed}}$	0.0328	Bortleson and Lee [7]
Rivers	Mn/Fe ratio	$f_{\mathrm{Mn:Fe}}^{\mathrm{riv}}$	0.2143	Sarmiento and Gruber [102 p. 2]
Hydrothermal	Mn fraction	$f_{\mathrm{Mn}}^{\mathrm{hydro}}$	696–880 (**716**) ppm	Wedepohl [50]
Settling of MnO_x	settling speed	w_s	$0.9 - 1.4$ (**1.15**) $\mathrm{m\,d^{-1}}$	Roy-Barman [125]
Oxidation	rate constant	k_{ox}	$0.34 \times 10^{-3}\,\mathrm{h^{-1}}$	Sunda and Huntsman [45], Bruland et al. [43]
Reduction	rate constant	$k_{\mathrm{red}}^{\mathrm{PZ}}$	$0.098\,\mathrm{h^{-1}}$	Sunda and Huntsman [45], Bruland et al. [43]
	rate constant	$k_{\mathrm{red}}^{\mathrm{AZ}}$	$1.7 \times 10^{-3}\,\mathrm{h^{-1}}$	Sunda and Huntsman [45]
Decay rate Mn(III)	rate constant	λ_{Mn}	$0.54 \times 10^{-3}\,\mathrm{h^{-1}}$	–
Biology	Mn/P ratio	$R_{\mathrm{Mn:P}}$	0.33–5 (**0.36**) ‰	Twining and Baines [165]
Settling of POM	settling speed	w_s'	$3.5 - 200\ \mathrm{m\,d^{-1}}$	Aumont and Bopp [96 supplement]

Table 7.2: Mn model parameters. There are two reduction parameters, one for the photic zone (PZ) and one for the aphotic zone (AZ). If an uncertainty range is given, the value used in the reference simulation are presented in boldface.

kept constant throughout all processes, the resulting biology equations are:

$$\frac{\partial M_{\text{phyt}}}{\partial t} = R_{\text{Mn:C}} \cdot (prod - resp - mort - graz) \ , \tag{7.7}$$

$$\frac{\partial M_{\text{pbiog}}}{\partial t} = R_{\text{Mn:C}} \cdot (mort + graz - diss) \ , \tag{7.8}$$

$$\frac{\partial M_{\text{diss}}}{\partial t} = R_{\text{Mn:C}} \cdot (-prod + resp + diss) \ . \tag{7.9}$$

Here C_{phyt} is the concentration of carbon in phytoplankton and C_{pbiog} is the concentration of phytoplankton detrital carbon, or Particulate Organic Carbon (POC). The extended Redfield ratio for Mn is represented by $R_{\text{Mn:C}} = R_{\text{Mn:P}} \cdot R_{\text{P:C}}$, where $R_{\text{Mn:P}}$ is the extended ratio (as it is usually reported), and $R_{\text{P:C}} = 1/106$ is the inverse of the Redfield C/P ratio. There is no growth limitation of phytoplankton by shortage of Mn(II).

The generalised Redfield ratio between manganese and phosphorus (Mn/P) varies from $0.33 \cdot 10^{-3}$ to $5 \cdot 10^{-3}$ [165]. The lower values are common, and Twining and Baines [165] note in their review paper that high values are from measurements that do not represent the correct open ocean stoichiometry, because they are from coastal waters or there is Mn adsorbed onto the particles. Twining and Baines [165] give a sort of consensus value of $0.36 \cdot 10^{-3}$, close to the observation of $0.38 \cdot 10^{-3}$ in the Southern Ocean [141]. However, Mn/P is much higher in the Arctic [140], namely $(3\text{–}10) \cdot 10^{-3}$, but probably other processes besides biological incorporation and remineralisation play a role here.

There are two types of phytoplankton in the model, nanophytoplankton and diatoms. Manganese is incorporated in both types. Since Mn is also an essential nutrient for zooplankton, in the future incorporation into the two modelled types of zooplankton (microzooplankton and mesozooplankton) may be included. The Mn model may even be extended to include growth limitation of phytoplankton by shortage of Mn(II). Equations **??**–**??**, and phytoplankton growth equations, would have to be extended accordingly if we wanted to model the biological ecosystem as completely as possible in PISCES. However, since this is the first global Mn model, the choice is here to keep it as simple as possible and only include the lowest trophic level for Mn cycling.

Settling and burial. There are two forms of settling Mn particles: oxidised/adsorbed particles and biogenic (Mn in dead particles which were incorporated during growth). Both are denoted here as M_{part}, both sink with some speed w_s:

$$\frac{\partial M_{\text{part}}}{\partial t}\Big|_{\text{settling}} = -\frac{\partial}{\partial z}(w_s \cdot M_{\text{part}}) \ . \tag{7.10}$$

They are buried when arriving at the ocean floor, which means that they are removed from the model domain. The addition of reduced Mn from sediments is a prescribed forcing, unrelated to the removal (Section 7.2.2.1).

The settling speed depends on the type of particle with which Mn is associated. Here w_s is different for incorporated Mn ($w_s' \geq 2 \ \text{m d}^{-1}$) and oxidised/adsorbed Mn ($w_s < 1.4 \ \text{m d}^{-1}$).

7.2.3 Simulations

The reference simulation uses $w_s = 1.15 \ \text{m d}^{-1}$, but only if $[\text{MnO}_x] > 25$ pM, keeping [Mn(II)] in check while still providing a deep ocean sink. The rational for not settling MnO_x below a certain threshold is that MnO_x is not heavy enough to sink by itself and it is not adsorbed to sufficiently heavy particles. Only if a critical concentration is reached (loosely a saturation concentration), aggregation of MnO_x colloids starts to form heavier particles that can settle.

Simulation	Short name	Difference with reference simulation
Reference simulation	`REFSIM`	-
No threshold	`NOTHRESH`	No threshold concentration for MnO_x
No biology	`NOBIO`	Biology for Mn(II) is turned off
Rivers excluded	`NORIV`	Without fluvial input of Mn(II)
Sediments excluded	`NOSED`	Without sediment diffusion of Mn(II)

Table 7.3: List of simulations.

Concentrations of Mn(II) and MnO_x were initialised such that [Mn(II)] is around 0.12 nM everywhere in the aphotic zone, a little less than the deep ocean average in the West Atlantic GEOTRACES observations. From that point the reference simulation was spun up for 600 yr, while from year 500 several sensitivity simulations were forked off.

In Table 7.3 all simulations are listed. The parameters for the reference simulation are listed in Table 7.2. The other simulations are variations on the reference simulation.

7.2.4 Observations

The following observational data sets are used for comparison with the model output:

- Pacific Ocean, VERTEX-4 [43 station near Hawaii]
- Pacific Ocean, Kilo Moana 2006 [136]
- Arctic Ocean, ARK XXII/2 [140]
- Southern Ocean, ANT XXIV/3 [141]
- West Atlantic Ocean, 64 PE *N* and JC057 [170]
- Pacific Ocean, CLIVAR P16 (unpublished data from Angela Milne and William Landing)

Of these observations, those of Middag et al. [170], together with the Zero-Meridian part of Middag et al. [141] are used for detailed visual comparison in Section 7.3. These measurements have been verified versus international reference samples and their consensus values of the SAFe and GEOTRACES programmes. The focus of this study is the West Atlantic Ocean for several reasons. Firstly, recently measurements have been carried out in that region, resulting in a large consistent (one method) dataset. Secondly, there are too few high-quality observations in other regions of the ocean, making it very difficult to define a reasonable goodness of fit. Thirdly, the West Atlantic Ocean is of large importance to the AMOC and hence the deep ocean cycling of nutrients. For these reasons all quantitative arguments in this study concern the West Atlantic GEOTRACES section.

For the visual comparison between model and observations, horizontal and vertical cross sections of the model data are plotted. Using the same colour scale observations are plotted as coloured dots to directly compare the model with the observations. Horizontal [Mn(II)] sections are presented for four different depths, where 'surface' signifies the average over the upper 30 m, '500 m' is 400–600 m averaged, '2500 m' is 2300–2700 m averaged and '4500 m' is 4000–5000 m averaged. The colour scale is not linear to better show the main features at both low and high concentrations of Mn(II). The vertical [Mn(II)] sections are calculated from the three-dimensional model data by converting the ORCA2 gridded model data to a rectilinear mapping and interpolating the rectilinear data onto the cruise track coordinates.

7.3 Results

7.3.1 Reference simulation

Figures 7.2 and 7.3 show the modelled and measured (dots) dissolved Mn concentration at four depths and in the West Atlantic Ocean for the reference simulation (`REFSIM`). The general characteristics of high [Mn(II)] at the ocean surface and lower concentrations in the deep ocean is reproduced by the model. Also low concentrations in the Southern Ocean are simulated well. However, in the West Atlantic Ocean at intermediate depths (200–3000 m) south of 40°N, the model overestimates [Mn(II)]. The model appears to show the effect of the AMOC and/or reversible scavenging, while the observations do not show that. Rather the observations show a relatively homogeneous distribution of Mn(II), except near the surface and near hydrothermal vents.

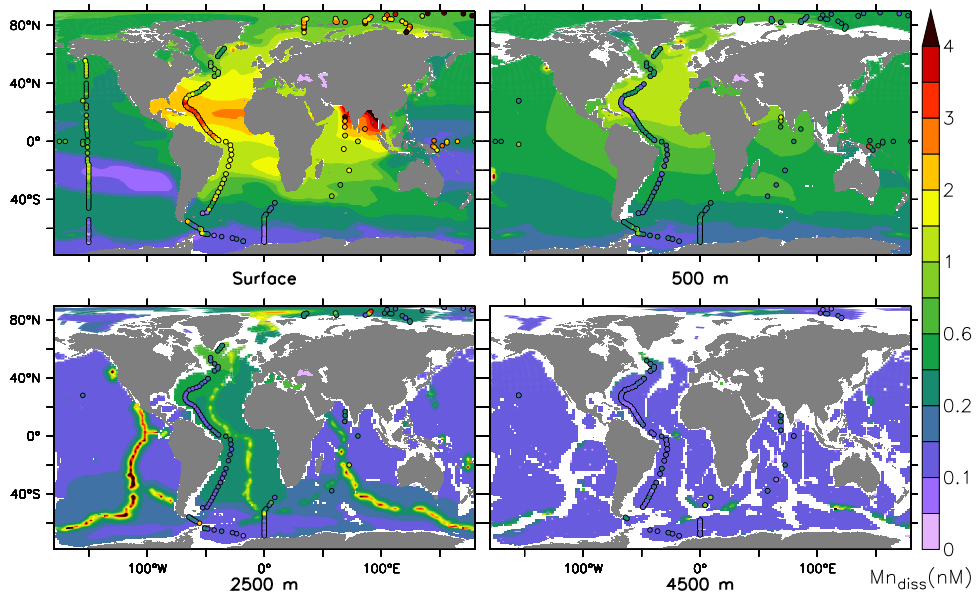

Figure 7.2: [Mn(II)] (nM) at four depth layers in the world ocean for the reference simulation (`REFSIM`). Observations are presented as coloured dots.

7.3.2 Sources of manganese

Rivers. Figure 7.4 shows the effect of fluvial sources on the [Mn(II)] distribution. After entering the ocean, Mn(II) is advected by the currents before it is oxidised/adsorbed and settles towards the seafloor. E.g. in the immediate neighbourhood of outflow of the Amazon River [Mn(II)] increased by at least 0.3 nM, while further upstream (following the North Brazil Current) the increase is at least 0.1 nM. Values may be higher or extend farther after running the model to a steady state, which is not yet the case for this simulation.

Shelves. Figure 7.5 shows the effect of shelf sediment sources on the [Mn(II)] distribution. The effect is much larger (after a shorter time) compared to the river simulation (different colour scale). Consistent with the sediment simulation of Van Hulten et al. [158], increases are relatively large in the Arctic Ocean, North Atlantic Ocean and in the Indian Ocean. There is almost no increase in the Southern Ocean. Even the relative difference (not presented here) does not show much of an increase in the Southern Ocean, while it should based on observations [162].

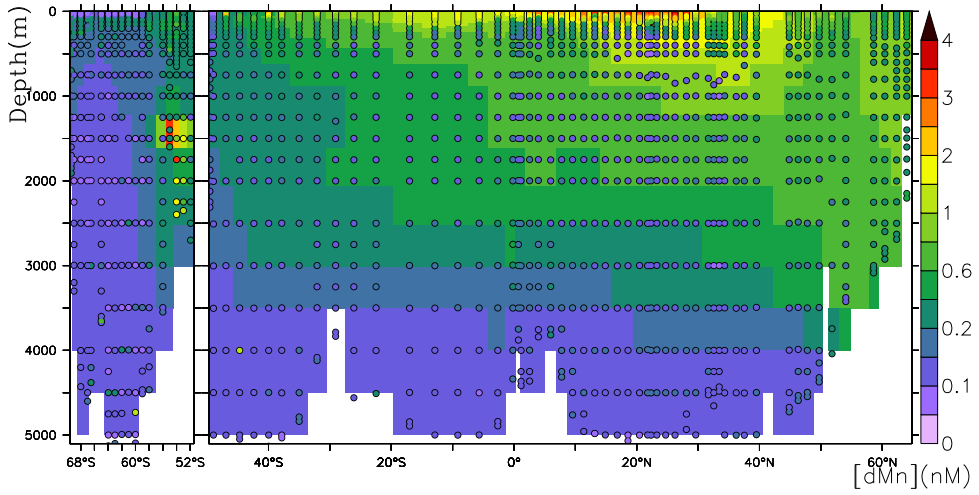

Figure 7.3: [Mn(II)] (nM) at the West Atlantic and Zero Meridian GEOTRACES cruise sections for `REFSIM`. Observations are presented as coloured dots.

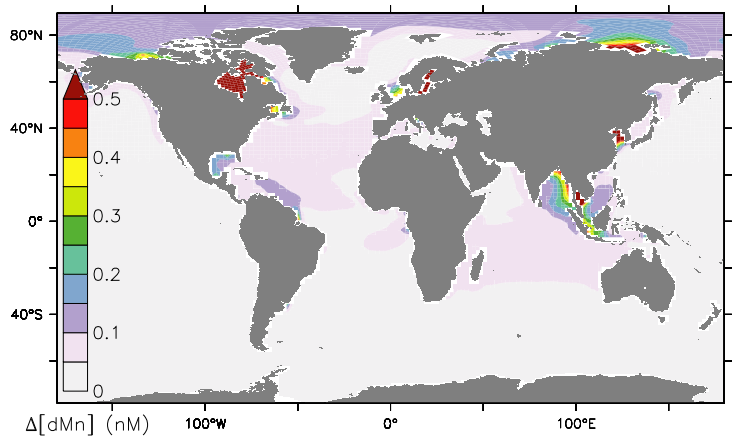

Figure 7.4: Difference between [Mn(II)] of simulations with and without river input of Mn(II) at the ocean surface. Changes below the mixed layer are negligible hence not plotted. Average over year 57.

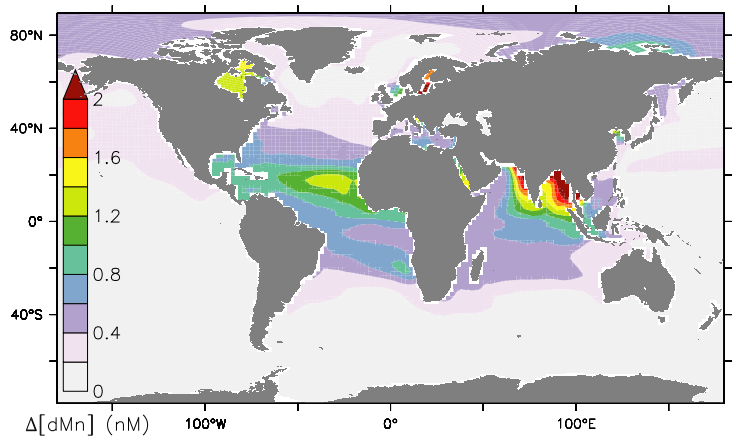

Figure 7.5: Difference between [Mn(II)] of simulations with and without shelf input of Mn(II) at the ocean surface. Changes below the mixed layer are negligible hence not plotted. Average over year 20 after forking from REFSIM.

Hydrothermal. Figure 7.6 shows the contribution from hydrothermal vents. Since outflux of Mn is high and removal from the model domain is fast, the pattern is very similar to that of Figure 3.4d, especially at 2500 m depth, where most hydrothermal activity takes place.

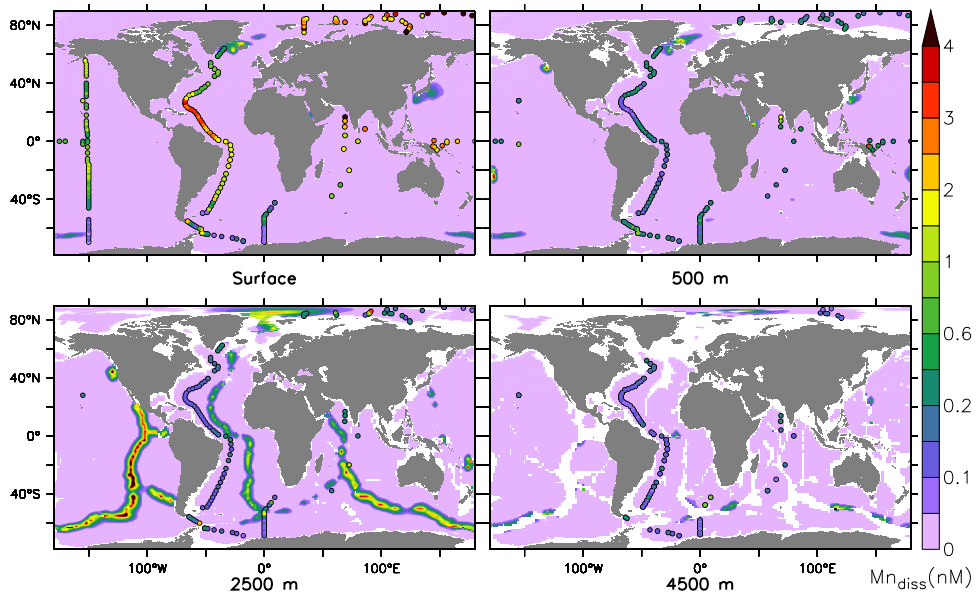

Figure 7.6: Hydrothermal-vent derived dissolved Mn concentration (nM) at four depths. This is a separate tracer in the model, hence plotted as an absolute concentration.

7.3.3 Effect of biology

Figure 7.7 shows the effect of biology in the ocean. There is a decrease in the ocean surface and an increase in the deep ocean.

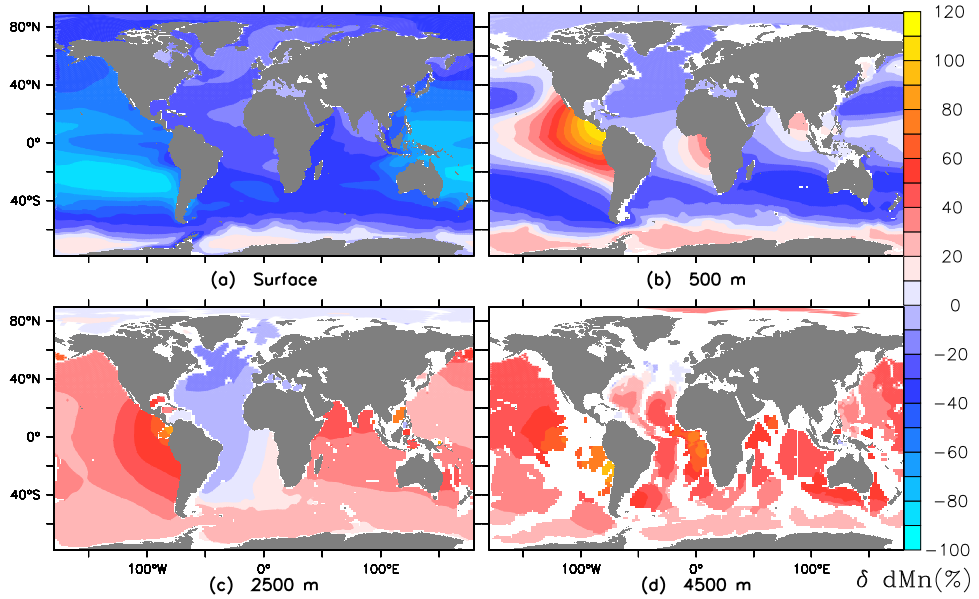

Figure 7.7: [Mn(II)] difference between a simulation with biology (`REFSIM`) and a corresponding one without biology (`NOBIO`), at four depths in the world ocean after 152 yr with biological incorporation and subsequent remineralisation of Mn.

7.3.4 Unconstrained settling

The limitation on settling of MnO_x as explained in Section 7.2.3 is introduced to keep [Mn(II)] in check. For this simulation (`NOTHRESH`) the limitation is removed. Figure 7.8 presents the yearly average concentration of Mn(II) 100 yr after forking from `REFSIM`.

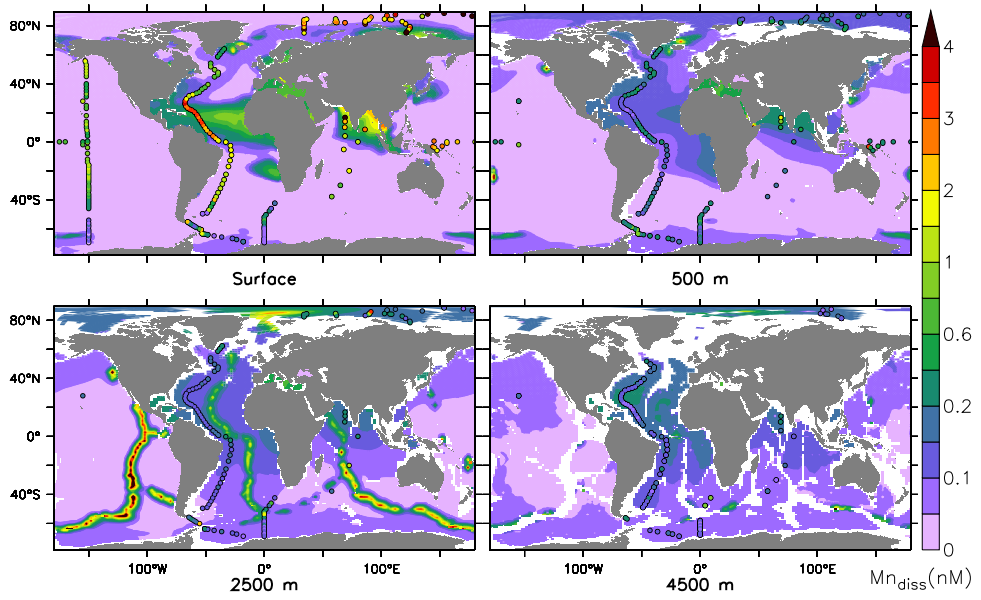

Figure 7.8: [Mn(II)] (nM) at four depth layers in the world ocean for the simulation with unconstrained settling of MnO_x (`NOTHRESH`) (after 100 yr).

Everywhere in the ocean [Mn(II)] is noticeably underestimated (except near the hydrothermal vents, but the dissolved hydrothermal Mn is a tracer subject to equations different from those of Mn(II)). Indeed, the correlation coefficient r (comparing the model with the observations) is significantly decreased (more than 2σ; see Section **??** for the criterium) in `NOTHRESH` in comparison to `REFSIM`, showing that the distribution of Mn(II) is less well represented. However, the Root Mean Square Deviation (RMSD) is significantly decreased, suggesting an *improvement*. This is possible since [Mn(II)] at intermediate depth was strongly overestimated in `REFSIM`, while it is close to the observations in `NOTHRESH`.

Smaller settling velocity `This simulations has not yet been performed -- discuss whether it should.`

Section	Short name	Spin-up time (yr)	$D_{\updownarrow}$ (nM)	σ (nM)	Significance	$r_{\updownarrow}$	σ	Significance
7.3.1	REFSIM	600	0.429	0.018	-	0.808	0.013	-
7.3.4	NOTHRESH	100	0.242	0.014	improvement	-0.071	0.097	worsening
7.3.2	NORIVER	57	0.114	0.008	n/a	0.899	0.004	n/a
7.3.2	NOMARGIN	20	0.125	0.009	n/a	0.898	0.004	n/a
7.3.3	NOBIO	200	1.107	0.038	n/a	0.765	0.016	n/a
			lower RMSD	upper RMSD		lower r	upper r	
	REFSIM	2-sigma range:	**0.39**	**0.47**		**0.78**	**0.83**	

Table 7.4: Statistical model–data comparison for [Mn(II)] at the GEOTRACES West Atlantic section. $D_{\updownarrow}$ denotes the vertically adjusted Root Mean Square Deviation and $r_{\updownarrow}$ the correlation coefficient. σ denotes the standard deviation for the respective statistics (see Section **??** for the method).

7.4 Discussion

Many of the properties of the Mn(II) distribution in the world ocean are reproduced (Section 7.3.1). Shortcomings are visible, among which the overestimation of [Mn(II)] at intermediate depths in the West Atlantic Ocean, and an underestimation of [Mn(II)] in the mixed layer of the Pacific Ocean (Figure 7.2). These apparent details may be related to a fundamental part of the model. Scavenging and aggregation are parameterised as a step function of [MnO_x] and [Mn(II)] (see Section 7.2.3). This is a drastic simplification of the underlying processes, which makes it very difficult to test them. There are several alternative possibilities that may keep [Mn(II)] in check.

Firstly, oxidation is mediated by microbes (bacteria and fungi) [91]. These organisms may prevent MnO_x from settling. However, there are neither bacteria nor fungi in PISCES. Even if there were, probably not all of these organisms would mediate oxidation. One may guess that this occurs only in the upper 200 m of the ocean, since there gradients in [O_2] are high [e.g. 160].

Secondly, a more explicit model for adsorption/desorption may be needed. Possibly much of the MnO_x is not settling; then another tracer Mn_{ads} is needed that is settling oxidised Mn (in adsorbed or aggregated form; doesn't matter). The adsorption should not take place on a homogeneous pool of particles, but rather on e.g. $CaCO_3$ [17] or lithogenic particles [125].

One may think that there is too much MnO_x produced compared to Mn(II), i.e. the ratio k_{ox}/k_{red} is too high. However, the k values are tuned to get values consistent with the ratio of concentration measurements of MnO_x and Mn(II). In Figure 7.9 the MnO_x/Mn(II) concentration ratio is plotted. The left panel shows that in the deep ocean this ratio is about 0.2, and the upper ocean (right panel) shows a value of less than 0.004, both consistent with Bruland et al. [43]. Interestingly, when removing the threshold for settling of MnO_x (`NOTHRESH`), the

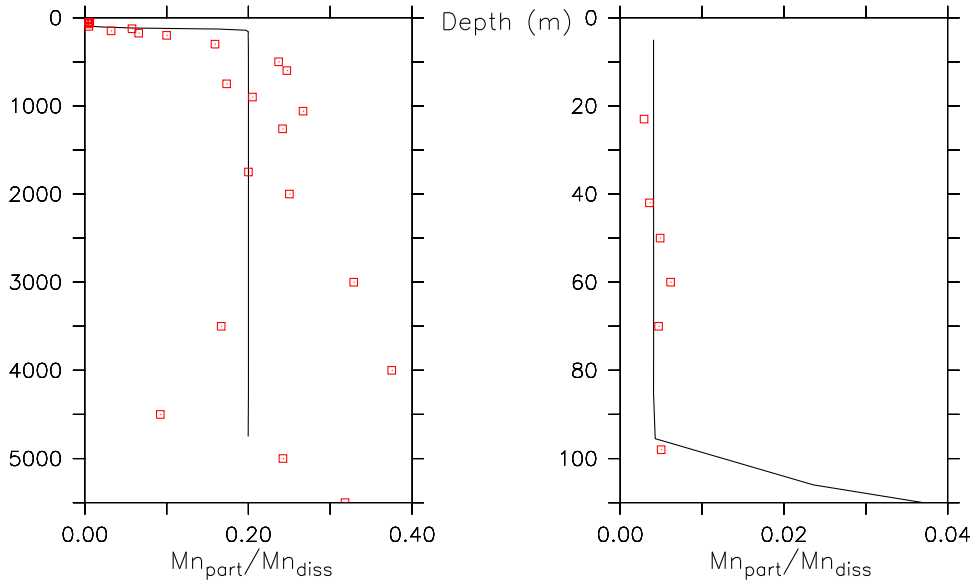

Figure 7.9: [Mn_{part}]/[Mn(II)] in the Pacific Ocean at VERTEX-IV (near Hawaii) at full depth (left) and in the upper 110 m (right). Squares are observations; the line is the model.

[MnO_x]/[Mn(II)] ratio in the photic zone increases too much. This suggests that k_{red}^{PZ} needs to be higher. That would result in higher and hence more realistic [Mn(II)] in most of the ocean surface.

Fundamental shortcomings. Modelling the manganese cycle better, or really well, may be difficult for the following potentially relevant fundamental shortcomings in PISCES, the underlying model:

- The sediment source is merely a function of sea floor topography. It may be too small in the Southern Ocean and too large in the Arctic Ocean. Using a sediment model may be necessary.
- Manganese oxidising microbes may be necessary, but PISCES does not explicitly model any bacteria or fungi.
- Manganese reducing microbes may be necessary, but PISCES does not explicitly model any bacteria or fungi.
- Apparently, sediment samples show a strong correlation between manganese and lithogenic particles, while Mn does not show any correlation with bSi, POC or $CaCO_3$ according to recent observations and modelling [125]. This suggests that only lithogenic particles are a scavenger of Mn. However, there are no lithogenic particles in PISCES.[1]
- Possibly co-limitation with iron can play an important role in modelling the Mn(II) distribution in the Southern Ocean. Iron is not well simulated by the used version of PISCES (Section 3.3.3), which makes it difficult to use the modelled iron distribution to model co-limitation.

7.5 Conclusion

This is the first published study in which the three-dimensional distributions of Mn(II) and MnO_x are modelled. Many of the features of the distribution of Mn(II) are captured by our model. However, there are notable shortcomings as well. There appears to be an inconsistency between the basic assumptions on scavenging of Mn and the measured [Mn(II)]. It is likely that at least one of the basic principles is wrong or incomplete.

Modelling is only one way to find out more about this issue. There need to be 3-D process studies of Mn in the ocean, as well as more measurements of $[MnO_x]$. When measuring $[MnO_x]$ it needs to be clear what is measured exactly. It would for instance be useful if (1) a range of particle sizes are measured and (2) structural analysis of the particles are preformed, such that one can unambiguously say on which particle Mn is adsorbed. Only then a realistic simulation of Mn can be performed that may confirm the basic principles.

Acknowledgement

Contributors to this research are Andreas Sterl, Hein de Baar, Rob Middag, Alessandro Tagliabue, Jean-Claude Dutay, Marion Gehlen, Mathieu Roy-Barman, Philippe Jean-Babtiste, Catherine Jeandel, William Landing, Angela Milne and Clifton Buck.

[1] Furthermore, we do not know whether the correlation comes from adsorption or dissolution from lithogenic sources (dust, rivers) (personal communication, A. Sterl and M. Roy-Barman, August 2013). If lithogenic particles do scavenge Mn, this does not seem consistent with the relatively small settling speed of 0.9–1.0 $\mathrm{m\,d^{-1}}$ for the inner Pacific Ocean (up to 1.9 $\mathrm{m\,d^{-1}}$ for the margins; 0.4 $\mathrm{m\,d^{-1}}$ for inner Arctic Ocean; 4.1 $\mathrm{m\,d^{-1}}$ marginal Arctic) [125] (personal communication, A. Sterl, August 2013).

Bibliography

[1] A.W. Burks, J. von Neumann, and H.H. Goldstine. "Preliminary discussion of the logical design of an electronic computing instrument". In: *Computer Structures: Readings & Examples* (1946).

[2] J. Monod. "The Growth of Bacterial Cultures". In: *Annual Review of Microbiology* 3.1 (1949), pp. 371–394. DOI: 10.1146/annurev.mi.03.100149.002103.

[3] Alfred Tarski. "I: A General Method in Proofs of Undecidability". In: *Studies in Logic and the Foundations of Mathematics* 13 (1953), pp. 1–34.

[4] J.C. Lewin. "The dissolution of silica from diatom walls". In: *Geochimica et Cosmochimica Acta* 21.3-4 (1961), pp. 182–198. DOI: 10.1016/S0016-7037(61)80054-9.

[5] P. Suppes. "A comparison of the meaning and uses of models in mathematics and empirical sciences". In: *The Concept and the role of the model in mathematics and natural and social sciences: proceedings of the colloquium sponsored by the Division of Philosophy of Sciences of the International Union of History and Philosophy of Sciences organized at Utrecht, January 1960*. Ed. by B.H. Kazemier and D. Vuysje. Vol. 3. D. Reidel Publishing Company, 1961, pp. 163–177.

[6] A.C. Redfield. "The influence of organisms on the composition of sea-water". In: *The Sea* 2 (1963), pp. 26–77. URL: http://ci.nii.ac.jp/naid/10003768545/en/.

[7] G.C. Bortleson and G.F. Lee. "Phosphorus, iron, and manganese distribution in sediment cores of six Wisconsin lakes". In: *Limnol. Oceanogr* 19.5 (1974), pp. 794–801.

[8] H. Elderfield. "Manganese fluxes to the oceans". In: *Marine Chemistry* 4.2 (1976), pp. 103–132.

[9] G. Klinkhammer, M. Bender, and R.F. Weiss. "Hydrothermal manganese in the Galapagos Rift". In: 269.5626 (1977), pp. 319–320. DOI: 10.1038/269319a0.

[10] J.G. Charney, A. Arakawa, D.J. Baker, B. Bolin, R.E. Dickinson, R.M. Goody, C.E. Leith, H.M. Stommel, and C.I. Wunsch. "Carbon dioxide and climate: a scientific assessment". In: *National Academy of Sciences Press: Washington DC* 33 (1979).

[11] M. Stoffyn. "Biological control of dissolved aluminum in seawater: experimental evidence". In: *Science* 203.4381 (1979), p. 651. DOI: 10.1126/science.203.4381.651.

[12] W.M. Landing and K.W. Bruland. "Manganese in the north Pacific". In: *Earth and Planetary Science Letters* 49.1 (1980), pp. 45–56. DOI: 10.1016/0012-821X(80)90149-1.

[13] J.E. Lupton, G.P. Klinkhammer, W.R. Normark, R. Haymon, K.C. MacDonald, R.F. Weiss, and H. Craig. "Helium-3 and manganese at the 21°N East Pacific Rise hydrothermal site". In: *Earth and Planetary Science Letters* 50.1 (1980), pp. 115–127. DOI: 10.1016/0012-821X(80)90123-5.

[14] W.S. Broecker and T.-H. Peng. *Tracers in the Sea*. Eldigio Press, 1982.

[15] M. Stoffyn and F.T. Mackenzie. "Fate of dissolved aluminum in the oceans". In: *Marine Chemistry* 11.2 (1982), pp. 105–127. DOI: 10.1016/0304-4203(82)90036-6.

[16] F. Azam, T. Fenchel, J.G. Field, J.S. Gray, L.A. Meyer-Reil, and F. Thingstad. "The ecological role of water-column microbes in the sea". In: *Estuaries* 50 (1983), p. 2.

[17] J.H. Martin and G.A. Knauer. "VERTEX: Manganese transport with $CaCO_3$". In: *Deep Sea Research Part A. Oceanographic Research Papers* 30.4 (1983), pp. 411–425.

[18] W.G. Sunda and S.A. Huntsman. "Effect of competitive interactions between manganese and copper on cellular manganese and growth in estuarine and oceanic species of the diatom Thallassiosira". In: *Limnology and oceanography* 28.5 (1983), pp. 924–934.

[19] G. Klinkhammer, P. Rona, M. Greaves, and H. Elderfield. "Hydrothermal manganese plumes in the Mid-Atlantic Ridge rift valley". In: 314.6013 (1985), pp. 727–731. DOI: 10.1038/314727a0.

[20] B. Sundby and N. Silverberg. "Manganese fluxes in the benthic boundary layer". In: *Limnology and Oceanography* (1985), pp. 372–381.

[21] D.J. Hydes, P.J. Statham, and J.D. Burton. "A vertical profile of dissolved trace metals (Al, Cd, Cu, Mn, Ni) over the median valley of the mid Atlantic ridge, 43°N: Implications for Hydrothermal activity". In: *Science of The Total Environment* 49 (1986), pp. 133–145. DOI: 10.1016/0048-9697(86)90236-6.

[22] J.E. Mackin. "Control of dissolved Al distributions in marine sediments by clay reconstitution reactions: experimental evidence leading to a unified theory". In: *Geochimica et Cosmochimica Acta* 50.2 (1986), pp. 207–214. DOI: 10.1016/0016-7037(86)90170-5.

[23] K.J. Orians and K.W. Bruland. "The biogeochemistry of aluminum in the Pacific Ocean". In: *Earth and planetary science letters* 78.4 (1986), pp. 397–410. DOI: 10.1016/0012-821X(86)90006-3.

[24] W.M. Landing and K.W. Bruland. "The contrasting biogeochemistry of iron and manganese in the Pacific Ocean". In: *Geochimica et Cosmochimica Acta* 51.1 (1987), pp. 29–43. DOI: 10.1016/0016-7037(87)90004-4.

[25] H.B. Maring and R.A. Duce. "The impact of atmospheric aerosols on trace metal chemistry in open ocean surface seawater, 1. Aluminum". In: *Earth and Planetary Science Letters* 84.4 (1987), pp. 381–392. DOI: 10.1016/0012-821X(87)90003-3.

[26] T.S. Bowers, A.C. Campbell, C.I. Measures, A.J. Spivack, M. Khadem, and J.M. Edmond. "Chemical controls on the composition of vent fluids at 13°–11°N and 21°N, East Pacific Rise". In: *Journal of Geophysical Research* 93.B5 (1988), pp. 4522–4536. DOI: 10.1029/JB093iB05p04522.

[27] S.B. Moran and R.M. Moore. "Evidence from mesocosm studies for biological removal of dissolved aluminium from sea water". In: *Nature* 335.6192 (1988), pp. 706–708. DOI: 10.1038/335706a0.

[28] A. Morel. "Optical modeling of the upper ocean in relation to its biogenous matter content (case I waters)". In: *Journal of Geophysical Research: Oceans (1978–2012)* 93.C9 (1988), pp. 10749–10768.

[29] W.G. Sunda and S.A. Huntsman. "Effect of sunlight on redox cycles of manganese in the southwestern Sargasso Sea". In: *Deep Sea Research Part A. Oceanographic Research Papers* 35.8 (1988), pp. 1297–1317. DOI: 10.1016/0198-0149(88)90084-2.

[30] S.B. Moran and R.M. Moore. "The distribution of colloidal aluminum and organic carbon in coastal and open ocean waters off Nova Scotia". In: *Geochimica et Cosmochimica Acta* 53.10 (1989), pp. 2519–2527. DOI: 10.1016/0016-7037(89)90125-7.

[31] B.C. Van Fraassen. "Laws and symmetry". In: *Clarendon Paperbacks, Oxford: Clarendon, 1989* (1989).

[32] N.A. Campbell, N. Caris, and R. Williams. *Biology*. Benjamin/Cummings Publishing Company, 1990. ISBN: 9780805318012.

[33] R. Chester. *Marine geochemistry*. Unwin Human Ltd, London, 1990. ISBN: 0-04-551108-X.

[34] P.R. Gent and J.C. McWilliams. "Isopycnal mixing in ocean circulation models". In: *Journal of Physical Oceanography* 20.1 (1990), pp. 150–155. DOI: 10.1175/1520-0485(1990)020<0150:IMIOCM>2.0.CO;2. URL: http://www.atmos.washington.edu/twiki/pub/Main/OceanModelingReadings/gentmcwilliams.pdf.

[35] T. Lunel, M. Rudnicki, H. Elderfield, and D. Hydes. "Aluminium as a depth-sensitive tracer of entrainment in submarine hydrothermal plumes". In: *Nature* 344.6262 (1990), pp. 137–139. DOI: 10.1038/344137a0.

[36] John A. Raven. "Predictions of Mn and Fe use efficiencies of phototrophic growth as a function of light availability for growth and of C assimilation pathway". In: *New Phytologist* 116.1 (1990), pp. 1–18. DOI: 10.1111/j.1469-8137.1990.tb00505.x.

[37] A. Stone and J.J. Morgan. "Kinetics of Chemical Transformation in the Environment". In: *Aquatic chemical kinetics: reaction rates of processes in natural waters*. Ed. by W. Stumm. Vol. 2. John Wiley and Sons, 1990. Chap. 1, pp. 1–42.

[38] Bennekom, A.J. van, A.G.J. Buma, and R.F. Nolting. "Dissolved aluminium in the Weddell-Scotia Confluence and effect of Al on the dissolution kinetics of biogenic silica". In: *Marine Chemistry* 35.1-4 (1991), pp. 423–434. DOI: 10.1016/S0304-4203(09)90034-2.

[39] S.B. Moran and R.M. Moore. "The potential source of dissolved aluminum from resuspended sediments to the North Atlantic Deep Water". In: *Geochimica et Cosmochimica Acta* 55.10 (1991), pp. 2745–2751. DOI: 10.1016/0016-7037(91)90441-7.

[40] Beusekom, J.E.E. van and A. Weber. "Decreasing diatom abundance in the North Sea: the possible significance of aluminium". In: *Marine Euthrophication and Population Dynamics* (1992), pp. 121–127.

[41] J. W. Lavelle, J. P. Cowen, and G. J. Massoth. "A model for the deposition of hydrothermal manganese near ridge crests". In: *Journal of Geophysical Research: Oceans* 97.C5 (1992), pp. 7413–7427. DOI: 10.1029/92JC00406.

[42] C.M. Lalli and T.R. Parsons. *Biological Oceanography: an introduction*. Pergamon Press, Oxford, 1993. ISBN: 0-08-041014-6.

[43] K.W. Bruland, K.J. Orians, and Cowen J.P. "Reactive trace metals in the stratified central North Pacific". In: *Geochimica et Cosmochimica Acta* 58.15 (1994), pp. 3171–3182. DOI: 10.1016/0016-7037(94)90044-2.

[44] C. Guieu, R. Duce, and R. Arimoto. "Dissolved input of manganese to the ocean: Aerosol source". In: *Journal of geophysical research* 99.D9 (1994), pp. 18789–18. DOI: 10.1029/94JD01120.

[45] W.G. Sunda and S.A. Huntsman. "Photoreduction of manganese oxides in seawater". In: *Marine chemistry* 46.1 (1994), pp. 133–152. DOI: 10.1016/0304-4203(94)90051-5.

[46] P.R. Gent, J. Willebrand, T.J. McDougall, and J.C. McWilliams. "Parameterizing eddy-induced tracer transports in ocean circulation models". In: *Journal of Physical Oceanography* 25.4 (1995), pp. 463–474. DOI: 10.1175/1520-0485(1995)025<0463:PEITTI>2.0.CO;2. URL: ftp://apapane.soest.hawaii.edu/users/kelvin/tracers/eddy_transport/gent95.pdf.

[47] T. Jickells. "Atmospheric inputs of metals and nutrients to the oceans: their magnitude and effects". In: *Marine Chemistry* 48.3-4 (1995), pp. 199–214. DOI: 10.1016/0304-4203(95)92784-P.

[48] W.M. Landing, G.A. Cutter, J.A. Dalziel, A.R. Flegal, R.T. Powell, D. Schmidt, A. Shiller, P. Statham, S. Westerlund, and J. Resing. "Analytical intercomparison results from the 1990 Intergovernmental Oceanographic Commission open-ocean baseline survey for trace metals: Atlantic Ocean". In: *Marine Chemistry* 49.4 (1995), pp. 253–265.

[49] D.M. Nelson, P. Tréguer, M.A. Brzezinski, A. Leynaert, and B. Quéguiner. "Production and dissolution of biogenic silica in the ocean: revised global estimates, comparison with regional data and relationship to biogenic sedimentation". In: *Global Biogeochem. Cycles* 9 (1995), pp. 359–359. DOI: 10.1029/95GB01070.

[50] K.H. Wedepohl. "The composition of the continental crust". In: *Geochimica et Cosmochimica Acta* 59.7 (1995), pp. 1217–1232. DOI: 10.1016/0016-7037(95)00038-2.

[51] H. Elderfield and A. Schultz. "Mid-ocean ridge hydrothermal fluxes and the chemical composition of the ocean". In: *Annual Review of Earth and Planetary Sciences* 24.1 (1996), pp. 191–224.

[52] P. Galison. "Computer simulations and the trading zone". In: *The disunity of science: Boundaries, contexts, and power* (1996), pp. 118–157.

[53] K.S. Johnson, K.H. Coale, W.M. Berelson, and R. Michael Gordon. "On the formation of the manganese maximum in the oxygen minimum". In: *Geochimica et Cosmochimica Acta* 60.8 (1996), pp. 1291–1299. DOI: 10.1016/0016-7037(96)00005-1.

[54] E. Kalnay, M. Kanamitsu, R. Kistler, W. Collins, D. Deaven, L. Gandin, M. Iredell, S. Saha, G. White, J. Woollen, Y. Zhu, A. Leetmaa, R. Reynolds, M. Chelliah, W. Ebisuzaki, W. Higgins, J. Janowiak, K. C. Mo, C. Ropelewski, J. Wang, Roy Jenne, and Dennis Joseph. "The NCEP/NCAR 40-Year Reanalysis Project". In: *Bull. Amer. Meteor. Soc.* 77.3 (1996), pp. 437–471. DOI: 10.1175/1520-0477(1996)077<0437:TNYRP>2.0.CO;2.

[55] G. Madec and M. Imbard. "A global ocean mesh to overcome the North Pole singularity". In: *Climate Dynamics* 12 (6 1996), pp. 381–388. DOI: 10.1007/BF00211684.

[56] R.J. Murray. "Explicit generation of orthogonal grids for ocean models". In: *Journal of Computational Physics* 126.2 (1996), pp. 251–273. DOI: 10.1006/jcph.1996.0136.

[57] W.G. Sunda and S.A. Huntsman. "Antagonisms between cadmium and zinc toxicity and manganese limitation in a coastal diatom". In: *Limnology and Oceanography* (1996), pp. 373–387. URL: http://www.aslo.org/lo/pdf/vol_41/issue_3/0373.pdf.

[58] L. Chou and R. Wollast. "Biogeochemical behavior and mass balance of dissolved aluminum in the western Mediterranean Sea". In: *Deep Sea Research Part II: Topical Studies in Oceanography* 44.3-4 (1997), pp. 741–768. DOI: 10.1016/S0967-0645(96)00092-6.

[59] Peter J Von Langen, Kenneth S Johnson, Kenneth H Coale, and Virginia A Elrod. "Oxidation kinetics of manganese (II) in seawater at nanomolar concentrations". In: *Geochimica et cosmochimica acta* 61.23 (1997), pp. 4945–4954. DOI: 10.1016/S0016-7037(97)00355-4.

[60] C.B. Field, M.J. Behrenfeld, J.T. Randerson, and P. Falkowski. "Primary production of the biosphere: integrating terrestrial and oceanic components". In: *Science* 281.5374 (1998), pp. 237–240. DOI: 10.1126/science.281.5374.237.

[61] S. Levitus, T.P. Boyer, M.E. Conkright, T. O'Brien, J. Antonov, C. Stephens, L. Stathoplos, D. Johnson, and R. Gelfeld. "NOAA Atlas NESDIS 18, World Ocean Database 1998: vol. 1: Introduction". In: *US Government Printing Office, Washington DC* 346 (1998).

[62] G. Madec, P. Delecluse, M. Imbard, and C. Lévy. "OPA 8.1 Ocean General Circulation Model reference manual". Anglais. In: *Note du Pole de Modélisation, Institut Pierre-Simon Laplace* 11 (1998), 91p. URL: http://hal.archives-ouvertes.fr/hal-00154217/en/.

[63] P.J. Statham, P.A. Yeats, and W.M. Landing. "Manganese in the eastern Atlantic Ocean: processes influencing deep and surface water distributions". In: *Marine Chemistry* 61.1 (1998), pp. 55–68.

[64] Lakshmi H. Kantha and Carol Anne Clayson. *Numerical Models of OCEANS and Oceanic Processes*. Academic Press, 2000.

[65] C.I. Measures and S. Vink. "On the use of dissolved aluminum in surface waters to estimate dust deposition to the ocean". In: *Global Biogeochem. Cycles* 14.1 (2000), pp. 317–327. DOI: 10.1029/1999GB001188.

[66] C. Rüth, R. Well, and W. Roether. "Primordial 3He in South Atlantic deep waters from sources on the Mid-Atlantic Ridge". In: *Deep Sea Research Part I: Oceanographic Research Papers* 47.6 (2000), pp. 1059–1075. DOI: 10.1016/S0967-0637(99)00077-1.

[67] W.G. Sunda and S.A. Huntsman. "Effect of Zn, Mn, and Fe on Cd accumulation in phytoplankton: Implications for oceanic Cd cycling". In: *Limnology and Oceanography* 45.7 (2000), pp. 1501–1516.

[68] S. Dixit, P. Van Cappellen, and A.J. van Bennekom. "Processes controlling solubility of biogenic silica and pore water build-up of silicic acid in marine sediments". In: *Marine Chemistry* 73.3-4 (2001), pp. 333–352. DOI: 10.1016/S0304-4203(00)00118-3.

[69] R. Kistler, W. Collins, S. Saha, G. White, J. Woollen, E. Kalnay, M. Chelliah, W. Ebisuzaki, M. Kanamitsu, V. Kousky, et al. "The NCEP-NCAR 50-year reanalysis: Monthly means CD-ROM and documentation". In: *Bulletin of the American Meteorological society* 82.2 (2001), pp. 247–267. DOI: 10.1175/1520-0477(2001)082<0247:TNNYRM>2.3.CO;2.

[70] G.P. Klinkhammer, C.S. Chin, R.A. Keller, A. Daehlmann, H. Sahling, G. Sarthou, S. Petersen, F. Smith, and C. Wilson. "Discovery of new hydrothermal vent sites in Bransfield Strait, Antarctica". In: *Earth and Planetary Science Letters* 193.3-4 (2001), pp. 395–407. DOI: 10.1016/S0012-821X(01)00536-2.

[71] E Douville, J.L. Charlou, E.H. Oelkers, P. Bienvenu, C.F. Jove Colon, J.P. Donval, Y. Fouquet, D. Prieur, and P. Appriou. "The rainbow vent fluids (36°14' N, MAR): the influence of ultramafic rocks and phase separation on trace metal content in Mid-Atlantic Ridge hydrothermal fluids". In: *Chemical Geology* 184.1 (2002), pp. 37–48. DOI: 10.1016/S0009-2541(01)00351-5.

[72] M. Gehlen, L. Beck, G. Calas, A.M. Flank, A.J. van Bennekom, and J.E.E. van Beusekom. "Unraveling the atomic structure of biogenic silica: evidence of the structural association of Al and Si in diatom frustules". In: *Geochimica et Cosmochimica Acta* 66.9 (2002), pp. 1601–1609. DOI: 10.1016/S0016-7037(01)00877-8.

[73] H.J.W. Baar and J. Roche. "Trace Metals in the Oceans: Evolution, Biology and Global Change". English. In: *Marine Science Frontiers for Europe*. Ed. by Gerold Wefer, Frank Lamy, and Fauzi Mantoura. Springer Berlin Heidelberg, 2003, pp. 79–105. ISBN: 978-3-540-40168-1. DOI: 10.1007/978-3-642-55862-7_6.

[74] M. Gehlen, C. Heinze, E. Maier-Reimer, and C.I. Measures. "Coupled Al-Si geochemistry in an ocean general circulation model: A tool for the validation of oceanic dust deposition fields?" In: *Global Biogeochem. Cycles* 17.1 (2003), p. 1028. DOI: 10.1029/2001GB001549.

[75] L.D. Talley, J.L. Reid, and P.E. Robbins. "Data-based meridional overturning streamfunctions for the global ocean". In: *Journal of Climate* 16.19 (2003), pp. 3213–3226. DOI: 10.1175/1520-0442(2003)016<3213:DMOSFT>2.0.CO;2.

[76] J.C. Dutay, P. Jean-Baptiste, J.M. Campin, A. Ishida, E. Maier-Reimer, R.J. Matear, A. Mouchet, I.J. Totterdell, Y. Yamanaka, K. Rodgers, et al. "Evaluation of OCMIP-2 ocean models' deep circulation with mantle helium-3". In: *Journal of marine systems* 48.1 (2004), pp. 15–36. DOI: 10.1016/j.jmarsys.2003.05.010.

[77] D.A. Hauglustaine, F. Hourdin, L. Jourdain, M.-A. Filiberti, S. Walters, J.-F. Lamarque, and E.A. Holland. "Interactive chemistry in the Laboratoire de Météorologie Dynamique general circulation model: Description and background tropospheric chemistry evaluation". In: *Journal of Geophysical Research: Atmospheres* 109.D4 (2004), p. D04314. DOI: 10.1029/2003JD003957.

[78] J. Kramer, P. Laan, G. Sarthou, K.R. Timmermans, and H.J.W. De Baar. "Distribution of dissolved aluminium in the high atmospheric input region of the subtropical waters of the North Atlantic Ocean". In: *Marine Chemistry* 88.3-4 (2004), pp. 85–101. DOI: 10.1016/j.marchem.2004.03.009.

[79] W.G. Large and S.G. Yeager. *Diurnal to decadal global forcing for ocean and sea-ice models: The data sets and flux climatologies*. National Center for Atmospheric Research, 2004.

[80] A. Leynaert, E. Bucciarelli, P. Claquin, RC Dugdale, V. Martin-Jézéquel, P. Pondaven, and O. Ragueneau. "Effect of iron deficiency on diatom cell size and silicic acid uptake kinetics". In: *Limnology and Oceanography* 49.4 (2004), pp. 1134–1143. DOI: 10.4319/lo.2004.49.4.1134.

[81] J.K. Moore, S.C. Doney, and K. Lindsay. "Upper ocean ecosystem dynamics and iron cycling in a global three-dimensional model". In: *Global Biogeochem. Cycles* 18.4 (2004), GB4028. DOI: 10.1029/2004GB002220.

[82] G. Peers and N.M. Price. "A Role for Managanese in Superoxide Dismutases and Growth of Iron-Deficient Diatoms". In: *Limnology and Oceanography* 49.5 (2004), pp. 1774–1783. DOI: 10.4319/lo.2004.49.5.1774.

[83] C.L. Sabine, R.A. Feely, N. Gruber, R.M. Key, K. Lee, J.L. Bullister, R. Wanninkhof, C.S. Wong, D.W.R. Wallace, B. Tilbrook, et al. "The oceanic sink for anthropogenic CO2". In: *Science* 305.5682 (2004), p. 367. DOI: 10.1126/science.1097403.

[84] B.M. Tebo, J.R. Bargar, B.G. Clement, G.J. Dick, K.J. Murray, D. Parker, R. Verity, and S.M. Webb. "BIOGENIC MANGANESE OXIDES: Properties and Mechanisms of Formation". In: *Annual Review of Earth and Planetary Sciences* 32.1 (2004), pp. 287–328. DOI: 10.1146/annurev.earth.32.101802.120213.

[85] K.R. Timmermans, B. van der Wagt, and H.J.W. de Baar. "Growth rates, half-saturation constants, and silicate, nitrate, and phosphate depletion in relation to iron availability of four large, open-ocean diatoms from the Southern Ocean". In: *Limnology and Oceanography* (2004), pp. 2141–2151. DOI: 10.4319/lo.2004.49.6.2141.

[86] H.J.W. de Baar, P.W. Boyd, K.H. Coale, M.R. Landry, A. Tsuda, P. Assmy, D.C.E. Bakker, Y. Bozec, R.T. Barber, M.A. Brzezinski, et al. "Synthesis of iron fertilization experiments: from the iron age in the age of enlightenment". In: *J. Geophys. Res* 110 (2005), C09S16. DOI: 10.1029/2004JC002601. URL: http://eprints.uni-kiel.de/8240/1/208_de%20Baar_2005_SynthesisOfIronFertilizationExperiments_Artzeit_pubid9976.pdf.

[87] T.D. Jickells, Z.S. An, K.K. Andersen, A.R. Baker, G. Bergametti, N. Brooks, J.J. Cao, P.W. Boyd, R.A. Duce, K.A. Hunter, H. Kawahata, N. Kubilay, J. de la Roche, P.S. Liss, N. Mahowald, J.M. Prospero, A.J. Ridgwell, I. Tegen, and R. Torres. "Global iron connections between desert dust, ocean biogeochemistry, and climate". In: *Science* 308.5718 (2005), pp. 67–71. DOI: 10.1126/science.1105959.

[88] C.I. Measures, M.T. Brown, and S. Vink. "Dust deposition to the surface waters of the western and central North Pacific inferred from surface water dissolved aluminum concentrations". In: *Geochem. Geophys. Geosyst.* 6.9 (Sept. 2005), Q09M03–. DOI: 10.1029/2005GC000922.

[89] M. Roy-Barman, C. Jeandel, M. Souhaut, M. Rutgers van der Loeff, I. Voege, N. Leblond, and R. Freydier. "The influence of particle composition on thorium scavenging in the NE Atlantic ocean (POMME experiment)". In: *Earth and Planetary Science Letters* 240.3 (2005), pp. 681–693. DOI: 10.1016/j.epsl.2005.09.059.

[90] C.L. Sabine, R.M. Key, A. Kozyr, R.A. Feely, R. Wanninkhof, F.J. Millero, T.H. Peny, J.L. Bullister, and K. Lee. *Global ocean data analysis project (GLODAP): Results and data*. Tech. rep. OAK RIDGE NATIONAL LABORATORY, 2005.

[91] B.M. Tebo, H.A. Johnson, J.K. McCarthy, and A.S. Templeton. "Geomicrobiology of manganese (II) oxidation". In: *TRENDS in Microbiology* 13.9 (2005), pp. 421–428. DOI: 10.1016/j.tim.2005.07.009.

[92] R. Timmermann, H. Goosse, G. Madec, T. Fichefet, C. Ethé, and V. Dulière. "On the representation of high latitude processes in the ORCA-LIM global coupled sea ice–ocean model". In: *Ocean Modelling* 8.1–2 (2005), pp. 175–201. DOI: 10.1016/j.ocemod.2003.12.009.

[93] S.M. Uppala, P.W. Kållberg, A.J. Simmons, U. Andrae, V. Bechtold, M. Fiorino, J.K. Gibson, J. Haseler, A. Hernandez, G.A. Kelly, et al. "The ERA-40 re-analysis". In: *Quarterly Journal of the Royal Meteorological Society* 131.612 (2005), pp. 2961–3012. DOI: 10.1256/qj.04.176.

[94] Samuel M. Webb, Gregory J. Dick, John R. Bargar, and Bradley M. Tebo. "Evidence for the presence of Mn(III) intermediates in the bacterial oxidation of Mn(II)". In: *Proceedings of the National Academy of Sciences of the United States of America* 102.15 (2005), pp. 5558–5563. DOI: 10.1073/pnas.0409119102. URL: http://www.pnas.org/content/102/15/5558.abstract.

[95] A.M. Aguilar-Islas and K.W. Bruland. "Dissolved manganese and silicic acid in the Columbia River plume: A major source to the California current and coastal waters off Washington and Oregon". In: *Marine chemistry* 101.3 (2006), pp. 233–247. DOI: 10.1016/j.marchem.2006.03.005.

[96] O. Aumont and L. Bopp. "Globalizing results from ocean in situ iron fertilization studies". In: *Global Biogeochem. Cycles* 20.2 (2006), GB2017. DOI: 10.1029/2005GB002591.

[97] A.R. Baker, T.D. Jickells, M. Witt, and K.L. Linge. "Trends in the solubility of iron, aluminium, manganese and phosphorus in aerosol collected over the Atlantic Ocean". In: *Marine Chemistry* 98.1 (2006), pp. 43–58. DOI: 10.1016/j.marchem.2005.06.004.

[98] K.W. Bruland and M.C. Lohan. "Controls of Trace Metals in Seawater". In: *The Oceans and Marine Geochemistry*. Ed. by H. Elderfield. Vol. 6. Elsevier, 2006. Chap. 6.02, pp. 23–47. URL: http://es.ucsc.edu/~kbruland/Manuscripts/BRULAND/BrulandChpt6_02_TraceMetals.pdf.

[99] C.S. Buck, W.M. Landing, J.A. Resing, and G.T. Lebon. "Aerosol iron and aluminum solubility in the northwest Pacific Ocean: Results from the 2002 IOC cruise". In: *Geochemistry, Geophysics, Geosystems* 7.4 (2006), Q04M07. DOI: 10.1029/2005GC000977.

[100] C. Ethé, O. Aumont, M-A Foujols, and M. Lévy. "NEMO reference manual, tracer component : NEMO-TOP. Preliminary version". In: *Note du Pole de Modélisation, Institut Pierre-Simon Laplace* (2006).

[101] R. Frigg. "Scientific representation and the semantic view of theories". In: *Theoria. Revista de Teoría, Historia y Fundamentos de la Ciencia* 55.1 (2006), pp. 37–53.

[102] J.L. Sarmiento and N. Gruber. *Ocean Biogeochemical Dynamics*. Princeton University Press, 2006. ISBN: 978-0-691-01707-5.

[103] J.B. Shurin, D.S. Gruner, and H. Hillebrand. "All wet or dried up? Real differences between aquatic and terrestrial food webs". In: *Proceedings of the Royal Society B: Biological Sciences* 273.1582 (2006), pp. 1–9. DOI: 10.1098/rspb.2005.3377.

[104] F. Wolfe-Simon, V. Starovoytov, J.R. Reinfelder, O. Schofield, and P.G. Falkowski. "Localization and role of manganese superoxide dismutase in a marine diatom". In: *Plant physiology* 142.4 (2006), pp. 1701–1709. DOI: 10.1104/pp.106.088963.

[105] S.A. Cunningham, T. Kanzow, D. Rayner, M.O. Baringer, W.E. Johns, J. Marotzke, H.R. Longworth, E.M. Grant, J.J.-M. Hirschi, L.M. Beal, et al. "Temporal variability of the Atlantic meridional overturning circulation at 26.5 N". In: *science* 317.5840 (2007), pp. 935–938. DOI: 10.1126/science.1141304.

[106] M. Gehlen, R. Gangstø, B. Schneider, L. Bopp, O. Aumont, and C. Ethe. "The fate of pelagic $CaCO_3$ production in a high CO_2 ocean: a model study". In: *Biogeosciences* 4.4 (2007), pp. 505–519. DOI: 10.5194/bg-4-505-2007.

[107] L.J. Hoffmann, I. Peeken, K. Lochte, et al. "Effects of iron on the elemental stoichiometry during EIFEX and in the diatoms *Fragilariopsis kerguelensis* and *Chaetoceros dichaeta*". In: *Biogeosciences* 4.4 (2007), pp. 569–579. URL: www.biogeosciences.net/4/569/2007/.

[108] Jong, J. de, M. Boyé, M.D. Gelado-Caballero, K.R. Timmermans, M.J.W. Veldhuis, R.F. Nolting, C.M.G. van den Berg, and H.J.W. de Baar. "Inputs of iron, manganese and aluminium to surface waters of the Northeast Atlantic Ocean and the European continental shelf". In: *Marine Chemistry* 107.2 (2007), pp. 120–142. DOI: 10.1016/j.marchem.2007.05.007.

[109] E. Koning, M. Gehlen, A.-M. Flank, G. Calas, and E. Epping. "Rapid post-mortem incorporation of aluminum in diatom frustules: Evidence from chemical and structural analyses". In: *Marine Chemistry* 106.1–2 (2007), pp. 208–222. DOI: 10.1016/j.marchem.2006.06.009.

[110] S.V. Pakhomova, P.O.J. Hall, M.Y. Kononets, A.G. Rozanov, A. Tengberg, and A.V. Vershinin. "Fluxes of iron and manganese across the sediment–water interface under various redox conditions". In: *Marine Chemistry* 107.3 (2007), pp. 319–331. DOI: 10.1016/j.marchem.2007.06.001.

[111] C. Tebaldi and R. Knutti. "The use of the multi-model ensemble in probabilistic climate projections". In: *Philosophical Transactions of the Royal Society A: Mathematical, Physical and Engineering Sciences* 365.1857 (2007), p. 2053.

[112] M.T. Brown and K.W. Bruland. "An improved flow-injection analysis method for the determination of dissolved aluminum in seawater". In: *Limnol. Oceanogr. Methods* 6 (2008), pp. 87–95. URL: https://www.aslo.org/lomethods/free/2008/0087.pdf.

[113] K.L. Denman. "Climate change, ocean processes and ocean iron fertilization". In: *Marine Ecology Progress Series* (2008). DOI: 10.3354/meps07542.

[114] T. Fenchel. "The microbial loop – 25 years later". In: *Journal of Experimental Marine Biology and Ecology* 366.1–2 (2008), pp. 99–103. DOI: 10.1016/j.jembe.2008.07.013.

[115] Q. Han, J.K. Moore, C. Zender, and D. Hydes. "Constraining oceanic dust deposition using surface ocean dissolved Al". In: *Global Biogeochem. Cycles* 22.2 (2008), GB2038. DOI: 10.1029/2007GB002975.

[116] G. Madec. "NEMO ocean engine". In: *Note du Pole de Modélisation, Institut Pierre-Simon Laplace* (2008).

[117] J.K. Moore and O. Braucher. "Sedimentary and mineral dust sources of dissolved iron to the world ocean". In: *Biogeosciences* 5.3 (2008), pp. 631–656. URL: http://hal.archives-ouvertes.fr/hal-00297688/.

[118] F.T.M. Nieuwstadt. *Turbulentie – inleiding in de theorie en toepassingen van turbulente stromingen*. Epsilon Uitgaven, 2008.

[119] T. Arsouze, J.-C. Dutay, F. Lacan, and C. Jeandel. "Reconstructing the Nd oceanic cycle using a coupled dynamical–biogeochemical model". In: *Biogeosciences* 6.12 (2009), pp. 2829–2846. DOI: 10.5194/bg-6-2829-2009.

[120] J.C. Dutay, F. Lacan, M. Roy-Barman, and L. Bopp. "Influence of particle size and type on ^{231}Pa and ^{230}Th simulation with a global coupled biogeochemical-ocean general circulation model: A first approach". In: *Geochemistry Geophysics Geosystems* 10.1 (2009), Q01011. DOI: 10.1029/2008GC002291.

[121] E. Hawkins and R. Sutton. "The potential to narrow uncertainty in regional climate predictions". In: *Bulletin of the American Meteorological Society* 90.8 (2009), pp. 1095–1107. DOI: 10.1175/2009BAMS2607.1.

[122] Heuven, S.M.A.C. van. "First direct observation of increasing CO2 over decadal time scale in deep ocean waters". PhD thesis. University of Groningen, 2009.

[123] R. Middag, H.J.W. de Baar, P. Laan, and K. Bakker. "Dissolved aluminium and the silicon cycle in the Arctic Ocean". In: *Marine Chemistry* 115.3-4 (2009), pp. 176–195. DOI: 10.1016/j.marchem.2009.08.002.

[124] G. Reverdin, M. Lévy, P. Raimbault, and D. Lefèvre. "Nutrients in mode waters of the northeast Atlantic". In: *Journal of Geophysical Research* 114 (2009). DOI: 10.1029/2009JC005546.

[125] M. Roy-Barman. "Modelling the effect of boundary scavenging on Thorium and Protactinium profiles in the ocean". In: *Biogeosciences* 6.4 (2009), pp. 3091–3107. DOI: 10.5194/bg-6-3091-2009.

[126] C.A. Stow, J. Jolliff, D.J. McGillicuddy Jr., S.C. Doney, J.I. Allen, M.A.M. Friedrichs, K.A. Rose, and P. Wallhead. "Skill assessment for coupled biological/physical models of marine systems". In: *Journal of Marine Systems* 76.1-2 (2009), pp. 4–15. DOI: 10.1016/j.jmarsys.2008.03.011.

[127] E. Breitbarth, E. P. Achterberg, M. V. Ardelan, A. R. Baker, E. Bucciarelli, F. Chever, P. L. Croot, S. Duggen, M. Gledhill, M. Hassellöv, C. Hassler, L. J. Hoffmann, K. A. Hunter, D. A. Hutchins, J. Ingri, T. Jickells, M. C. Lohan, M. C. Nielsdóttir, G. Sarthou, V. Schoemann, J. M. Trapp, D. R. Turner, and Y. Ye. "Iron biogeochemistry across marine systems – progress from the past decade". In: *Biogeosciences* 7.3 (2010), pp. 1075–1097. DOI: 10.5194/bg-7-1075-2010.

[128] L. Brodeau, B. Barnier, A.-M. Treguier, T. Penduff, and S. Gulev. "An ERA40-based atmospheric forcing for global ocean circulation models". In: *Ocean Modelling* 31.3-4 (2010), pp. 88–104. DOI: 10.1016/j.ocemod.2009.10.005.

[129] M.T. Brown, S.M. Lippiatt, and K.W. Bruland. "Dissolved aluminum, particulate aluminum, and silicic acid in northern Gulf of Alaska coastal waters: Glacial/riverine inputs and extreme reactivity". In: *Marine Chemistry* 122.1 (2010), pp. 160–175. DOI: 10.1016/j.marchem.2010.04.002.

[130] C.S. Buck, W.M. Landing, J.A. Resing, and C.I. Measures. "The solubility and deposition of aerosol Fe and other trace elements in the North Atlantic Ocean: Observations from the A16N CLIVAR/CO2 repeat hydrography section". In: *Marine Chemistry* 120.1-4 (2010), pp. 57–70. DOI: 10.1016/j.marchem.2008.08.003.

[131] John M. Lyman, Simon A. Good, Viktor V. Gouretski, Masayoshi Ishii, Gregory C. Johnson, Matthew D. Palmer, Doug M. Smith, and Josh K. Willis. "Robust warming of the global upper ocean". In: *Nature* 465 (2010), pp. 334–337. DOI: 10.1038/nature09043.

[132] A.M.P. McDonnell and K.O. Buesseler. "Variability in the average sinking velocity of marine particles". In: *Limnol. Oceanogr* 55.5 (2010), pp. 2085–2096. DOI: 10.4319/lo.2010.55.5.2085.

[133] C.I. Measures, T. Sato, S. Vink, S. Howell, and Y.H. Li. "The fractional solubility of aluminium from mineral aerosols collected in Hawaii and implications for atmospheric deposition of biogeochemically important trace elements". In: *Marine Chemistry* 120.1-4 (2010), pp. 144–153. DOI: 10.1016/j.marchem.2009.01.014.

[134] Jeffrey Mendez, Cecile Guieu, and Jess Adkins. "Atmospheric input of manganese and iron to the ocean: Seawater dissolution experiments with Saharan and North American dusts". In: *Marine Chemistry* 120.1 (2010), pp. 34–43. DOI: 10.1016/j.marchem.2008.08.006.

[135] R. Middag. "Dissolved Aluminium and Manganese in the Polar Oceans". PhD thesis. University of Groningen, 2010.

[136] L.O. Slemons, J.W. Murray, J. Resing, B. Paul, and P. Dutrieux. "Western Pacific coastal sources of iron, manganese, and aluminum to the Equatorial Undercurrent". In: *Global Biogeochem. Cycles* 24.3 (2010). DOI: 10.1029/2009GB003693.

[137] A. Tagliabue, L. Bopp, J.-C. Dutay, A.R. Bowie, F. Chever, P. Jean-Baptiste, E. Bucciarelli, D. Lannuzel, T. Remenyi, G. Sarthou, O. Aumont, M. Gehlen, and C. Jeandel. "Hydrothermal contribution to the oceanic dissolved iron inventory". In: *Nature Geoscience* 3.4 (2010), pp. 252–256. DOI: 10.1038/NGEO818.

[138] B. Cushman–Roisin and J.-M. Beckers. *Introduction to Geophysical Fluid Dynamics: physical and numerical aspects*. Elsevier, 2011.

[139] S.M.A.C. van Heuven, M. Hoppema, O. Huhn, H.A. Slagter, and H.J.W. de Baar. "Direct observation of increasing CO_2 in the Weddell Gyre along the Prime Meridian during 1973–2008". In: *Deep Sea Research Part II: Topical Studies in Oceanography* 58.25 (2011), pp. 2613–2635.

[140] R. Middag, H.J.W. de Baar, P. Laan, and M.B. Klunder. "Fluvial and hydrothermal input of manganese into the Arctic Ocean". In: *Geochimica et Cosmochimica Acta* 75.9 (2011), pp. 2393–2408. DOI: 10.1016/j.gca.2011.02.011.

[141] R. Middag, H.J.W. de Baar, P. Laan, P.H. Cai, and J.C. van Ooijen. "Dissolved manganese in the Atlantic sector of the Southern Ocean". In: *Deep Sea Research Part II: Topical Studies in Oceanography* 58 (2011), pp. 2661–2677. DOI: 10.1016/j.dsr2.2010.10.043.

[142] D. Rayner, J.J.-M. Hirschi, T. Kanzow, W.E. Johns, P.G. Wright, E. Frajka-Williams, H.L. Bryden, C.S. Meinen, M.O. Baringer, J. Marotzke, et al. "Monitoring the Atlantic meridional overturning circulation". In: *Deep Sea Research Part II: Topical Studies in Oceanography* 58.17 (2011), pp. 1744–1753. DOI: 10.1016/j.dsr2.2010.10.056. URL: http://www.researchgate.net/publication/223416810_Monitoring_the_Atlantic_meridional_overturning_circulation/file/3deec528f82e945999.pdf.

[143] M.J.A. Rijkenberg, R.J. Langlois, M.M. Mills, M.D. Patey, P.G. Hill, M.C. Nielsdóttir, T.J. Compton, J. LaRoche, and E.P. Achterberg. "Environmental Forcing of Nitrogen Fixation in the Eastern Tropical and Sub-Tropical North Atlantic Ocean". In: *PloS one* 6.12 (2011), e28989. DOI: 10.1371/journal.pone.0028989.

[144] S.G. Sander and A. Koschinsky. "Metal flux from hydrothermal vents increased by organic complexation". In: *Nature Geoscience* 4.3 (2011), pp. 145–150. DOI: 10.1038/ngeo1088.

[145] A. Tagliabue and C. Völker. "Towards accounting for dissolved iron speciation in global ocean models". In: *Biogeosciences* 8.10 (2011), pp. 3025–3039. DOI: 10.5194/bg-8-3025-2011.

[146] G.A. Cutter and K.W. Bruland. "Rapid and noncontaminating sampling system for trace elements in global ocean surveys". In: *Limnol. Oceanogr. Methods* 10 (2012), pp. 425–436. DOI: 10.4319/lom.2012.10.425.

[147] R. Frigg and S. Hartmann. "Models in Science". In: *The Stanford Encyclopedia of Philosophy*. Ed. by Edward N. Zalta. Fall 2012. 2012. URL: http://plato.stanford.edu/entries/models-science/.

[148] H. Halvorson. "What Scientific Theories Could Not Be". In: *Philosophy of science* 79.2 (2012), pp. 183–206.

[149] Q. Han, C.S. Zender, J.K. Moore, C.S. Buck, Y. Chen, A. Johansen, and C.I. Measures. "Global estimates of mineral dust aerosol iron and aluminum solubility that account for particle size using diffusion-controlled and surface-area-controlled approximations". In: *Global Biogeochem. Cycles* 26.2 (2012), GB2038. DOI: 10.1029/2011GB004186.

[150] D.C. Ince, L. Hatton, and J. Graham-Cumming. "The case for open computer programs". In: *Nature* 482.7386 (2012), pp. 485–488. DOI: 10.1038/nature10836.

[151] M.T. Jones, C.R. Pearce, and E.H. Oelkers. "An experimental study of the interaction of basaltic riverine particulate material and seawater". In: *Geochimica et Cosmochimica Acta* 77 (2012), pp. 108–120. DOI: 10.1016/j.gca.2011.10.044.

[152] J. Katzav, H.A. Dijkstra, and A.T.J. de Laat. "Assessing climate model projections: State of the art and philosophical reflections". In: *Studies in History and Philosophy of Science Part B: Studies in History and Philosophy of Modern Physics* 43.4 (2012), pp. 258–276. DOI: 10.1016/j.shpsb.2012.07.002. URL: http://www.sciencedirect.com/science/article/pii/S1355219812000536.

[153] G. Madec et al. "NEMO ocean engine". In: *Note du Pole de Modélisation, Institut Pierre-Simon Laplace* (2012).

[154] R. Middag, H.J.W. de Baar, P. Laan, and O. Huhn. "The effects of continental margins and water mass circulation on the distribution of dissolved aluminum and manganese in Drake Passage". In: *J. Geophys. Res.* 117.C1 (2012), p. C01019. DOI: 10.1029/2011JC007434.

[155] A.C. Petersen. "Simulating nature: a philosophical study of computer-simulation uncertainties and their role in climate science and policy advice". PhD thesis. 2012.

[156] R.M. Stallman. *The Free Software Definition*. 2012. URL: https://www.gnu.org/philosophy/free-sw.html.

[157] A. Tagliabue, T. Mtshali, O. Aumont, A. R. Bowie, M. B. Klunder, A. N. Roychoudhury, and S. Swart. "A global compilation of dissolved iron measurements: focus on distributions and processes in the Southern Ocean". In: *Biogeosciences* 9.6 (2012), pp. 2333–2349. DOI: 10.5194/bg-9-2333-2012.

[158] Hulten, M.M.P. van, A. Sterl, J.-C. Dutay, A. Tagliabue, M. Gehlen, H.J.W. de Baar, and R. Middag. "Aluminium in an ocean general circulation model compared with the West Atlantic Geotraces cruises". In: *Journal of Marine Systems* 126 (Oct. 2013), pp. 3–23. DOI: 10.1016/j.jmarsys.2012.05.005. URL: http://arxiv.org/abs/1202.4679.

[159] IPCC. *Fifth Assessment Report: Climate Change 2013: The AR5 Synthesis Report – Working Group I: The Physical Science Basis*. Geneva: IPCC, 2013. URL: http://www.climatechange2013.org/.

[160] J.E. Johnson, S.M. Webb, K. Thomas, S. Ono, J.L. Kirschvink, and W.W. Fischer. "Manganese-oxidizing photosynthesis before the rise of cyanobacteria". In: *Proceedings of the National Academy of Sciences* 110.28 (2013), pp. 11238–11243. DOI: 10.1073/pnas.1305530110.

[161] A.S. Madison, B.M. Tebo, A. Mucci, B. Sundby, and G.W. Luther. "Abundant Porewater Mn(III) Is a Major Component of the Sedimentary Redox System". In: *Science* 341.6148 (2013), pp. 875–878. DOI: 10.1126/science.1241396.

[162] R. Middag, H.J.W. de Baar, M.B. Klunder, and P. Laan. "Fluxes of dissolved aluminum and manganese to the Weddell Sea and indications for manganese co-limitation". In: *Limnol. Oceanogr* 58.1 (2013), pp. 287–300. DOI: 10.4319/lo.2013.58.1.0287.

[163] H. Thi Dieu Vu and Y. Sohrin. "Diverse stoichiometry of dissolved trace metals in the Indian Ocean". In: 3 (2013). DOI: 10.1038/srep01745.

[164] P.J. Tréguer and C.L. De La Rocha. "The World Ocean Silica Cycle". In: *Annual Review of Marine Science* (2013). DOI: 10.1146/annurev-marine-121211-172346.

[165] B.S. Twining and S.B. Baines. "The Trace Metal Composition of Marine Phytoplankton". In: *Annual Review of Marine Science* 5.1 (2013). DOI: 10.1146/annurev-marine-121211-172322.

[166] A. Yool, E. E. Popova, and T. R. Anderson. "MEDUSA-2.0: an intermediate complexity biogeochemical model of the marine carbon cycle for climate change and ocean acidification studies". In: *Geoscientific Model Development* 6.5 (2013), pp. 1767–1811. DOI: 10.5194/gmd-6-1767-2013.

[167] Hulten, M.M.P. van, A. Sterl, R. Middag, H.J.W. de Baar, M. Gehlen, J.-C. Dutay, and A. Tagliabue. "An improved ocean model of aluminium: the effects of circulation, sediment resuspension and biological incorporation". In: *Biogeosciences Discussion* (Oct. 2013). DOI: 10.5194/bgd-10-14539-2013.

[168] K. Schmidt, C. L. De La Rocha, M. Gallinari, and G. Cortese. "Not all calcite ballast is created equal: differing effects of foraminiferan and coccolith calcite on the formation and sinking of aggregates". In: *Biogeosciences* 11.1 (2014), pp. 135–145. DOI: 10.5194/bg-11-135-2014. URL: http://www.biogeosciences.net/11/135/2014/.

[169] O. Aumont. "PISCES: An ocean biogeochemical model for carbon and ecosystem studies". In: *Geoscientific Model Development* (in preparation).

[170] R. Middag, H.M. van Aken, M.M.P. van Hulten, and H.J.W. de Baar. "Aluminium in the ocean: unique mirror image of the biological cycle". in preparation.

[171] M.J.A. Rijkenberg, R. Middag, P. Laan, L.J.A. Gerringa, H.M. van Aken, A. Schoemann, J.T.M. de Jong, H. van Haren, and H.J.W. de Baar. "Multiple sources of dissolved iron to the West Atlantic Ocean". In: (in preparation).